공학석사 학위논문

Behavior and Design Strength of Block Shear in Steel Lap Joints with High-Strength Steel

고강도 강재를 적용한 겹침이음 접합부의 블록전단 거동 및 강도

2017 년 2 월

서울대학교 대학원

건축학과

김 근 형

Behavior and Design Strength of Block Shear in Steel Lap Joints with High-Strength Steel

지도 교수 이 철 호

이 논문을 공학석사 학위논문으로 제출함

2017 년 2 월

서울대학교 대학원

건축학과

김 근 형

김근형의 공학석사 학위논문을 인준함

2017 년 2 월

위 원 장 _____ **(인)**

부위원장 _____ **(인)**

위 원 _____ **(인)**

Abstract

Behavior and Design Strength of Block Shear in Steel Lap Joints with High-Strength Steel

Kim, Keunhyung

Department of Architecture and Architectural Engineering

College of Engineering

Seoul National University

Bolting is a common connecting method in steel construction. In steel structures, block shear rupture is one of the very critical failure modes of bolted connections. The block shear failure is that shear failure and perpendicular tension failure simultaneously occur in the bolted connection. Although abundant test results on the block shear of bolted connections are available, the failure mechanism is not clearly explained. Since AISC Specification 1978, the design equation for block shear failure have continued to change in various forms. Design equation of current codes including AISC 2010 propse considerably conservative design strength of block shear rupture and inaccurately predict the failure mode.

Abstract

The application of high-strength steel for structural members has diverse technical advantages from design to construction. As the current design equation of the block shear is based on the experiments with conventional steels, the applicability of the high-strength steel for current design standards are unconfirmed. In this study, the behavior of bolted connections with the high-strength steel, HSA800, was experimentally evaluated.

In order to better understand and describe the failure mechanism of the block shear and its capacity, 10 lap joints fabricated from conventional and high-strength steels were tested in this study. Numerical analyses of bolted connections were conducted using the general-purpose finite element (FE) software, ABAQUS. Key test variables included the grades of the steels, the geometrical configuration of the number of bolts and distance.

This study evaluated the design criteria for the block shear and the applicability of the high-strength steels. Based on the experimental results and the finite element analysis, a new design equation for the block shear applicable to both the convention and high-strength steel was suggested.

Keywords: Block Shear, High-Strength Steel, Bolted Connection, Lap Joint, Design Equation

Student Number: 2015-21095

Contents

Abstract ..... **i**

Contents ..... **iii**

List of Tables ..... **vi**

List of Figures ..... **vii**

Chapter 1. Introduction **1**

1.1 Research Background 1

1.2 Objectives and Scope 3

Chapter 2. Previous Research **7**

2.1 Introduction 7

2.2 Block Shear Researches in Lap Joints 7

2.2.1 Birkemoe and Gilmor (1978) 7

2.2.2 Hardash and Bjorhovde (1985) 8

2.2.3 Rabinovitch and Cheng (1994) 9

2.2.4 Nast, Grondin, and Cheng (1999) 10

2.2.5 Aalberg and Larsen (2000) 10

2.2.6 Swanson and Leon (2000) 11

2.2.7 Kulak and Grondin (2001a) 11

2.2.8 Huns, Driver, and Grondin (2002) 12

2.2.9 Driver, Grondin, and Kulak (2006) 12

2.2.10 Teh and Yazici (2013) 13

2.3 Review of Current Design Codes 13
2.3.1 AISC (1999) 15
2.3.2 AISC (2005) and AISC (2010) 16
2.3.3 CSA S16-09 16
2.4 Summary 17

Chapter 3. Experimental Study 21
3.1 Introduction 21
3.2 Experimental Program 21
3.3 Test Set-up 27
3.4 Test Result and Contemplation 28
3.4.1 Specimen 25T-490-3-60 30
3.4.2 Specimen 25T-490-7-40 32
3.4.3 Specimen 25T-570-3-60 34
3.4.4 Specimen 25T-570-7-40 36
3.4.5 Specimen 25T-800-3-60 38
3.4.6 Specimen 25T-800-7-40 40
3.4.7 Specimen 15T-490-3-60 42
3.4.8 Specimen 15T-490-4-60 44
3.4.9 Specimen 15T-800-3-60 46
3.4.10 Specimen 15T-800-4-60 48
3.5 Summary 50

Chapter 4. Numerical Parametric Study and Suggestion of New Design Equation 51
4.1 Introduction 51
4.2 Finite Element Model 52
4.3 Verification 54

4.4 Numerical Analysis Results 60
4.4.1 Specimens with 25mm Plate 60
4.4.2 Specimens with 15mm Plate 78
4.5 Connection Length Effect 98
4.6 Proposed a New Design Equation 99
4.7 Summary 101

Chapter 5. Summary and Conclusion 103

References 105

Korean Abstract 108

List of Tables

Table 2-1. Block Shear Design Eqaution of AISC 14
Table 2-2 Mean Test-to-Design Strength Ratio 19
Table 2-3 Summary of Previous Researches 20
Table 3-1. Specification of Test Specimens in Test Series I 23
Table 3-2 Specification of Test Specimens in Test Series II 25
Table 3-3 Tensile Test Results of Steel Plate 26
Table 3-4. Block Shear Test Results for Specimens with 25 mm plate 29
Table 3-5 Block Shear Test Results for Specimens with 15mm Plate 29
Table 3-6 Test Result of Specimens with Block Shear Failure 50
Table 4-1 Comparison of Test and FE Analysis Results 60
Table 4-2 FE Analysis Results for SM490 Steel 75
Table 4-3 FE Analysis Results for SM570 Steel 76
Table 4-4 FE Analysis Results for HSA800 Steel 77
Table 4-5 FE Analysis Results for SM490 Steel 95
Table 4-6 FE Analysis Results for SM570 Steel 96
Table 4-7 FE Analysis Results for HSA800 Steel 97
Table 4-8 Results of the Regression Analyses 101

List of Figures

Figure 1-1 Block Shear in Bolted Connection 2

Figure 1-2 Example of Block Shear Behavior 2

Figure 1-3 Two Possible Case of Block Shear 2

Figure 1-4 Stress-Strain Curves of Conventional and High-Strength Steel 3

Figure 1-5 Typical Mechanism of Block Shear with Net Shear Plane 5

Figure 1-6 Typical Mechanism of Block Shear with Gross Shear Plane 5

Figure 2-1 Connection Length Factor from Hardash and Bjorhovde (1985) ... 9

Figure 2-2 Test-to-Design Strength Ratio for AISC 1999 Specification 18

Figure 2-3 Test-to-Design Strength Ratio for 2010 AISC Specification 18

Figure 2-4 Test-to-Design Strength Ratio for CSA S16-09 19

Figure 3-1 Bloted Connection in Flage of H-beam 23

Figure 3-2 Typical Specimen with Non-Staggered Configuration in Test Series I 24

Figure 3-3 Typical Specimen with Staggered Configuration in Test Series I 24

Figure 3-4 Typical Specimen with 12 Bolts in Test Series II 25

Figure 3-5 Typical Specimen with 16 Bolts in Test Seires II 26

Figure 3-6 Test Set-up 27

Figure 3-7 Test Set-up 28

Figure 3-8 Specimen 25T-490-3-60 at end of test 30

Figure 3-9 Block Shear Failure of Specimen 25T-490-3-60 31

Figure 3-10 Load and Deformation for Specimen 25T-490-3-60 31

Figure 3-11 Specimen 25T-490-7-40 at end of test 32

Figure 3-12 Net Section Failure of Specimen T25-490-7-40 33

Figure 3-13 Load and Deformation for Specimen 25T-490-7-40 33
Figure 3-14 Specimen 25T-570-3-60 at end of test..... 34
Figure 3-15 Block Shear Failure of Specimen 25T-570-3-60 35
Figure 3-16 Load and Deformation for Specimen 25T-570-3-60 35
Figure 3-17 Specimen 25T-570-7-40 at end of test..... 36
Figure 3-18 Gross Section Failure of Specimen 25T-570-7-40 37
Figure 3-19 Load and Deformation for Specimen 25T-570-7-40 37
Figure 3-20 Specimen 25T-800-3-60 at end of test..... 38
Figure 3-21 Bolt Shear Rupture of Specimen 25T-800-3-60 39
Figure 3-22 Load and Deformation for Specimen 25T-800-3-60 39
Figure 3-23 Specimen 25T-800-7-40 at end of test..... 40
Figure 3-24 Bolt Shear Rupture of Specimen 25T-800-7-40 41
Figure 3-25 Load and Deformation for Specimen 25T-800-7-40 41
Figure 3-26 Specimen 15T-490-3-60 at end of test..... 42
Figure 3-27 Block Shear Failure of Specimen 15T-490-3-60 43
Figure 3-28 Load and Deformation for Specimen 15T-490-3-60 43
Figure 3-29 Specimen 15T-490-4-60 at end of test..... 44
Figure 3-30 Block Shear Failure of Specimen 15T-490-4-60 45
Figure 3-31 Load and Deformation for Specimen 15T-490-4-60 45
Figure 3-32 Specimen 15T-800-3-60 at end of test..... 46
Figure 3-33 Block Shear Failure of Specimen 15T-800-3-60 47
Figure 3-34 Load and Deformation for Specimen 15T-800-3-60 47
Figure 3-35 Specimen 15T-800-4-60 at end of test..... 48
Figure 3-36 Block Shear Failure of Specimen 15T-800-4-60 49
Figure 3-37 Load and Deformation for Specimen 15T-800-4-60 49
Figure 4-1 Engineering and True Stress-Strain Curve of SM490 53
Figure 4-2 Engineering and True Stress-Strain Curve for SM570..... 53
Figure 4-3 Enginnering and True Stress-Strain Curve of HSA800..... 54

Figure 4-4 Finite Element Mesh and Boundary Condition 55

Figure 4-5 Comparison of the Finite Element Analysis and the Test Result for Specimen 25T-490-3-60 56

Figure 4-6 Comparison of the Finite Element Analysis and the Test Result for Specimen 25T-570-3-60 56

Figure 4-7 Comparison of the Finite Element Analysis and the Test Result for Specimen 25T-800-3-60 57

Figure 4-8 Failure Shape of Experiment and Finite Element Analysis for Specimen 25T-490-3-60 58

Figure 4-9 Failure Shape of Experiment and Finite Element Analysis for Specimen 25T-570-3-60 59

Figure 4-10 Failure Shape of Finite Element Analysis for Specimen 25T-800-3-60 60

Figure 4-11 Failure Shape of FE Analysis for 25 mm Specimen with SM490 Steel 63

Figure 4-12 Failure Shape of FE Analysis for 25 mm Specimen with HSA800 Steel 66

Figure 4-13 Load-Deformation Curves for FE Models with 25mm Thick SM490 Steel 68

Figure 4-14 Load-Deformation Curves of FE Models with the Same Connection Length 69

Figure 4-15 Load-Deformation Curves for FE Models with 25mm Thick SM570 Steel 71

Figure 4-16 Load-Deformation Curves of FE Models with the Same Connection Length 72

Figure 4-17 Load-Deformation Curves for FE Models with 25mm Thick HSA800 Steel 73

Figure 4-18 Load-Deformation Curves of FE Models with the Same Connection Length 74

Figure 4-19 Failure Shape of FE Analysis for 15 mm Specimen with SM490 Steel 81

Figure 4-20 Failure Shape of FE Analysis for 15 mm Specimen with HSA800 Steel 85

Figure 4-21 Load-Deformation Curves for FE Models with 15mm Thick

SM490 Steel 87

Figure 4-22 Load-Deformation Curves of FE Models with the Same Connection Length 88

Figure 4-23 Load-Deformation Curves for FE Models with 15mm Thick SM570 Steel 90

Figure 4-24 Load-Deformation Curves of FE Models with the Same Connection Length 91

Figure 4-25 Load-Deformation Curves for FE Models with 15mm Thick HSA800 Steel 93

Figure 4-26 Load-Deformation Curves of FE Models with the Same Connection Length 94

Figure 4-27 Relationship between Connection Length and α from FE Analysis 99

Figure 4-28 Relationship between Connection Length and α factor from FE Analysis and Experiments 100

Figure 4-29 Test-to-Design Strength Ratio for New Design Equation 101

Chapter 1. Introduction

1.1 Research Background

Bolting is a common connecting method in steel construction. Although ther are various different modes of rupture in steel structures, block shear is one of the critical failure mode, which governs bolted connetion with high strength bolt. The failure mode of the block shear is combined with a rupture on the tension plane and yielding on the shear plane. The block shear failure is that shear failure and perpendicular tension failure simultaneously occur in the bolted connection. Figure 1-1 shows the basic examples of block shear based on the conndection of different members.

In spite of the name of the block shear failure, practically the whole block is not torn out of the material. As decribed in Figure 1-2, rupture and yielding arose following the tesion and shear plane. Although design standards proposed two types of design equation for the block shear by comparing the tensile and shear strength, all of test data show that block shear rupture occurred when the shear strength is larger than the tensile strength. This means that the rupture on the tension plane occurs with the shear yielding on the shear plane. Additionaly, the current design codes based on the previous researches inconsistently suggest using the gross and net area of tension and shear plane in the equation of block shear.

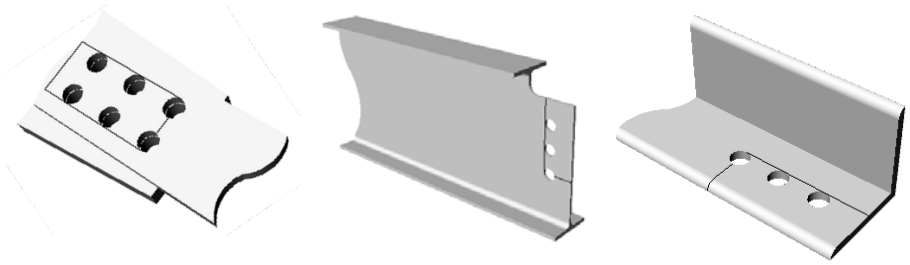

Gusset Plate **Coped Beam** **Angle**

Figure 1-1 Block Shear in Bolted Connection

Figure 1-2 Example of Block Shear Behavior

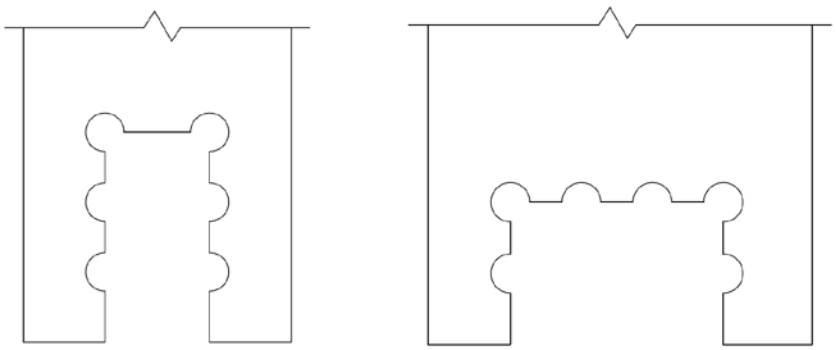

Figure 1-3 Two Possible Case of Block Shear

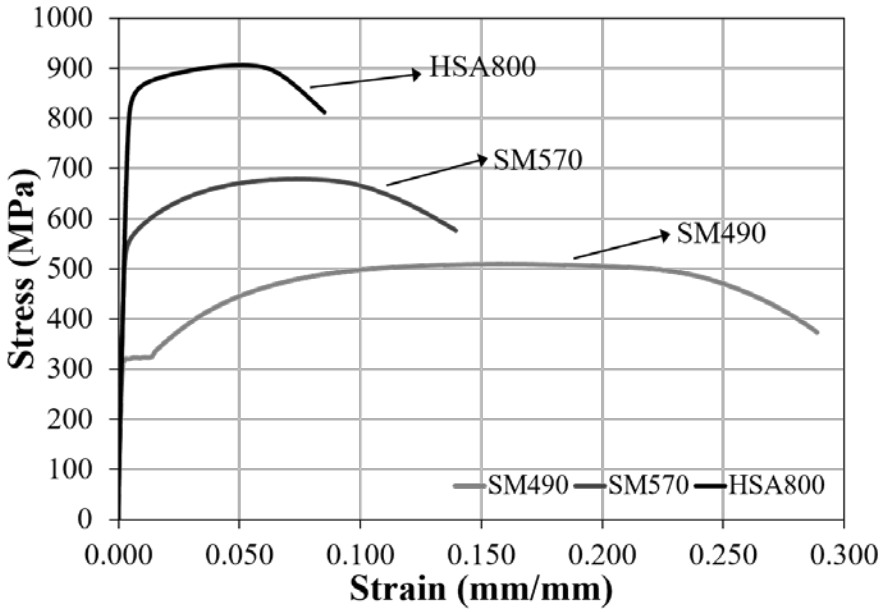

Figure 1-4 Stress-Strain Curves of Conventional and High-Strength Steel

Figure 1-4 shows the stress-strain relationship of typical conventional and high-strength steel (SM490, SM570, and HSA800). Despite having significantly higher tensile strength, the high-strength steel have relatively low ductility. The use of high-strength steel on connections for bolted tension joints provides the higher capacity without increasing the member size compared to the conventional steel. Due to the insufficient deformation capacity and ductility of high-strength steel, the uncertainty of bolted connections with high-strength steel has been raised.

1.2 Objectives and Scope

Since AISC Specification 1978, the design equation for block shear failure have continued to change due to the uncertainty of the possible

mechanism of block shear. As using the net and gross area for the block shear strength, design equation of current codes including AISC 210 propsed considerably conservative design strength of block shear rupture. In addition, the design standard have an inconsistency with the strength of the shear rupture because the mechanism with shear yielding and tensile rupture is precedable. In this sense, this study focuses on a clear explaination of the failure mechanism related to the block shear.

The application of high-strength steel for structural members has diverse technical advantages from design to construction. Although abundant test results on the block shear of bolted connections are available, the experimental studies with hgh-strength steel are not widely known. In this sense, the applicability of the high-strength steel for most of current design standards are unconfirmed. In order to better understand and describe the failure mechanism of the block shear and its capacity, the lap joints fabricated from conventional and high-strength steels were tested in this study. Key test variables included the grades of the steels, the geometrical configuration of the bolts, and the failure modes of bolted connections.

Based on the results from the experimental studies, this study takes varibles that are not included in the test into the adanced finite element method in order to investigate the process of the block shear failure. This research proposes a new design equation for the block shear failure with the test results from previous researches, and the data of experimental and finite element analysis in this study.

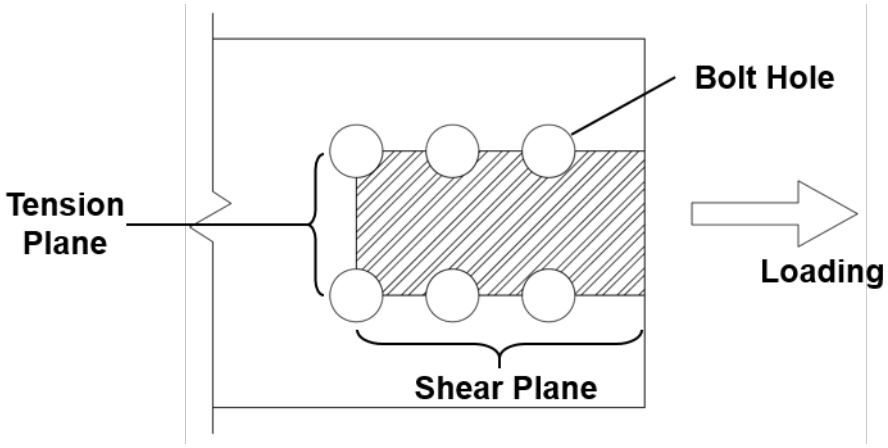

Figure 1-5 Typical Mechanism of Block Shear with Net Shear Plane

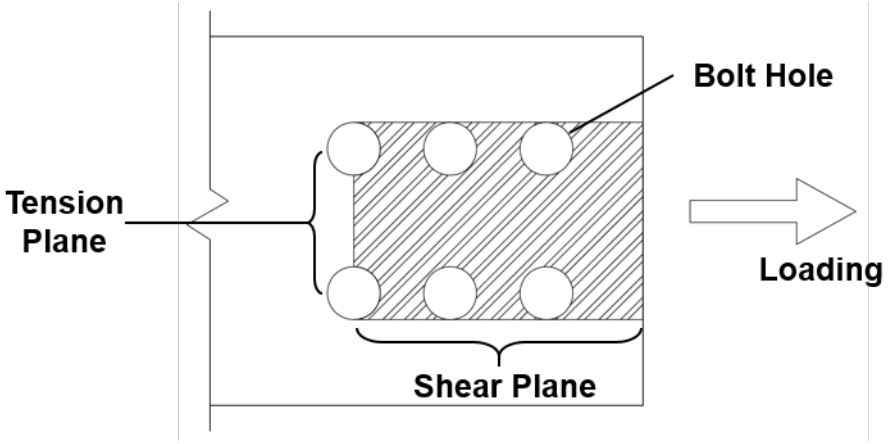

Figure 1-6 Typical Mechanism of Block Shear with Gross Shear Plane

Chapter 2. Previous Research

2.1 Introduction

Lap joints of bolted connection are commonly used in steel structures. This section provides literatural reviews on experimental studies of block shear of the bolted connections. This section has two sub-sections: Section 2.2, which presents a summary of previous researches related to the block shear and design equations to better estimate; and Section 2.3, which presents a summary of the current design codes.

2.2 Block Shear Researches in Lap Joints

2.2.1 Birkemoe and Gilmor (1978)

In a research of 1978, Birkemoe and Gilmor carried out the full-scale test of the shear resistance of coped and uncoped beam bolted connection. A distinct failure mode in the coped beam test consisted of a tearing out of a block from the web. The research demonstrated the block shear failure shearing out of a block in the web. The test result had been developed to the concept of block shear failure and a failure model suggested predicting the block shear strength of bolted connections.

2.2.2 Hardash and Bjorhovde (1985)

Hardash and Bjorhovde (1985) carried out 28 full-scaled tests using gussets paltes. In the tests of Hardash and Bjorhovde, test varialbes were the gauge distance, bolt spacing, and the number of the bolts. The test specimen were composed of 0.237 in. and 0.253 in. plate of ASTM-A36 steel with 1/2 in. diameter of A325 bolts. The research of Hardash and Bjorhovde (1985) presented that the block shear failure occurred on the last row of the bolts with the ultimate tensile stress, and the uniformly distributed shear stress acted on the gross shear area along the bolt path. The test results also demonstrated that the rupture on the net tension area always were prior to the fracture on the gross shear area and the effective tensile stress were vary from the connection length. With the result of the test, Hardash and Bjorhovde derived an equation of the block shear including the connection length effect as follows:

$$R_n = F_u S_{net} t + 1.15 F_{eff} l t \qquad 2\text{-}1$$

where F_{eff} is an effective tensile stress on the shear plane.

$$F_{eff} = (1 - C_l) F_y + C_l F_u \qquad 2\text{-}2$$

$$C_l = 0.95 - 0.047 l \qquad 2\text{-}3$$

F_y and F_u are the yield and tensile strength of the material, repecitively. S_{net} is net area on the tension plane, l is the connection length along outter bolt path, and t is the thickness of the plate. C_l is the connection length factor.

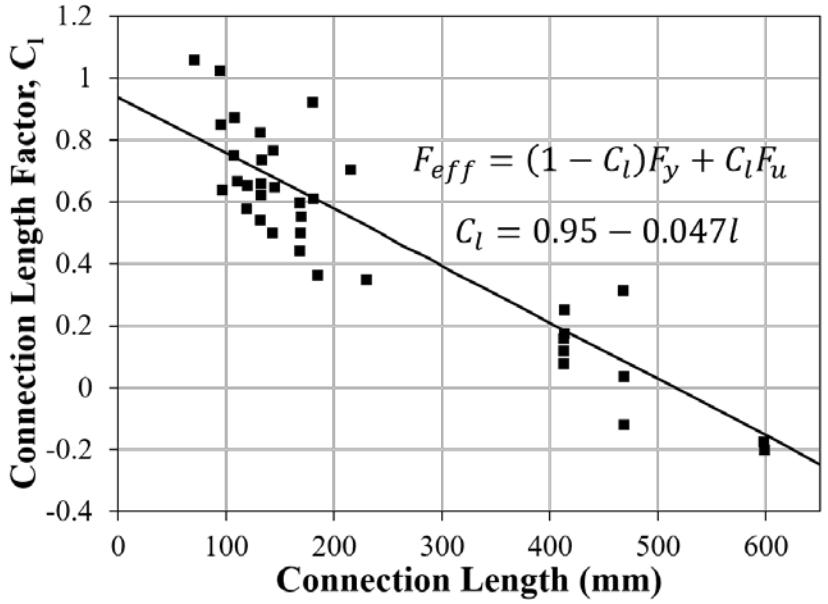

Figure 2-1 Connection Length Factor from Hardash and Bjorhovde (1985)

2.2.3 Rabinovitch and Cheng (1994)

Rabinovitch and Cheng (1994) performed tests of gusset plate under cyclic loading in order to investigate the general behavior of gusset plate connections. The full-scale gusset plates connected to a bracing member at the joint of a beam and column were used for the test. A series of five specimens were fabricated from CSA S40.21-M 300W structural steel and test variables were the thickness of plate, palte configuration, and boundary conditions. The block shear failer occurred in the all five test specimens. According to the test results, rupture on the net tension area were observed before the rupture on the gross shear area.

2.2.4 Nast, Grondin, and Cheng (1999)

Nast et al. (1999) researched the effect of gusset plate-brace member interaction on stiffened and unsiffened gusset plates using four full-scale test. Two specimens had a gusset plate with free edge stiffeners and other specimens had a gusset plate without
the stiffeners. All four specimens had identically the same bolt geometry. The test results represented that rupture on the net tension area were observed before the rupture on the gross shear area.

2.2.5 Aalberg and Larsen (2000)

Aalberg and Larsen (2000) researched block shear in tension member and I-shaped coped beam with conventional and high-strengh steel. Total eight specimens in the research have two bolt lines and from two to four rows of bolt. Four specimens were fabricated from the high-strength steel, Weldox 700. The measured tensile strength of this high-strength steel is 822 MPa and a yield ratio is 0.96. The specimens with high-strength steel have the same bolt configuration comparing to specimens with conventional steel. This study also tested two specimens with the cutting on tension plane at the last row of the bolt in order to measure the effective shear strength. The research showed that the rupture on the net tension plane occurred before the rupture on the gross shear plane. Aalberg and Larsen (2000) also investigated that strength dropping after the rupture of the net tension plane were associated with the tensile strength of the tension plane.

2.2.6 Swanson and Leon (2000)

Swanson and Leon (2000) carried out a test with bolted T-subs under cyclic load. Although total fifty-eigh specimens were tested, only one specimen showed the block shear failure. All the specimens had two bolt lines and four rows. The main varibles of the test were bolt diameter, gauge distance, and spacing of the bolts. The research used the 22 mm and 25 mm diameter tension control bolts. The bolt spacing was varied from 63.5 mm to 76 mm, and the block shear failure took place in the specimen with 63.5 mm bolting space. The research represented that the rupture of the net tension plane was observed when the block shear failure began.

2.2.7 Kulak and Grondin (2001)

Kulak and Grondin (2001) presented that the possibility of the block shear failure with shear ultimate strength and tensile yield strength is low. It can be seen that the tensile ducility on the tension plane is not sufficient to permit the fracture on the shear plane. The research indicated that the failure mode of the block shear is separated into two parts: gusset plate connections and web of coped beams. Kulak and Grondin (2001) propsed that adding the ultimate tensile strength on the net tension area and the shear yield strength on the gross shear area gives better prediction for gusset plate connections. However, due to the fact that the tensile stress is not uniform in the coped beam connections, the research recommended that multiplying the ultimate tensile strength by 0.5.

U_{bs} factor in the 2005 and 2010 AISC Specification is based on this research.

2.2.8 Huns, Driver, and Grondin (2002)

Huns, Driver, and Grondin (2002) performed five tests of gusset plates with a variety of bolt patterns under either cyclic load (tension only) or monotonic loading. The test of this research were focused on the progression of the block shear failure. The test specimens have two different types of connection: one is the long and narrow connection and the other one is a short and wide connection. In order to verify the progression of the block shear failure from the yielding to fracture, removing the splice plates during the tests was needed. According to the test results, the rupture on the net tension area indeed took place prior to the rupture on the shear planes.

2.2.9 Driver, Grondin, and Kulak (2006)

Driver, Grondin, and Kulak (2006) proposed a unified equation for the prediction of the block shear capacity. The research used the database of 205 block sheare tests with various connection types, gusset plates, angles, tees, and coped beams for the reliability study. All tests data showed that the ultimate strength of the block shear failure is when the rupture of the net tension area occurs with shear yielding on the gross shear area. Driver, Grondin, and Kulak (2006) recommended that using the average of the yield and tensile strength of the material for the shear stress on the gross shear plane. The unified equaltion for the block shear capcity is as follow:

$$R_n = F_u A_{nt} + A_{gv}\left(\frac{F_y + F_u}{2\sqrt{3}}\right) \quad 2\text{-}4$$

Although the proposed equation gives well-predicted block shear strength comparing to AISC 1999 and 2005 specification, the test data of high-strength steel is inaccurate with the equation.

2.2.10 Teh and Yazici (2013)

Teh and Yazici (2013) presented that European steel structers code, ECS (2005), using the net shear area gives conservative prediction for the block shear capacity. The research demontstrated that the block shear equation in AISC (2010) specification also presents conservative results. Teh and Yazici (2013) proposed an equation for the block shear capacity in hot-rolled steel with active shear plane. The active shear plane is located along the bolt paths between the gross and net shear plane.

$$R_n = F_u A_{nt} + 0.6 F_u A_{av} \quad 2\text{-}5$$

where A_{av} is the area of the active shear plane.

The research presented that using the shear tulimate stress gives better prediction for the block shear capacity in hot-rolled steel plates due to the full or almost full strain hardening.

2.3 Review of Current Design Codes

Block shear failure is a critical limit state of bolted connections in steel structures. Current design codes, such as AISC Specification for Structural

Steel Buildings (AISC 2010), and Canadian steel structures standards (CSA S16-09), incorporate design strength of the block shear failure in the limit states. However, since it was discovered by (Birkemoe & Gilmor, 1978) and first incorporated into the AISC specification (AISC 1978), the design provisions for determining the block shear capacity of a bolted connection have continued to change and even oscillate between certain equations, as described in Table 2-1.

Table 2-1. Block Shear Design Eqaution of AISC

	Block Shear Design Equation of AISC
1978	$R_n = F_u A_{nt} + 0.6F_u A_{nv}$
1986	$R_n = F_u A_{nt} + 0.6F_y A_{gv}$ or $R_n = F_y A_{gt} + 0.6F_u A_{nv}$
1989	$R_n = F_u A_{nt} + 0.6F_u A_{nv}$
1993	Where $F_u A_{nt} \geq 0.6F_u A_{nv}$, $R_n = F_u A_{nt} + 0.6F_u A_{nv}$ Where $F_u A_{nt} < 0.6F_u A_{nv}$, $R_n = F_y A_{gt} + 0.6F_u A_{nv}$
1999	Where $F_u A_{nt} \geq 0.6F_u A_{nv}$, $R_n = \left[06F_y A_{gv} + F_u A_{nt} \right] \leq \left[0.6F_u A_{nv} + F_u A_{nt} \right]$ Where $F_u A_{nt} < 0.6F_u A_{nv}$, $R_n = \left[06F_u A_{nv} + F_y A_{gt} \right] \leq \left[0.6F_u A_{nv} + F_u A_{nt} \right]$
2005 / 2010	$R_n = 0.6F_u A_{nv} + F_u A_{nt} \leq 0.60F_y A_{gv} + F_u A_{nt}$

2.3.1 AISC (1999)

The Load and Resistance Factor Design (LRFD) equations in the 1999 AISC Specification proposed two equations of block shear failure. The first one is the net tension rupture with shear yielding on the gross shear area. The other one is the shear rupture on the net shear area with yielding on the gross tension area. The strength of the shear yield and rupture is taken as 0.6 times the tensile yield or rupture strength, respectively. These equations are

When $F_u A_{nt} \geq 0.6 F_u A_{nv}$:

$$R_n = \left[06 F_y A_{gv} + F_u A_{nt} \right] \leq \left[0.6 F_u A_{nv} + F_u A_{nt} \right] \qquad 2\text{-}6$$

When $F_u A_{nt} < 0.6 F_u A_{nv}$:

$$R_n = \left[06 F_u A_{nv} + F_y A_{gt} \right] \leq \left[0.6 F_u A_{nv} + F_u A_{nt} \right] \qquad 2\text{-}7$$

F_y and F_u are the yield and tensile strength of the material, respectively. A_{gt} and A_{nt} are the gross and the net tension area and A_{gv} and A_{nv} are the gross and net shear area, respectively. According to the AISC LRFD 1999, the block shear strength combines the rupture on the net tension area with the shear yielding on the gross shear area or the yielding on the gross tension area with the shear rupture on the net shear area.

Equation 2-6 applies when the tensile strength on the net tension area is larger or equal to the shear strength on the net shear area. Otherwise, the

second equation applies for the block shear strength. Upper bound of these equations are the rupture on the net tension section with rupture on the gross shear area.

2.3.2 AISC (2005) and AISC (2010)

The Load and Resistance Factor Design (LRFD) equations in the 2010 AISC Specification offers one equation of block shear failure. The last version of AISC incorporates the simultaneous shear and tensile rupture mechanism and the shear yielding and tensile rupture mechanism. The block shear design equation is

$$R_n = 0.6F_u A_{nv} + U_{bs} F_u A_{nt} \leq 0.60F_y A_{gv} + U_{bs} F_u A_{nt} \qquad 2\text{-}8$$

If the tension stress is uniform, U_{bs} is equal to 1, but if the tension stress is not uniform, U_{bs} factor is 0.5. The equation of the block shear strength combines the tension rupture strength on the net tension area with the shear rupture strength on the net shear area. The upper bound of the equation is the rupture strength on the net tension section with yielding on the gross shear area.

2.3.3 CSA S16-09

The Canadian steel structures standard (CSA 2001) used the same block shear euation of AISC 1999. CSA S16-09, however, proposes a single equation for block shear capacity. The design code of CSA S16-09 incorporates

the simulataneous shear and tensile rupture mechanism.

$$R_n = F_u A_{nt} + 0.6\left(\frac{F_y + F_u}{2}\right) A_{gv} \qquad 2\text{-}9$$

Due to the failure mechanim of the block shear, CSA S16-09 uses an average value of yield and tensile strength of the material for the shear section. In the block shear failure mode, the rupture on the tension plane was observed prior to the shear rupture on the gross shear area. CSA S16-09 only uses the gross shear area to calculate the block shear strength.

2.4 Summary

Figure 2 2, Figure 2 3, and Figure 2 4 graphically show the test-to-design strength ratio of the database from previous researches. As can be seen in the figures, the block shear equation from AISC 1999 and AISC 2010 provide conservative design strength. Although CSA S16-09 offers well-predicted design strength in comparion with AISC 1999 and 2010, there are still significant margin with the data of a large capacity and high-strength steel.

Table 2-2 shows the list of the block shear data from the previous researches. The research of Aalberg and Larsen (2000) included the test results with the high-strength steel whose tensile strength is over 700 MPa.

Table **2-3** shows a summary of the previous researches related to block shear failure. Birkemoe and Gilmor (1978) reported the block shear failure for the first time.

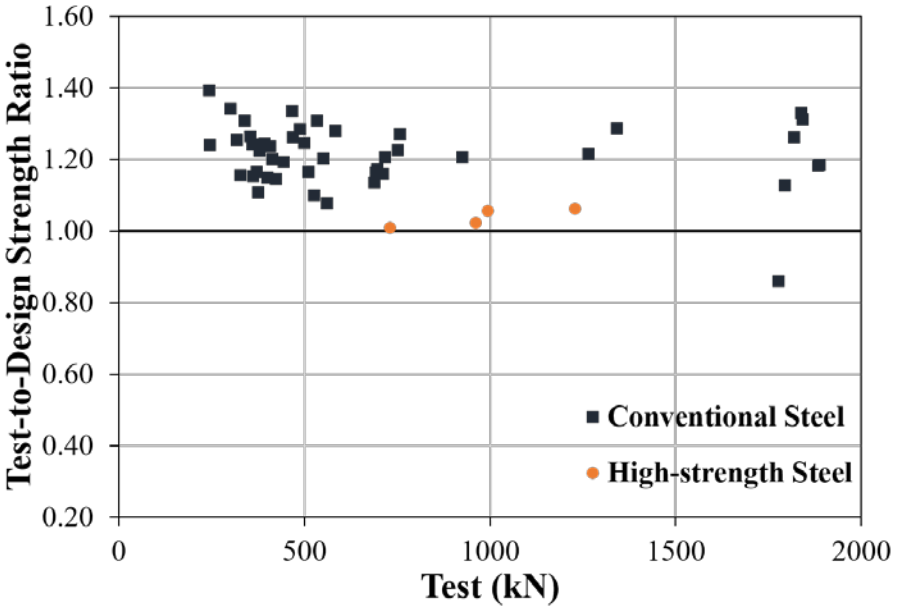

Figure 2-2 Test-to-Design Strength Ratio for AISC 1999 Specification

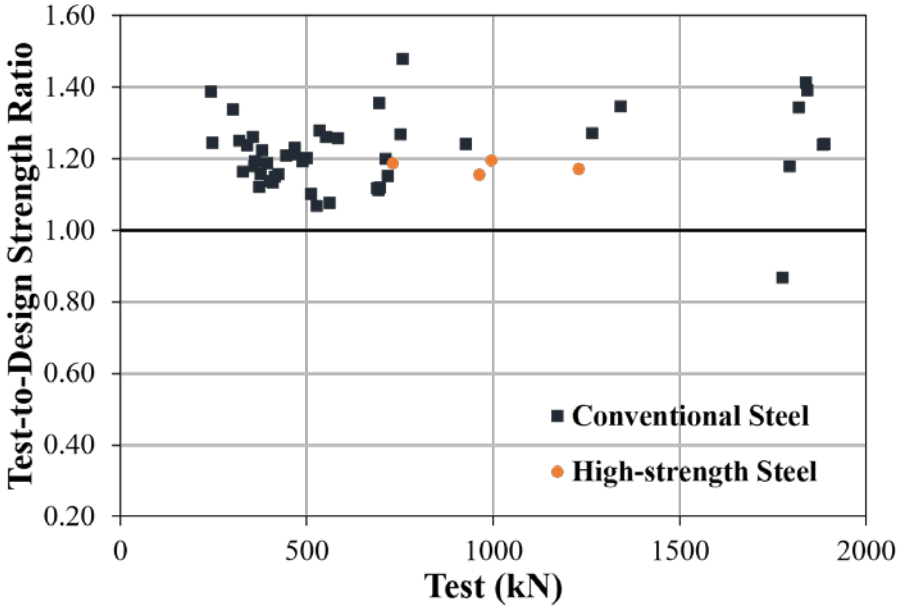

Figure 2-3 Test-to-Design Strength Ratio for 2010 AISC Specification

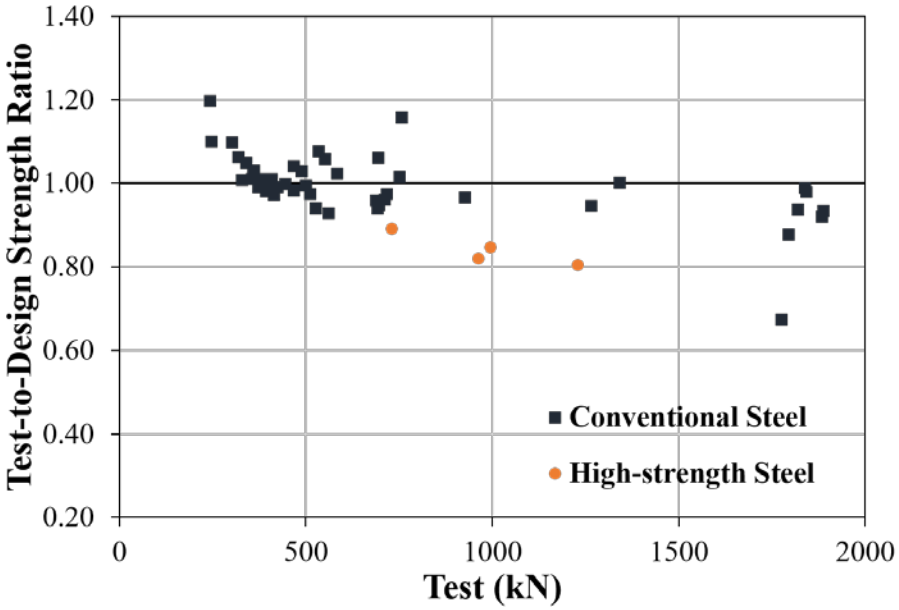

Figure 2-4 Test-to-Design Strength Ratio for CSA S16-09

Table 2-2 Mean Test-to-Design Strength Ratio

Source	Number of Tests	Test-to-Design Strength Ratio		
		AISC 2010	AISC 1999	CSA S16-09
Hardash and Bjorhovde (1985)	28	1.2	1.22	1.02
Rabinovitch and Cheng (1993)	5	1.26	1.2	0.94
Nast et al. (1999)	3	1.34	1.31	1.01
Aalberg and Larsen (2000)	8	1.26	1.19	0.99
Huns et al. (2002)	5	1.24	1.2	1.02

Table 2-3 Summary of Previous Researches

Researcher	Review of Comment
Birkemoe and Gilmor (1978)	The research demonstrated the block shear failure shearing out of a block in the web for the first time.
Hardash and Bjorhovde (1985)	The research suggested the block shear eqaution including Connection Length Effect for the better prediction.
Rabinovitch and Cheng (1994)	The researcher performed gusset plate test under cyclic loading.
Nast, Grondin, and Cheng (1999)	The researcher investigated the effect of both stiffened and unstiffened gusset plate.
Aalberg and Larsen (2000)	The researcher performed the experimental study of block shear in tension member with conventional and high-strength steel
Swanson and Leon (2000)	The researcher carried out the test with bolted T-subs under cylcic load.
Kulak and Grondin (2001)	The researcher proposed the block shear mechanism of tensile strength on the net tension area and the shear yield strength on the gross shear area. The researcher suggested the multiplying the ultimate tensile strength by 0.5.
Huns, Driver, and Grondin (2002)	The researcher tested two different type of connection: the long and narrow connection and the short and wide connection.
Driver, Grondin, and Kulak (2006)	The researcher proposed a unified equation for the block shear capacity using the average value of Fy and Fu.
Teh and Yazici (2013)	The researcher suggested an equation for the block shear capacity in hot-rolled steel with active shear plane.

Chapter 3. Experimental Study

3.1 Introduction

Abundant experimental studies related to block shear failure have been perfomed in various types of bolted connection. However, test results of these experimental studies do not clearly explained the failure mechanism of the block shear. In this research, the experimental study focuses on the block shear strength and the failure mechanism. In order to obtain understanding of the effects of high-strength steel, the experimental study used bolted connection with high-strength steel. This chapter descirbes the test specimens in the experimental program, the procedure of the test, and results of the test.

3.2 Experimental Program

Experimental program deals with investigation on the static behavior on bolted connection in lap joints under axial loading. Investigating the behavior and strength of the lap joints with various types of geometry condtions and materials was the focus of the block shear tests.

As described in Figure 3-1, the test specimens imitated a bolted connection on the flange of H-beam. The test specimens copied the situation that the tension load acted on the bottom flange of H-beam. Key test varibles included the grade of the steels, the geometrical configuration of the bolts, and

the failure modes of bolted connections. Two different types of specimen were considered.

In Series I, the lap joint specimens were fabricated with 25 mm thick plate and 20 mm and 30 mm diameter high-strength bolts. Diameter of holes are 22 mm and 33 mm, respectively. Test specimens have two different bolt arrangement, staggered and non-staggered configuration. 20 mm and 30 mm diatmeter bolts are for staggered and non-staggered configuration, respectively. Bolt distance was 60mm for non-staggered configuration and 40mm for staggered configuration. The bolt connection specimens were fabricated from SM490, SM570, and HSA800. Test specimens was designed based on the block shear equation of AISC 2010. On the other hand, Series II had the total four test specimens with 15 mm thick plate and 30 mm diameter high-strength bolts. The specimens in the Seires II had only non-staggered bolt configuration. Although bolt distance of the specimen in series II was 60mm, the specimens had the different number of the bolt in order to make different connection length. SM490 and HSA800 steel were used in the specimens of Series II. In the test Series II, test specimens were also designed based on the block shear equation of AISC 2010. This study used F10T high-strength bolts in both Series I and II. The basic difference between Series I and II was the thickness of the plate, 25 mm and 15 mm. The test specimens are illustrated in Figure 3-2 and Figure 3-3, and Table 3-1 shows the specification of the specimens.

Figure 3-1 Bloted Connection in Flage of H-beam

Table 3-1. Specification of Test Specimens in Test Series I

Specimen	Steel Grade	Plate Thickness (mm)	Bolt Diameter (mm)	Bolt Distance (mm)	Number of Bolts
25T-490-3-60	SM490	25	30	60	12
25T-490-7-40	SM490	25	20	40	28
25T-570-3-60	SM570	25	30	60	12
25T-570-7-40	SM570	25	20	40	28
25T-800-3-60	HSA800	25	30	60	12
25T-800-7-40	HSA800	25	20	40	28

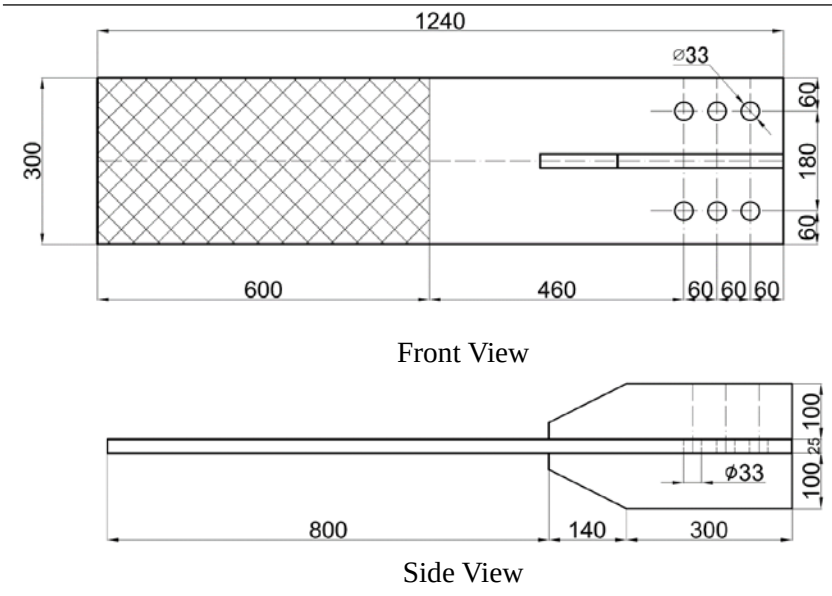

Figure 3-2 Typical Specimen with Non-Staggered Configuration in Test Series I

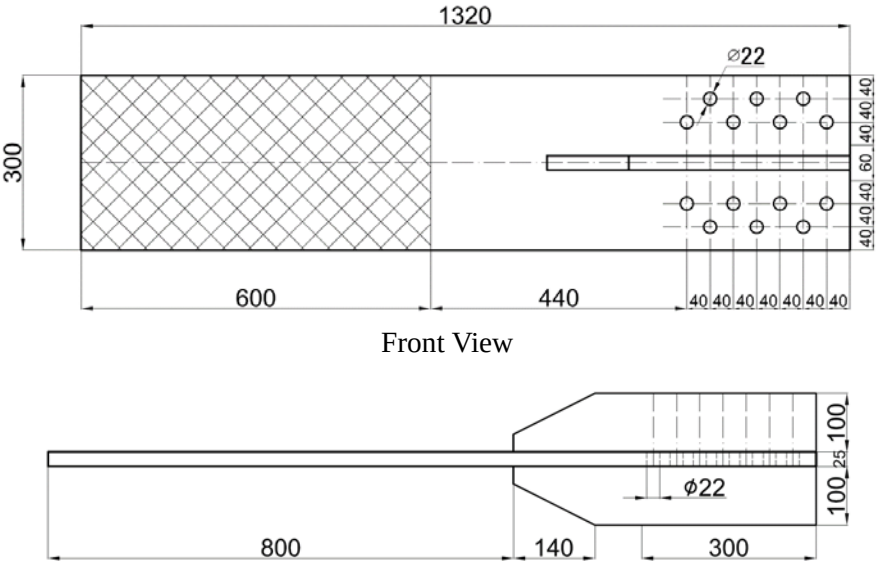

Figure 3-3 Typical Specimen with Staggered Configuration in Test Series I

Table 3-2 Specification of Test Specimens in Test Series II

Specimen	Steel Grade	Plate Thickness (mm)	Bolt Diameter (mm)	Bolt Distance (mm)	Number of Bolts
15T-490-3-60	SM490	15	30	60	12
15T-490-4-60	SM490	15	30	60	16
15T-800-3-60	HSA800	15	30	60	12
15T-800-4-60	HSA800	15	30	60	16

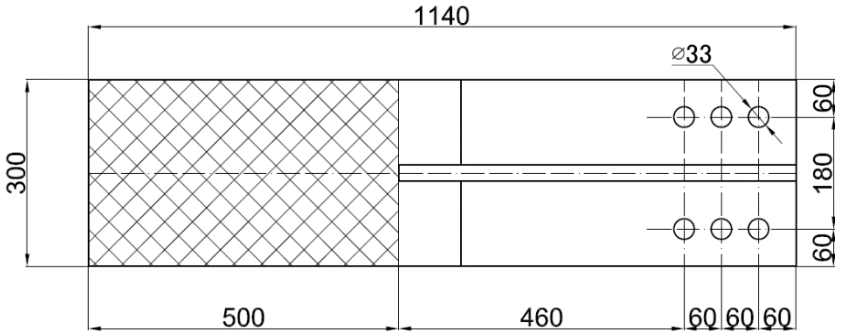

Front View

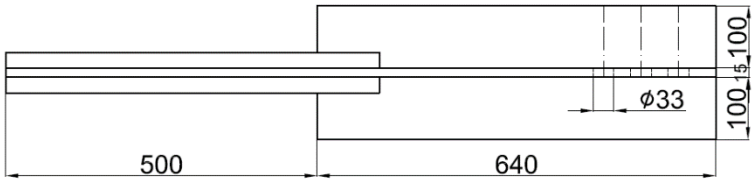

Side View

Figure 3-4 Typical Specimen with 12 Bolts in Test Series II

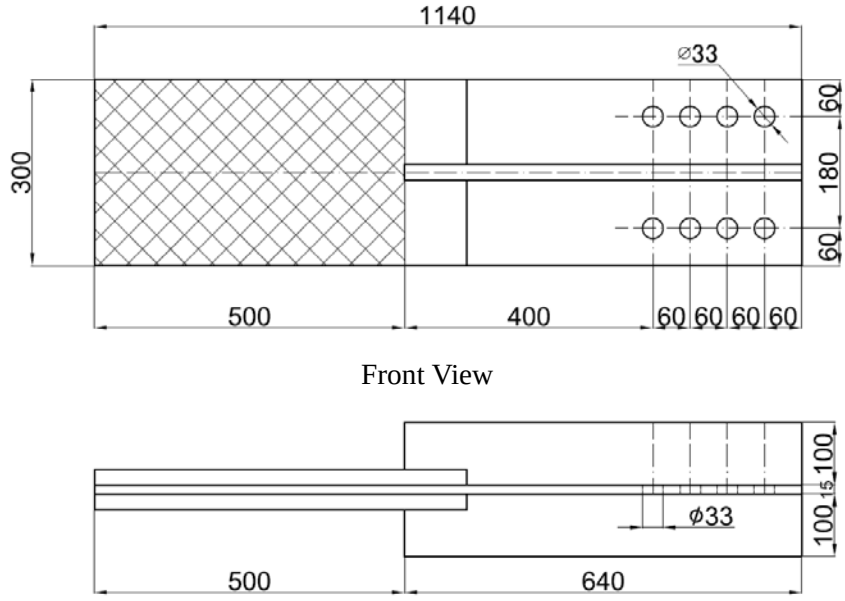

Figure 3-5 Typical Specimen with 16 Bolts in Test Seires II

Table 3-3 Tensile Test Results of Steel Plate

	Steel Grade	Nominal F_y (MPa)	Measured F_y (MPa)	Nominal F_u (MPa)	Measured F_u (MPa)	Yield Ratio
Test Ⅰ	SM490	325	325	490	516	0.63
	SM570	420	553	570	690	0.80
	HSA800	650	839	800	905	0.93
Test Ⅱ	SM490	325	333	490	500	0.67
	HSA800	650	784	800	814	0.96

3.3 Test Set-up

The tests of block shear were carried out by using a 10,000 kN UTM (Universal Testing Machine). The specimens were tested by under the tension loading. The test specimens mounted on the UTM in the vertical position. Both the upper and lower brace of the test machine pulled the test specimen to cause block shear failure. The intention of the tests was to examine the mechanism of the block shear failure. Figure 3-6 shows the typical test set-up.

Front View **Side View**

Figure 3-6 Test Set-up

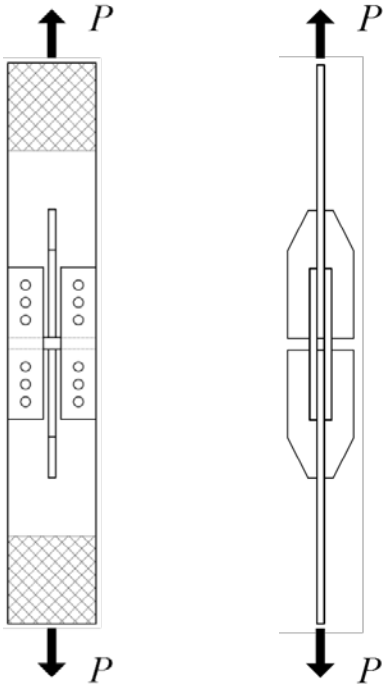

Figure 3-7 Test Set-up

3.4 Test Result and Contemplation

Table 3-4 shows the results of the tests for the block shear failure. Various types of failure modes were observed during the tests. Although the ultimate strength of all the specimens exceeded the design strength of the current codes for block shear, the block shear rupture only occurred in the specimens of 25T-490-1 and 25T-570-1.

Table 3-4. Block Shear Test Results for Specimens with 25 mm plate

Specimen	Steel Grade	Ultimate Strength (kN)	Deformation at Ultimate Load (mm)	Failure Mode
25T-490-3-60	SM490	3416	43.06	Block Shear Rupture
25T-490-7-40	SM490	4859	56.00	Net Section Rupture
25T-570-3-60	SM570	4260	31.59	Block Shear Rupture
25T-570-7-40	SM570	4947	51.26	Gross Section Rupture
25T-800-3-60	HSA800	5824	17.17	Bolt Shear Rupture
25T-800-7-40	HSA800	5146	21.27	Bolt Shear Rupture

Table 3-5 Block Shear Test Results for Specimens with 15mm Plate

Specimen	Steel Grade	Ultimate Strength (kN)	Deformation at Ultimate Load (mm)	Failure Mode
15T-490-3-60	SM490	1974	37.64	Block Shear Rupture
15T-490-4-60	SM490	2488	32.92	Block Shear Rupture
15T-800-3-60	HSA800	3139	22.66	Block Shear Rupture
15T-800-4-60	HSA800	3512	21.92	Block Shear Rupture

3.4.1 Specimen 25T-490-3-60

Specimen 25T-490-3-60 fabricated from SM490 steel had a non-staggered blot configuration. Figure 3-8 and Figure 3-9 show block shear failure in specimen 25T-490-3-60. The load-deformation curve is plotted in Figure 3-10 and the initial slip was eliminated. The ultimate strength of the spciemen was 3416 kN and the deformation at the peak strength was 43.06 mm. Block shear failure with the rupture on the net tension plane after the shear yield on the gross shear plane occurred in the test.

Figure 3-8 Specimen 25T-490-3-60 at end of test

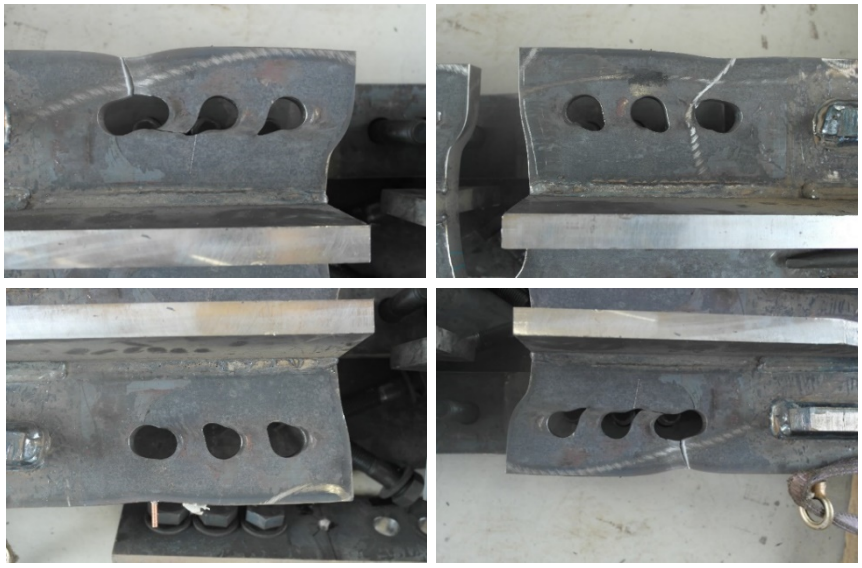

Figure 3-9 Block Shear Failure of Specimen 25T-490-3-60

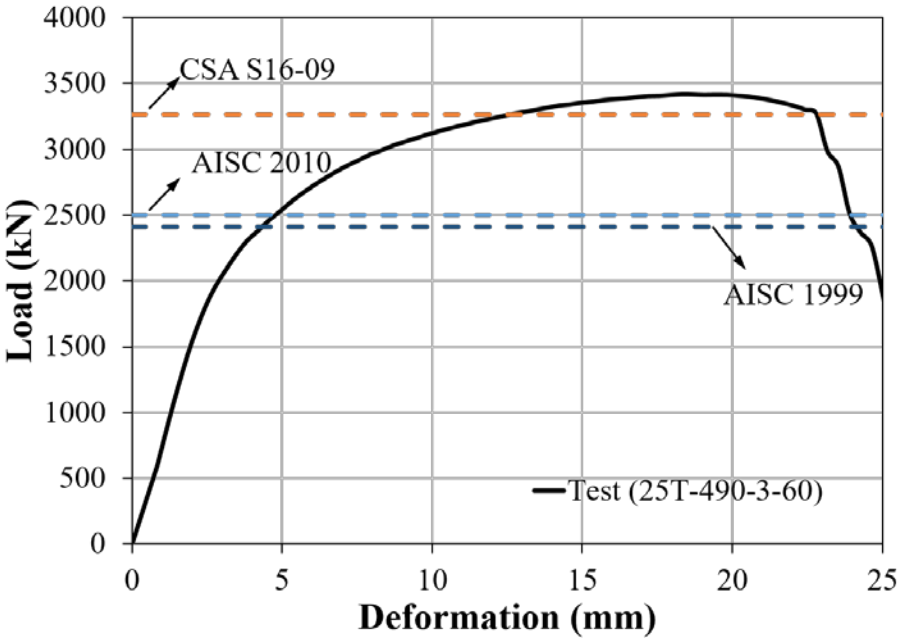

Figure 3-10 Load and Deformation for Specimen 25T-490-3-60

3.4.2 Specimen 25T-490-7-40

Specimen 25T-490-7-40 fabricated from SM490 steel had a staggered blot configuration. Figure 3-11 and Figure 3-12 present the net section failure of the gusset plate in specimen 25T-490-7-40. The load-deformation curve is plotted in Figure 3-13 and the initial slip was eliminated. Based on AISC 2010, the net section strength of the gusset plate was slightly higher than the block shear strength. The ultimate strength of the spciemen was 4859 kN and the deformation at the peak strength was 56.00 mm. Although the deformation of the bolt holes was observed, the test ended with the rupture on the net section on the connecting plate.

Figure 3-11 Specimen 25T-490-7-40 at end of test

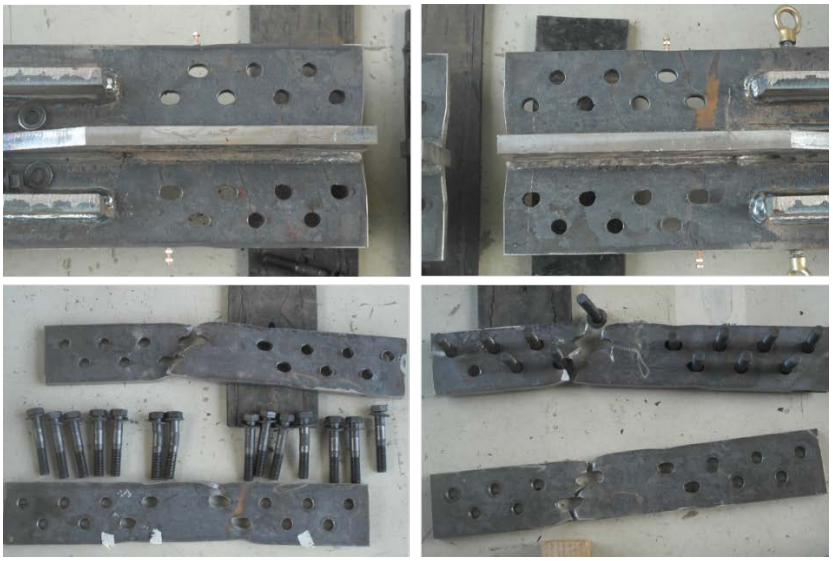

Figure 3-12 Net Section Failure of Specimen T25-490-7-40

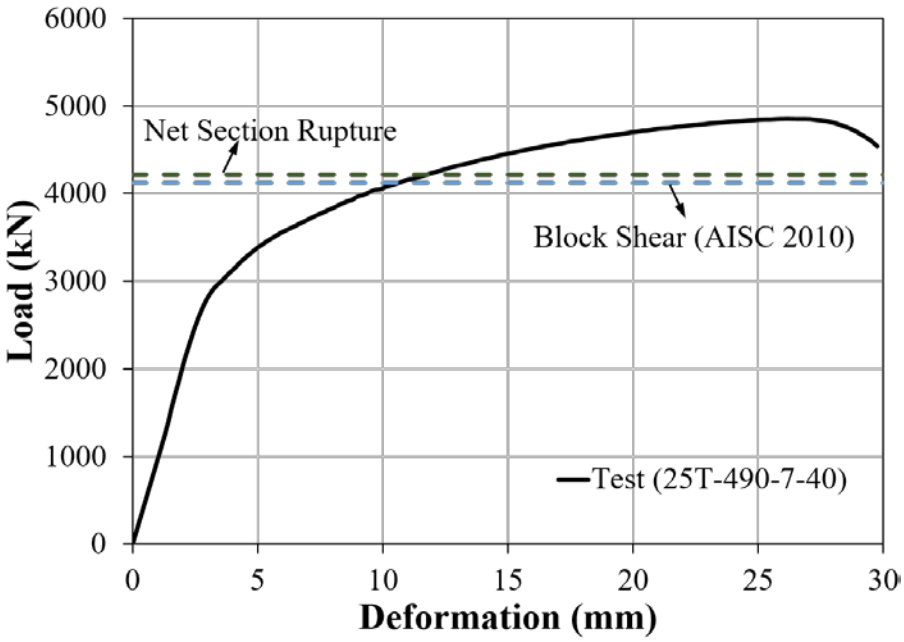

Figure 3-13 Load and Deformation for Specimen 25T-490-7-40

3.4.3 Specimen 25T-570-3-60

Specimen 25T-570-3-60 fabricated from SM570 steel had a non-staggered blot configuration. The test result of this specimen demonstrates the mechanism of block shear failure in high-strength steel. It can be seen that Figure 3-14 and Figure 3-15 present the block shear failure in specimen 25T-570-3-60 with high-strength steel. The load-deformation curve is plotted in Figure 3-16 and the initial slip was eliminated. The ultimate strength of the spciemen was 4260 kN and the deformation at the peak strength was 31.59 mm. Block shear failure with the rupture on the net tension plane after the shear yield on the gross shear plane occurred in the test.

Figure 3-14 Specimen 25T-570-3-60 at end of test

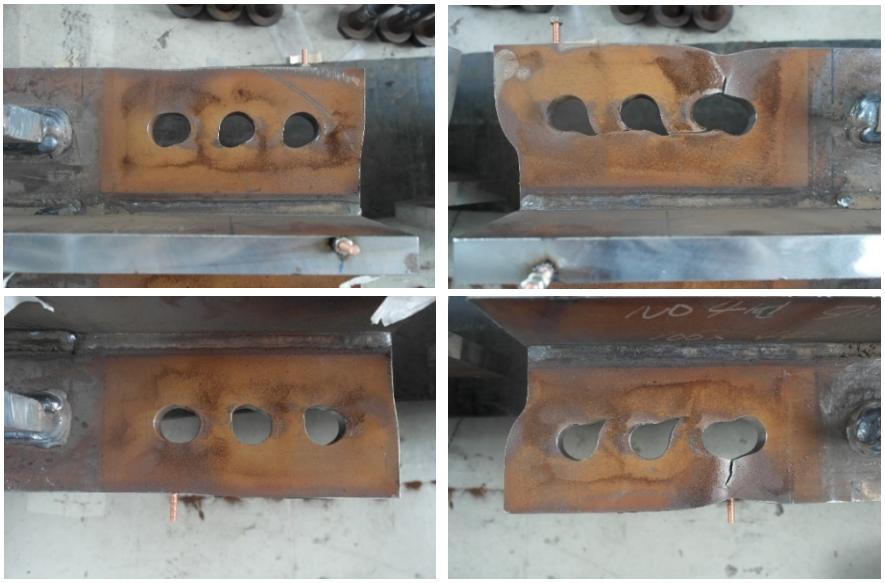

Figure 3-15 Block Shear Failure of Specimen 25T-570-3-60

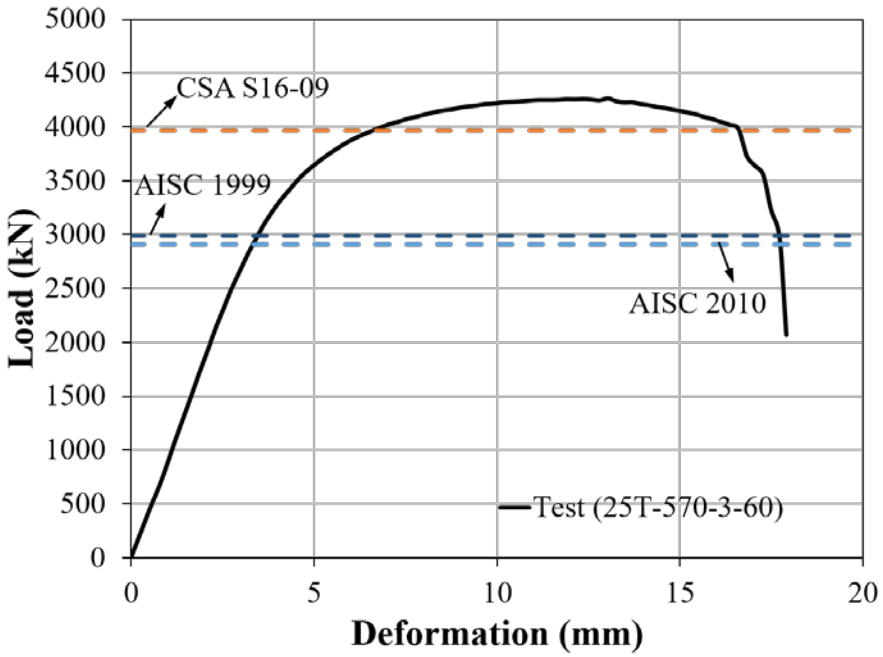

Figure 3-16 Load and Deformation for Specimen 25T-570-3-60

3.4.4 Specimen 25T-570-7-40

Specimen 25T-570-7-40 fabricated from SM570 steel had a staggered blot configuration. As Figure 3-17 and Figure 3-18 present, the failure mode of the gross section rupture occurred in the specimen 25T-570-7-40. The load-deformation curve is plotted in Figure 3-19 and the initial slip was eliminated. The ultimate strength of the spciemen was 4947 kN and the deformation at the peak strength was 51.26 mm. The test ended with the failure mode of the gross section rupture after the necking on the specimen. Due to the gross section rupture, the strength of the specimen did not reach the design strength of the block shear failure.

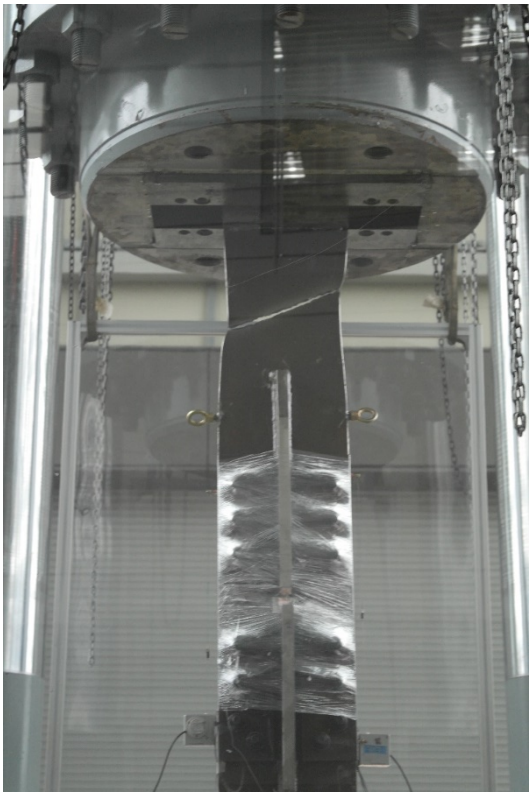

Figure 3-17 Specimen 25T-570-7-40 at end of test

Figure 3-18 Gross Section Failure of Specimen 25T-570-7-40

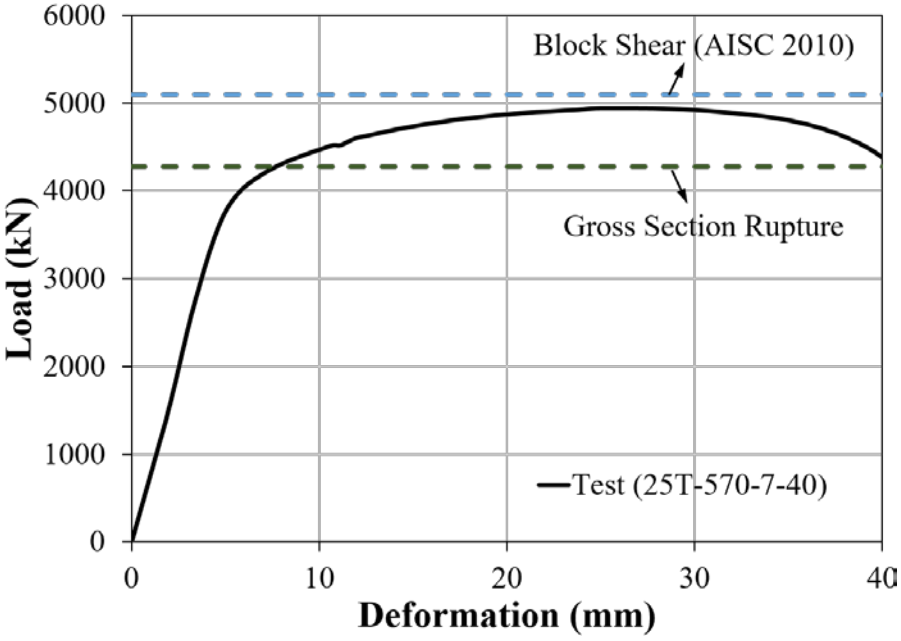

Figure 3-19 Load and Deformation for Specimen 25T-570-7-40

3.4.5 Specimen 25T-800-3-60

Specimen 25T-800-3-60 fabricated from HSA800 steel had a non-staggered blot configuration. Figure 3-20 and Figure 3-21 present a failure mode of the blot shear rupture in specimen 25T-800-3-60. The load-deformation curve is plotted in Figure 3-22 and the initial slip was eliminated. The ultimate strength of the spciemen was 5824 kN and the deformation at the peak strength was 17.17 mm. The test ended with the bolt shear rupture. Deformation of the bolt holes were not observed during the test of specimen 25T-800-3-60. The limit state of the blot shear rupture governed the specimen with HSA800 steel because the blot strength was not sufficient for the 25 mm thick plate.

Figure 3-20 Specimen 25T-800-3-60 at end of test

Figure 3-21 Bolt Shear Rupture of Specimen 25T-800-3-60

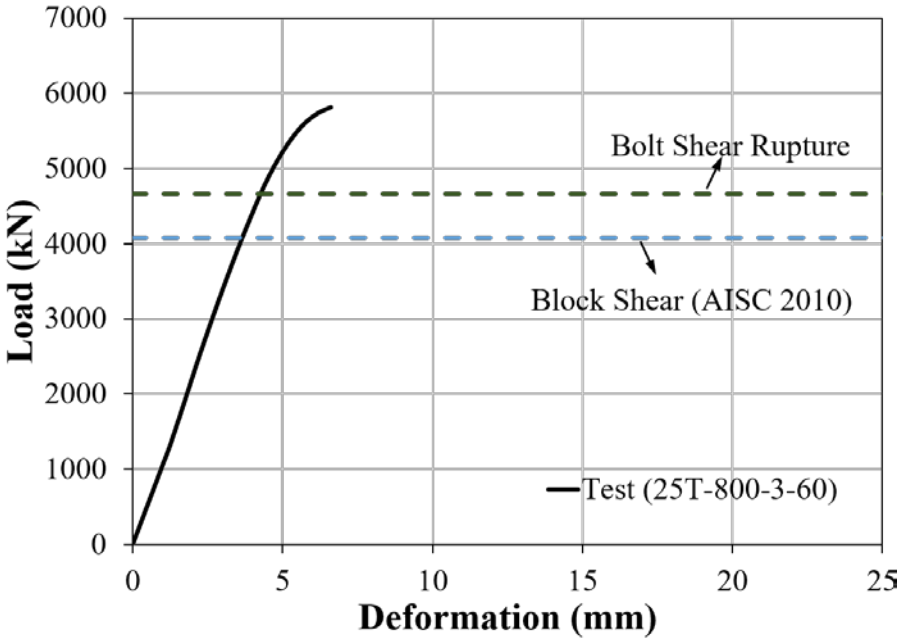

Figure 3-22 Load and Deformation for Specimen 25T-800-3-60

3.4.6 Specimen 25T-800-7-40

Specimen 25T-800-7-40 fabricated from HSA800 steel had a staggered blot configuration. Figure 3-23 and Figure 3-24 demonstrate a failure mode of the blot shear rupture in specimen 25T-800-7-40. The load-deformation curve is plotted in Figure 3-25 and the initial slip was eliminated. The ultimate strength of the spciemen was 5146 kN and the deformation at the peak strength was 21.27 mm. The test ended with the bolt shear rupture. Deformation of the bolt holes were not observed during the test of specimen 25T-800-7-40. The limit state of the blot shear rupture governed the specimen with HSA800 steel because the blot strength was not sufficient for the 25 mm thick plate.

Figure 3-23 Specimen 25T-800-7-40 at end of test

Figure 3-24 Bolt Shear Rupture of Specimen 25T-800-7-40

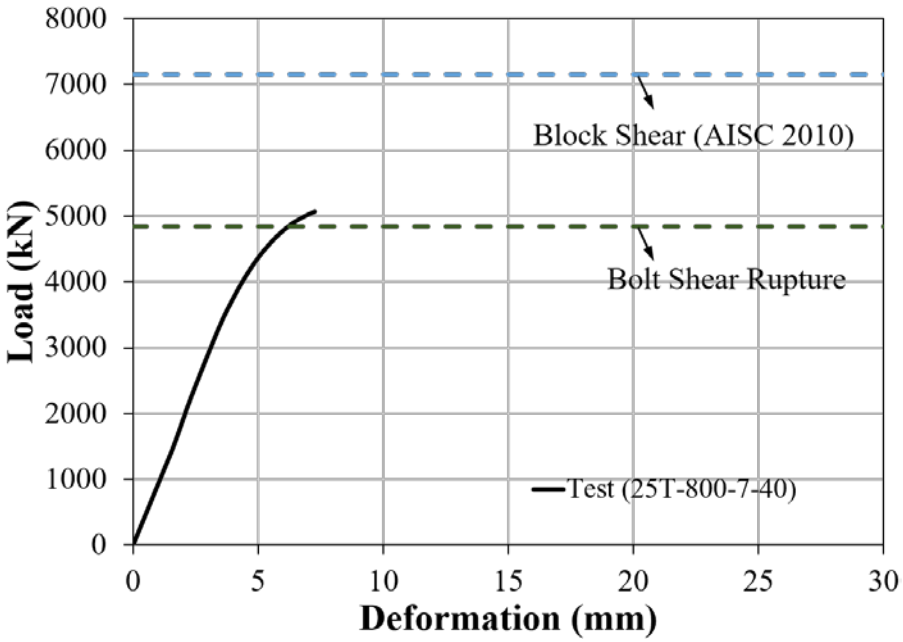

Figure 3-25 Load and Deformation for Specimen 25T-800-7-40

3.4.7 Specimen 15T-490-3-60

Specimen 15T-490-3-60 fabricated from SM490 steel had a non-staggered blot configuration. Both bolt distance and end distance were 60mm. The specimen had three bolts on each side. The test result of this specimen demonstrates the mechanism of block shear failure in high-strength steel. It can be seen that Figure 3-26 and Figure 3-27 present the block shear failure in specimen 15T-490-3-60. The load-deformation curve is plotted in Figure 3-28 and the initial slip was eliminated. The ultimate strength of the spciemen was 1974 kN and the deformation at the peak strength was 37.64 mm. Block shear failure with the rupture on the net tension plane after the shear yield on the gross shear plane occurred in the test.

Figure 3-26 Specimen 15T-490-3-60 at end of test

Figure 3-27 Block Shear Failure of Specimen 15T-490-3-60

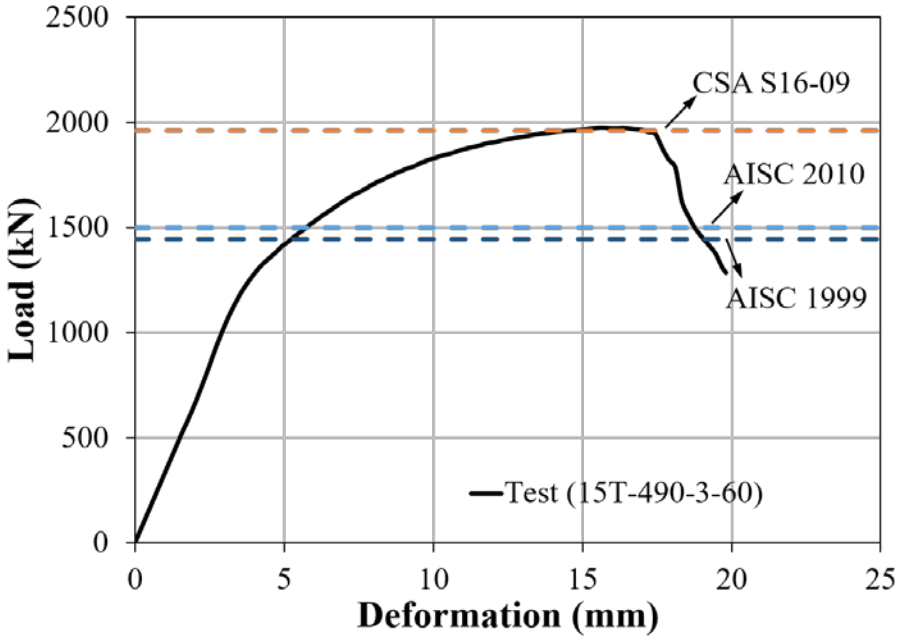

Figure 3-28 Load and Deformation for Specimen 15T-490-3-60

3.4.8 Specimen 15T-490-4-60

Specimen 15T-490-4-60 fabricated from SM490 steel had a non-staggered blot configuration. Both bolt distance and end distance were 60mm. The specimen had four bolts on each side. This specimen had longer connection length comparing to specimen 15T-490-3-60. The test result of this specimen demonstrates the mechanism of block shear failure in high-strength steel. It can be seen that Figure 3-29 and Figure 3-30 present the block shear failure in specimen 15T-490-4-60. The load-deformation curve is plotted in Figure 3-31 and the initial slip was eliminated. The ultimate strength of the spciemen was 2488 kN and the deformation at the peak strength was 32.92 mm. Block shear failure with the rupture on the net tension plane after the shear yield on the gross shear plane occurred in the test.

Figure 3-29 Specimen 15T-490-4-60 at end of test

Figure 3-30 Block Shear Failure of Specimen 15T-490-4-60

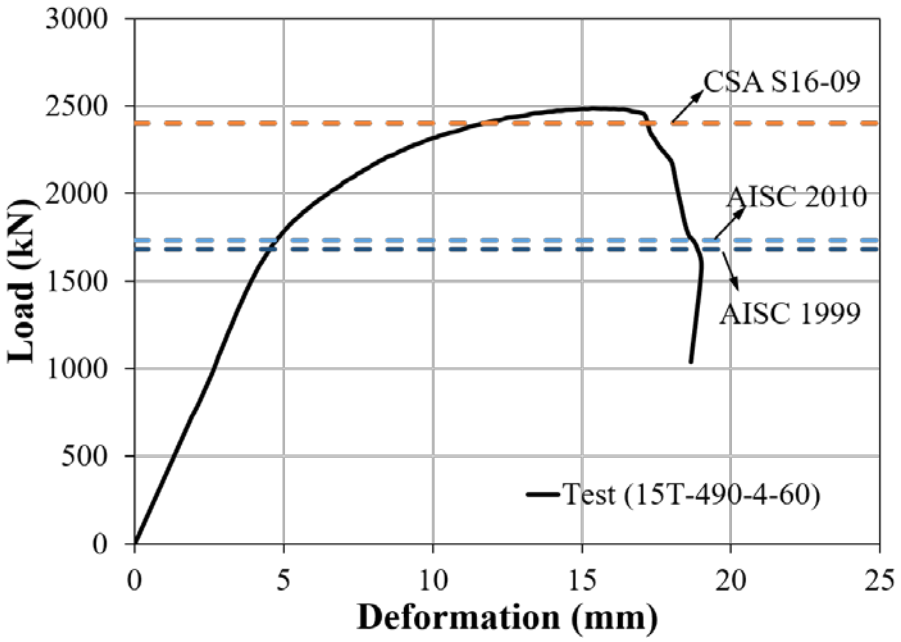

Figure 3-31 Load and Deformation for Specimen 15T-490-4-60

3.4.9 Specimen 15T-800-3-60

Specimen 15T-800-4-60 fabricated from HSA800 steel had a non-staggered blot configuration. Both bolt distance and end distance were 60mm. The specimen had four bolts on each side. The test result of this specimen demonstrates the mechanism of block shear failure in high-strength steel. It can be seen that Figure 3-32 and Figure 3-33 present the block shear failure in specimen 15T-800-4-60. The load-deformation curve is plotted in Figure 3-34 and the initial slip was eliminated. The ultimate strength of the spciemen was 3139 kN and the deformation at the peak strength was 22.66 mm. Block shear failure with the rupture on the net tension plane after the shear yield on the gross shear plane occurred in the test.

Figure 3-32 Specimen 15T-800-3-60 at end of test

Figure 3-33 Block Shear Failure of Specimen 15T-800-3-60

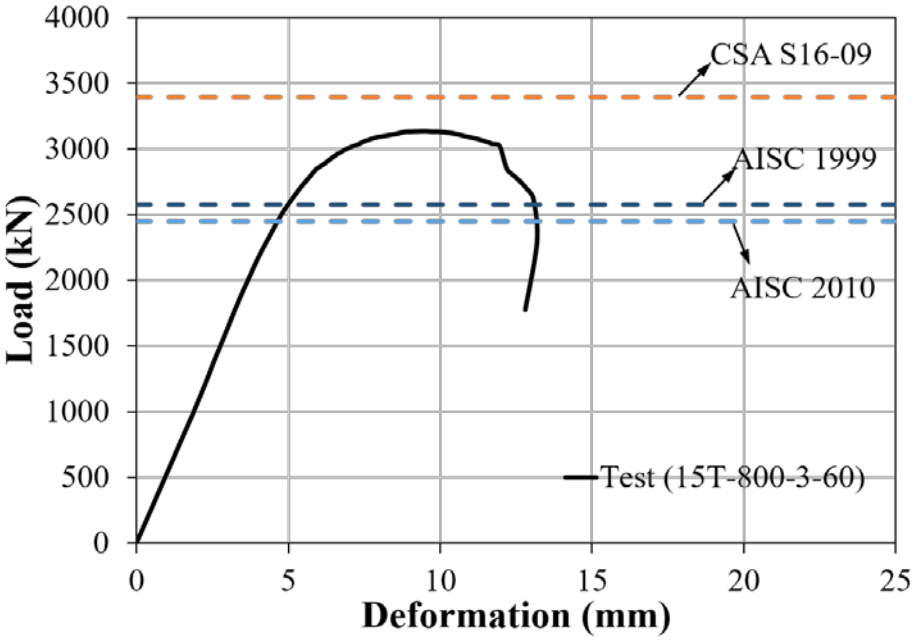

Figure 3-34 Load and Deformation for Specimen 15T-800-3-60

3.4.10 Specimen 15T-800-4-60

Specimen 15T-800-4-60 fabricated from HSA800 steel had a non-staggered blot configuration. Both bolt distance and end distance were 60mm. The specimen had four bolts on each side. This specimen had longer connection length comparing to specimen 15T-800-3-60. The test result of this specimen demonstrates the mechanism of block shear failure in high-strength steel. It can be seen that Figure 3-35 and Figure 3-36 present the block shear failure in specimen 15T-800-4-60. The load-deformation curve is plotted in Figure 3-37 and the initial slip was eliminated. The ultimate strength of the spciemen was 3512 kN and the deformation at the peak strength was 21.92 mm. Block shear failure with the rupture on the net tension plane after the shear yield on the gross shear plane occurred in the test.

Figure 3-35 Specimen 15T-800-4-60 at end of test

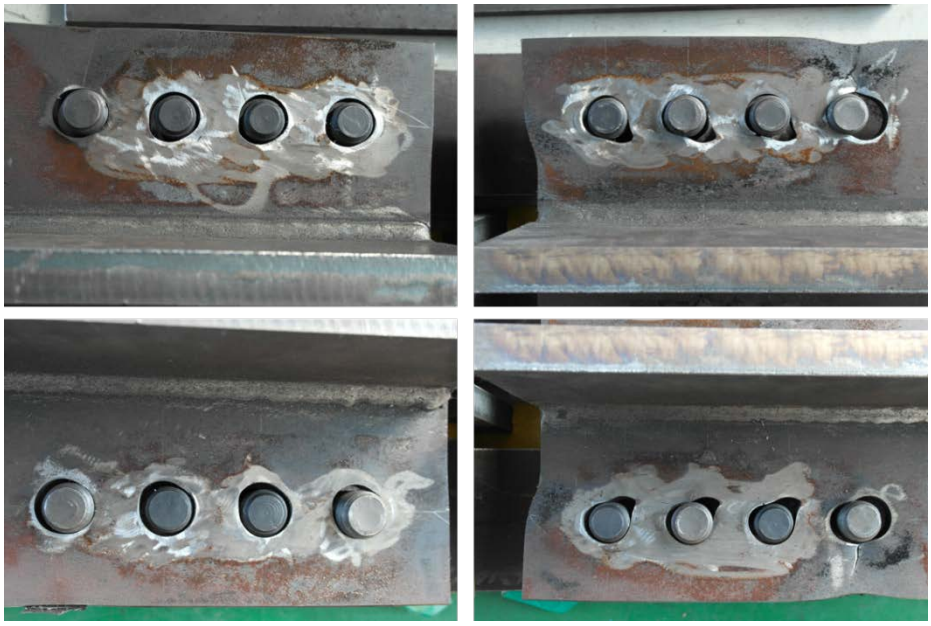

Figure 3-36 Block Shear Failure of Specimen 15T-800-4-60

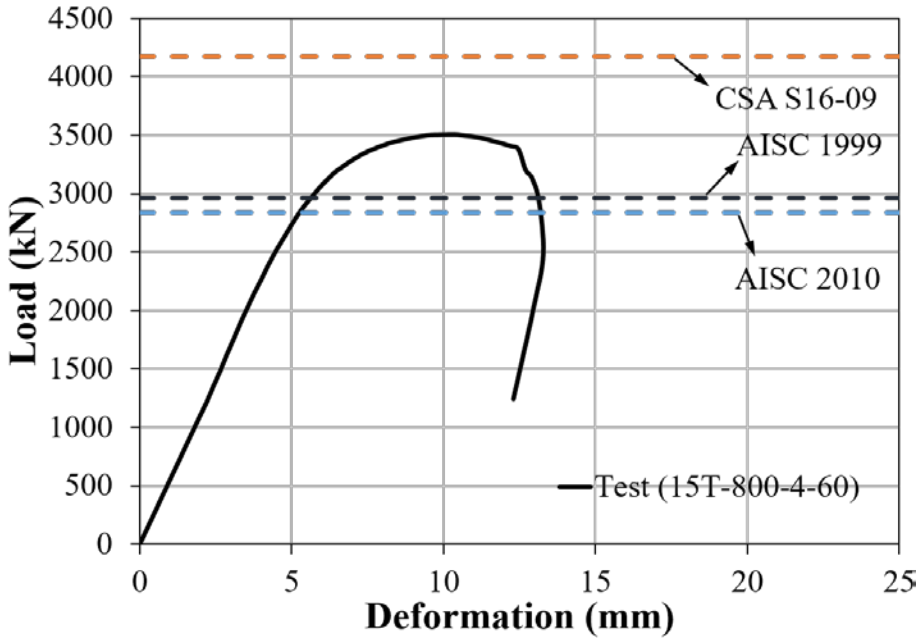

Figure 3-37 Load and Deformation for Specimen 15T-800-4-60

3.5 Summary

Table 3-6 shows the summary of the experimental study of block shear failure. The block shear failure occurred in 25mm thick specimens of SM490 and SM490 steel and all specimens of 15 mm thick including HSA800 steel. In the test series II, the deformation at the ultimate load of speicmens with the high-strength steel is about two third of that of the specimens with the conventional steel. All test specimens with block shear failure showed that the yielding on the gross shear area and the fracture on the net tension. The shear deformation of the bolt holes occured along the gross shear plane. Comparing the test results and the design strength of the current design standards, the block shear strength of AISC 1999 and 2010 provided a considerably conservative capacity. Although block shear strength of CSA S16-09 was relatively close to the test results, CSA S16-09 predicted an inaccurate strength.

Table 3-6 Test Result of Specimens with Block Shear Failure

Specimen	Steel Grade	Test (kN)	Design Strength		
			AISC 2010	AISC 1999	CSA S16-09
25T-490-3-60	SM490	3415	2499	2408	3266
25T-570-3-60	SM570	4260	2907	2987	3967
15T-490-3-60	SM490	1973	1591	1570	2112
15T-490-4-60	SM490	2488	1844	1822	2590
15T-800-3-60	HSA800	3138	2448	2574	3393
15T-800-4-60	HSA800	3511	2837	2963	4176

Chapter 4. Numerical Parametric Study and Suggestion of New Design Equation

4.1 Introduction

Finite element analysis has been widely used in the researches to study the behavior and strength of bolted connection in steel structures. The puropose of finite element analysis is carrying out various conditions to predict the strength and behavior of the block shear failure. The finite element model can increase the number of database related to the test results of block shear. Analyzing all the different variables is unavailable in the real experimental study due to the variuos limtaion of condtion, such as limitation of loading or diverse bolting configuration. The finite element method can include the various effect of diverse geometric parameters and material properties through parametric study. Based on finite element model, the precise information, such as stress distribution and failure mechanism can be obtained. In this chapter, the verification of the finite element models is described by comparing he results of the experiments on lap joints of the bolted connetions from Chapter 3.

The general-purpose finite element software, ABAQUS/CAE is used for the finite element analyses. The general aspect of finite modeling, referring to the geometry, material properties, element type, and boundary conditions are presented in the subchapters.

4.2 Finite Element Model

Procedure of the finite element analysis focuses on validation of the strength and behavior of lap joints failing in the block shear against the results of the experimental study in Chapter 3. The investigation for the finite element method of the block shear used the model of non-staggered bloted connection in Chapter 3, which failed in block shear.

Either shell or solid elements to model bolted connections were used in the previous researches. However, the finite elements models with solid elements accurately demonstrate the representation of the geometric shapes including loading and boundary conditions. In this study, solid element C3D8R from ABAQUS was used to model the lap joints.

Non-linear behavior of the material corresponded with the von Mises yield criterion with isotropic hardening in the finite element analysis. In the non-linear ABAQUS analysis, NLGEOM was activated to initiate the large deformation analysis. The following equation were used to convert the engineering stress-strain curve from the data of steel coupon test into the relation of true stress-strain.

$$\varepsilon_t = \ln\left(1+\varepsilon_e\right) \qquad 4\text{-}1$$

$$\sigma_t = \sigma_e\left(1+\varepsilon_e\right) \qquad 4\text{-}2$$

where ε_t and σ_t refer to the true stress and ture stain respectively, while ε_e

and σ_e denote the engineering stress and engineering strain. Figure 4-1 to Figure 4-3 present the comparison between the engineering stress-strain and true stress-strain relationship for SM490, SM570, and HSA800 used in the finite element analysis.

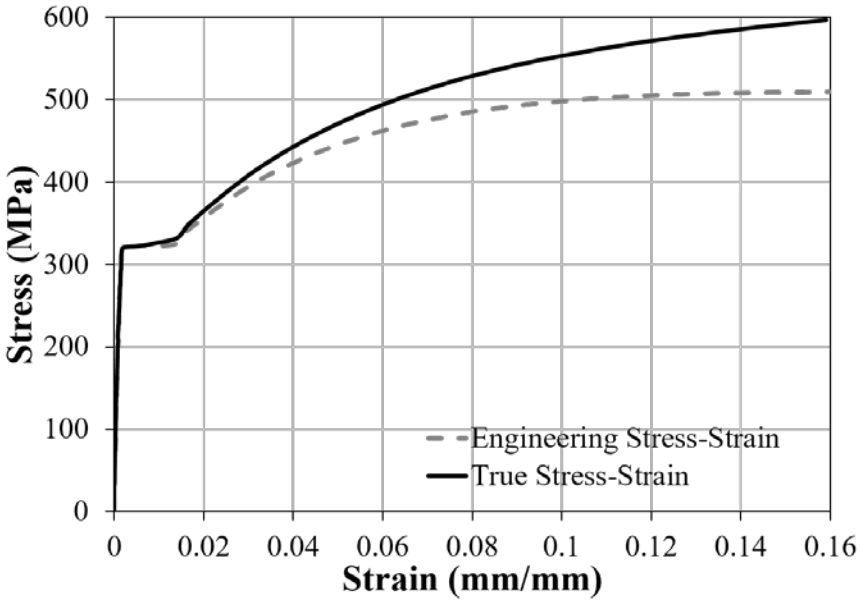

Figure 4-1 Engineering and True Stress-Strain Curve of SM490

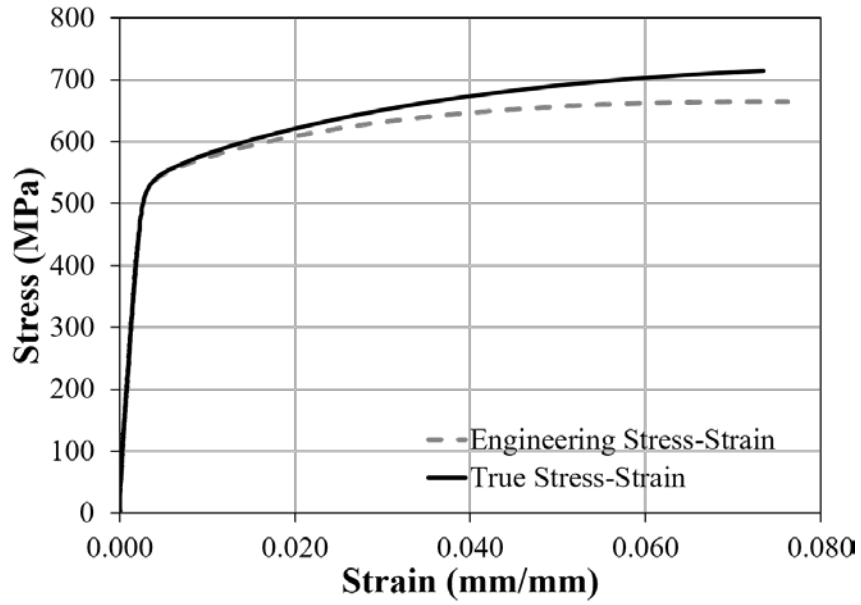

Figure 4-2 Engineering and True Stress-Strain Curve for SM570

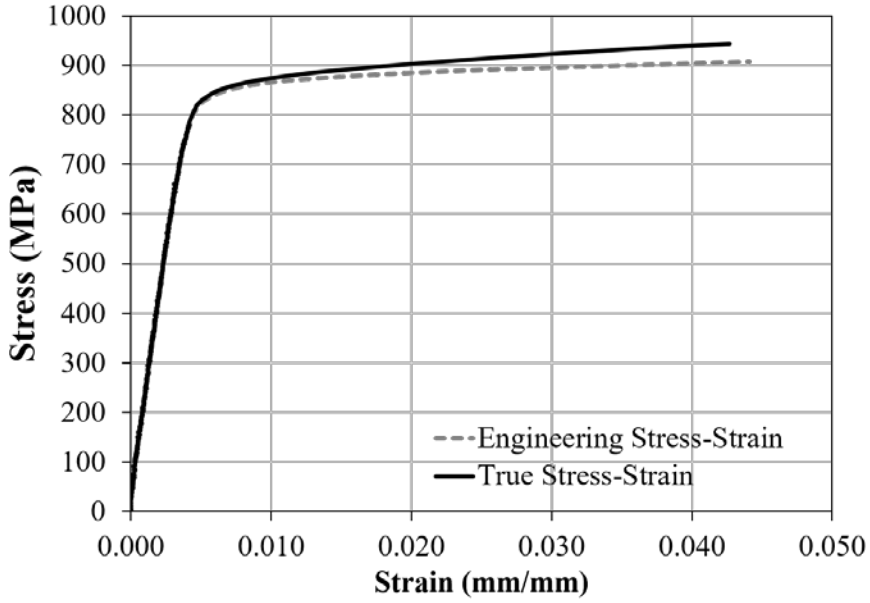

Figure 4-3 Enginnering and True Stress-Strain Curve of HSA800

4.3 Verification

The finite element models are verified against the results from the experiment results from Chapter 3 of the specimen with 25mm thick plate. Test specimens in the experimental study possessed a symmetric plane along the length. Using the symmetricity, a quarter of the specimen is modeld for efficiency. In the finite element models, the bolts are analytic rigid and the bolt shear rupture is not considered. The main purpose of the finite element analysis was the investigation of the mechanism of the block shear failure and the strength instead of the block shear rupture. Figure 4-4 shows the boundary condition of the FE models corresponding to those in the test set-up. The

material properties obtained from the coupon test are used and their stress-strain curves described in the Figure 4-1 to Figure 4-3.

Figure 4-5 to Figure 4-7 compare the results of FE analysises with the test records from Chapter 3. As depicted in Figure 4-5 to Figure 4-7, FE analysies and the test results show the different initial slope. However, FE models and the experiments represent the similar level of ultimate strength in the three specimens. Table 4-1 shows the comparison result from the experimental study and the finite element analyses.

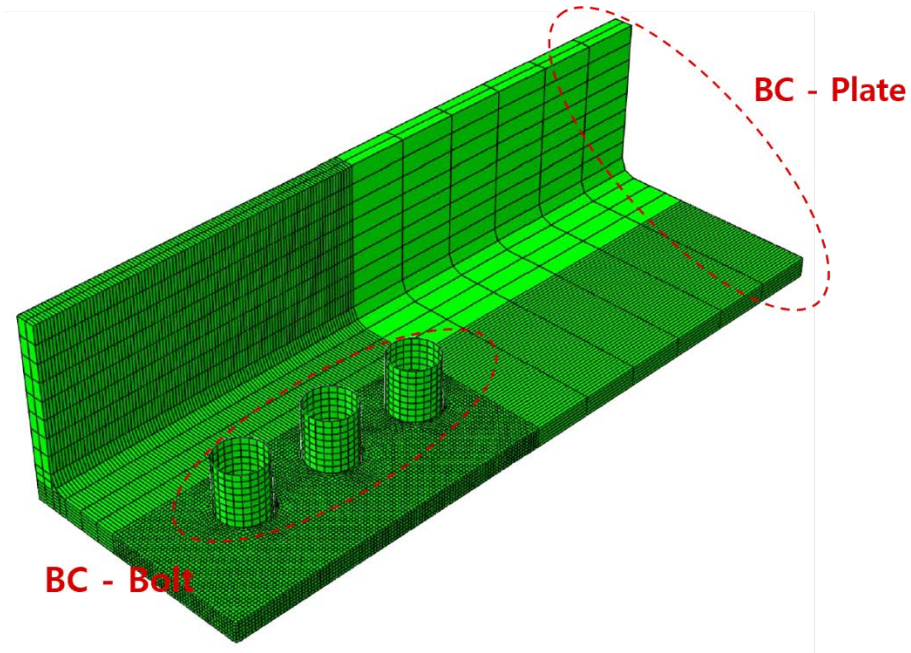

Figure 4-4 Finite Element Mesh and Boundary Condition

	Plate	**Bolt**
U1	Restrained	Restrained
U2	Restrained	Restrained
U3	Restrained	Loading

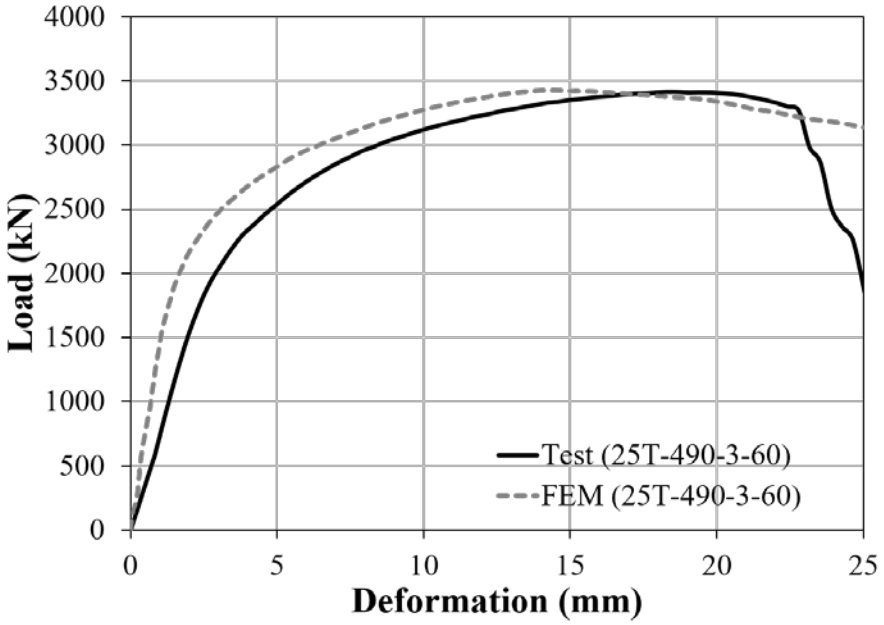

Figure 4-5 Comparison of the Finite Element Analysis and the Test Result for Specimen 25T-490-3-60

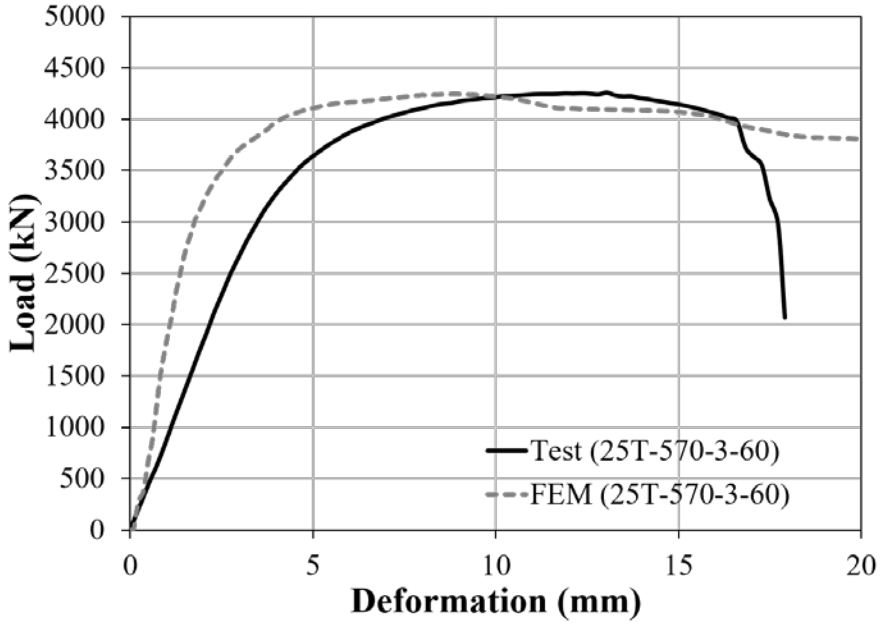

Figure 4-6 Comparison of the Finite Element Analysis and the Test Result for Specimen 25T-570-3-60

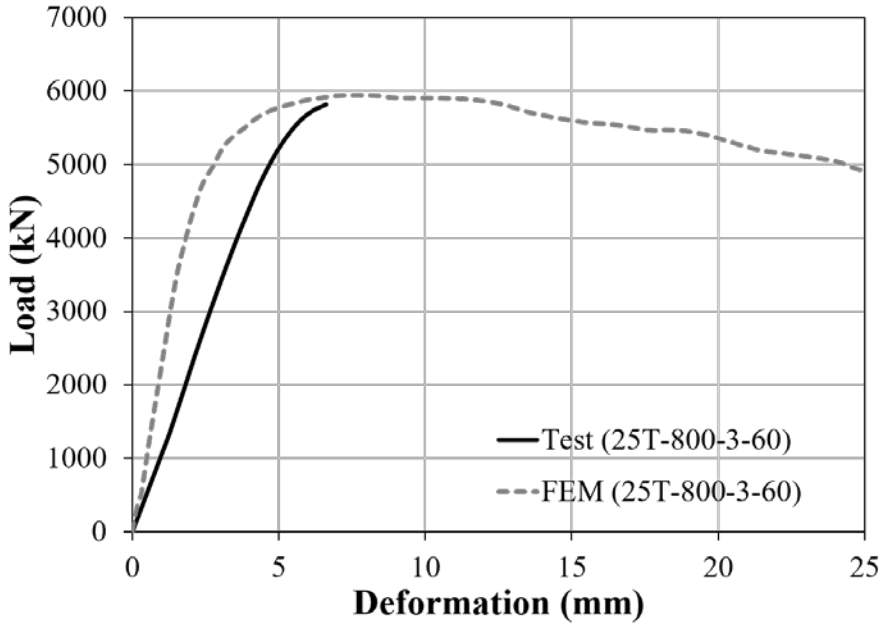

Figure 4-7 Comparison of the Finite Element Analysis and the Test Result for Specimen 25T-800-3-60

(a) Experimental Study

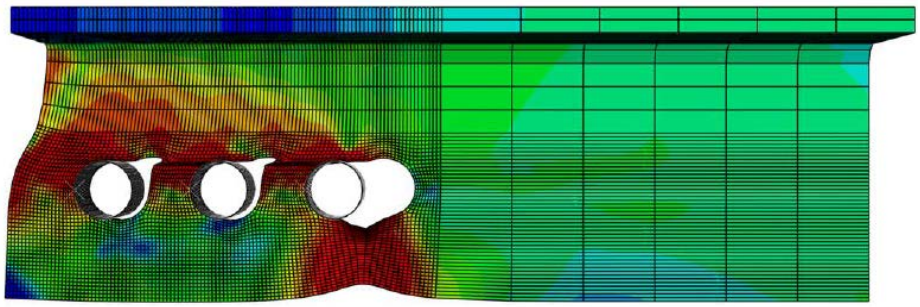

(b) Finite Element Model

Figure 4-8 Failure Shape of Experiment and Finite Element Analysis for Specimen 25T-490-3-60

(a) Experimental Study

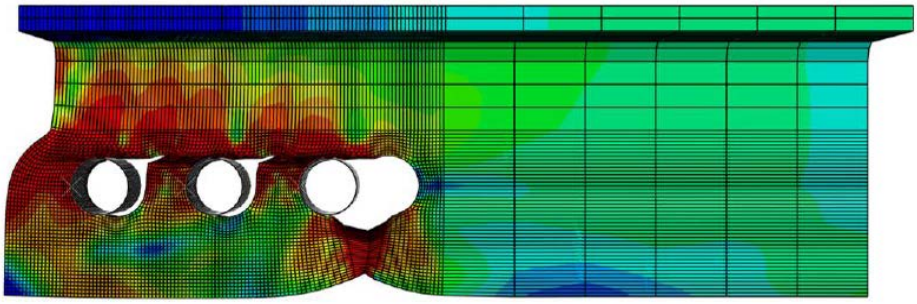

(b) Finite Element Model

Figure 4-9 Failure Shape of Experiment and Finite Element Analysis for Specimen 25T-570-3-60

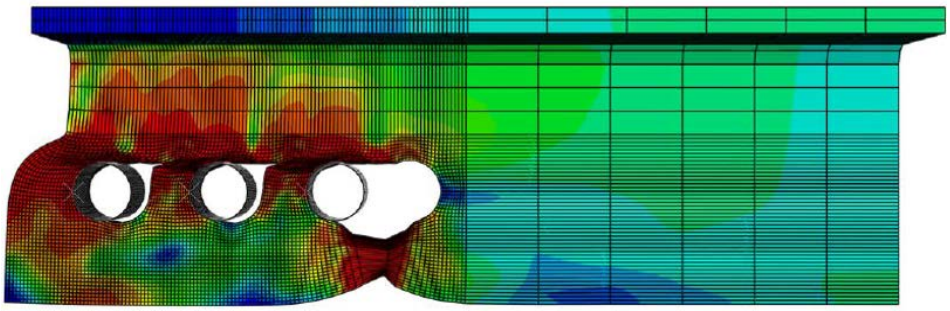

(a) Finite Element Model

Figure 4-10 Failure Shape of Finite Element Analysis for Specimen 25T-800-3-60

Table 4-1 Comparison of Test and FE Analysis Results

Specimen	Steel Grade	Test (kN)	FE Analysis (kN)	Difference (%)
25T-490-3-60	SM490	3415	3452	1.1
25T-570-3-60	SM570	4260	4243	0.4
25T-800-3-60	HSA800	N.A	5948	N.A

4.4 Numerical Analysis Results

4.4.1 Specimens with 25mm Plate

The FE models use the different number of bolts and the bolt distance to make various connection length of the specimen. The finite element models with 25mm plate have total eleven different bolt configurations. The number of

bolts is from 2 to 6 for 60mm bolt distance, from 2 to 4 for 80mm bolt distance, from 2 to 3 for 100mm bolt distance and 3 for 75mm bolt distance. Because SM490, SM570, and HSA800 steel were used in the finite elment analysis, the total number of FE models is 33 for 25mm thick plate. Figure 4-11 and Figure 4-12 show the shape of the block shear failure from results of the finite element analysis. The tensile plane is the section of impeding fracture. Table 4-2 to Table 4-4 show the result of the finite elment analysis.

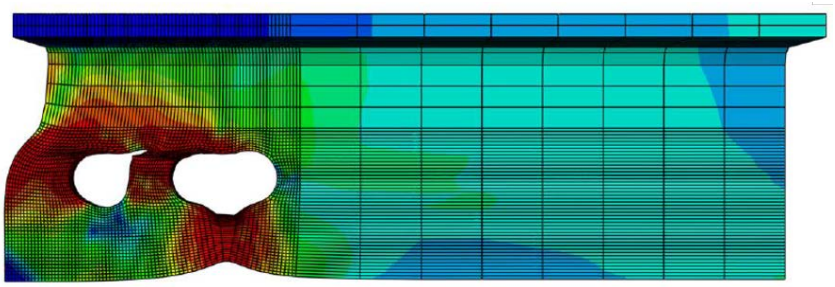

(a) 25T-490-2-60

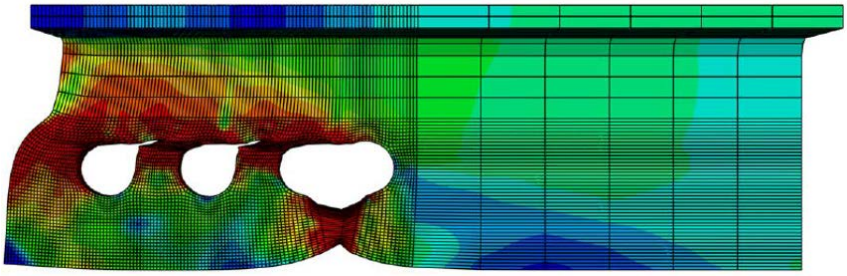

(b) 25T-490-3-60

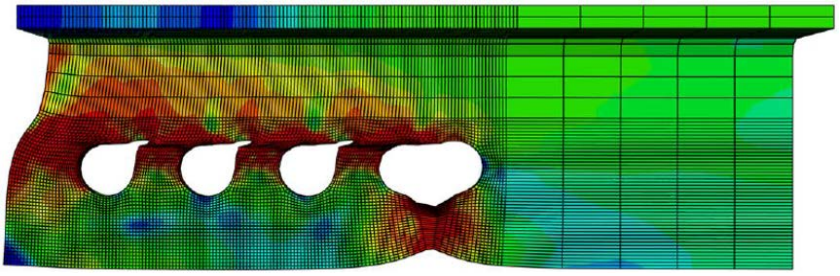

(c) 25T-490-4-60

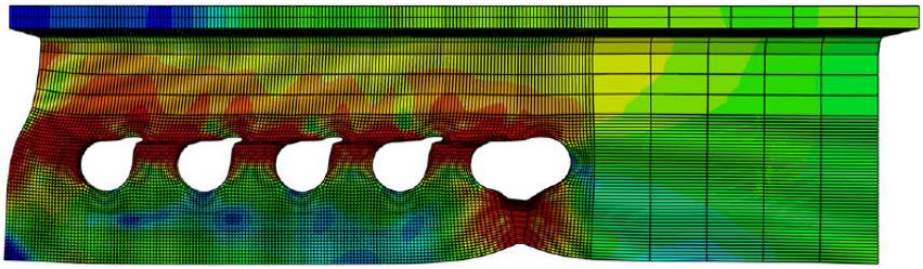

(d) 25T-490-5-60

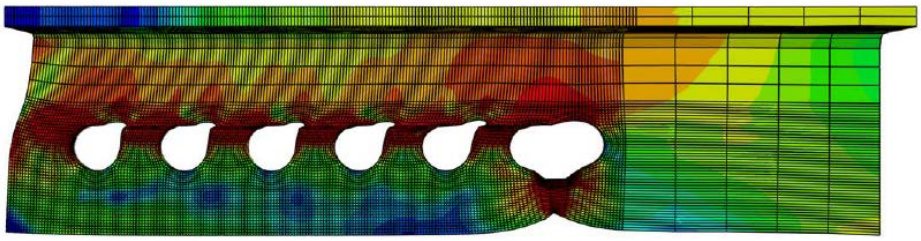

(e) 25T-490-6-60

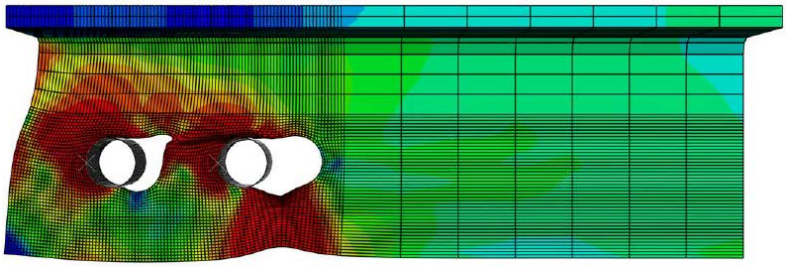

(f) 25T-490-2-80

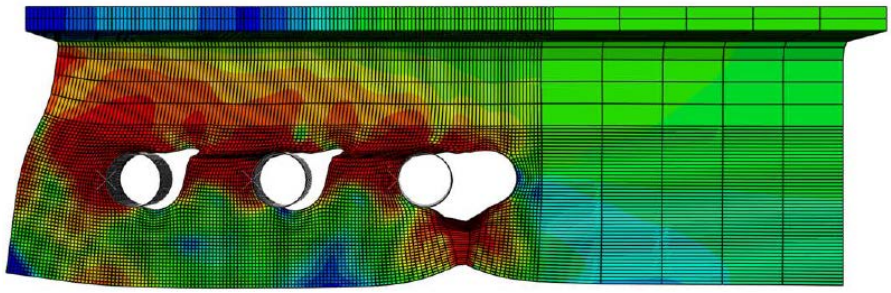

(g) 25T-490-3-80

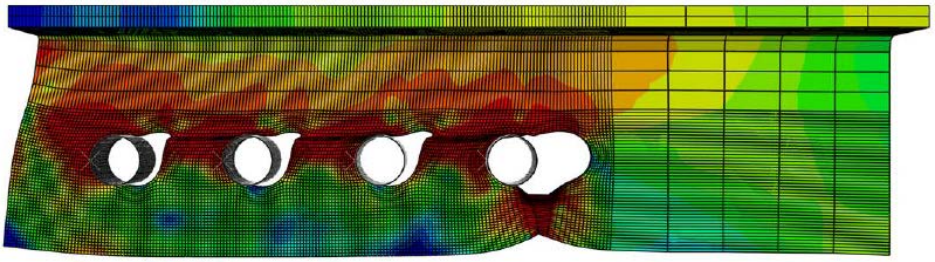

(h) 25T-490-4-80

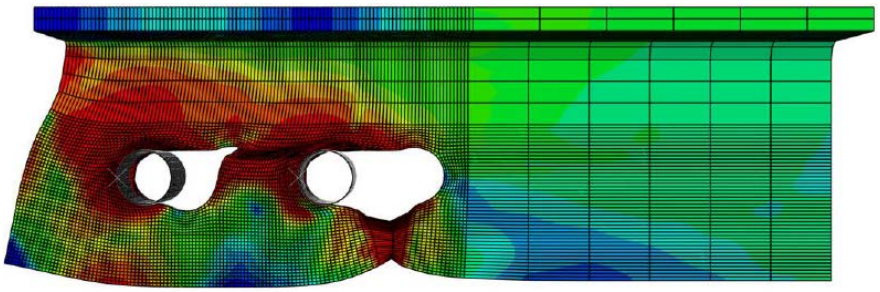

(i) 25T-490-2-100

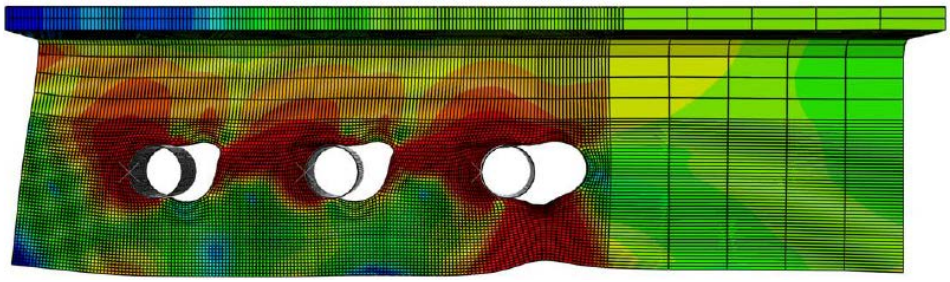

(j) 25T-490-3-100

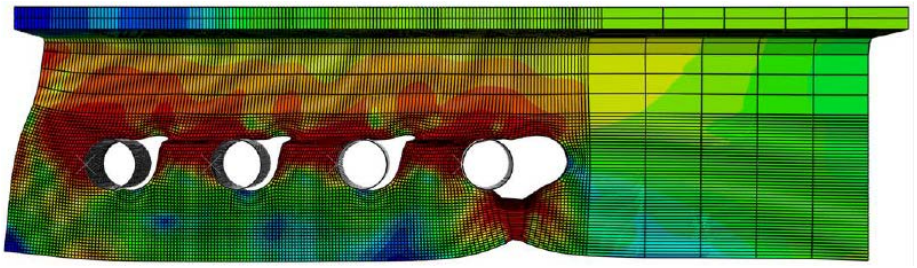

(k) 25T-490-4-750

Figure 4-11 Failure Shape of FE Analysis for 25 mm Specimen with SM490 Steel

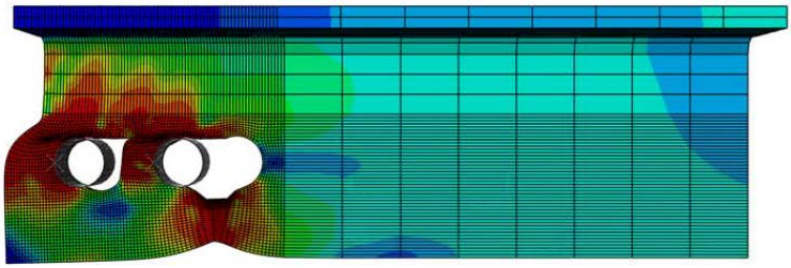

(a) 25T-800-2-60

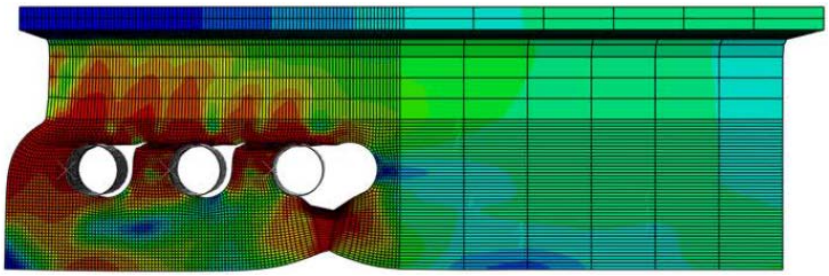

(b) 25T-800-3-60

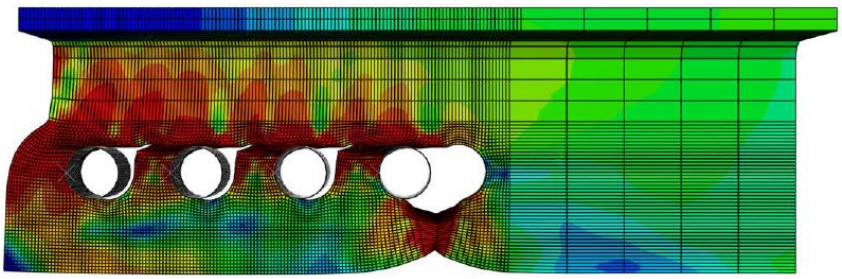

(c) 25T-800-4-60

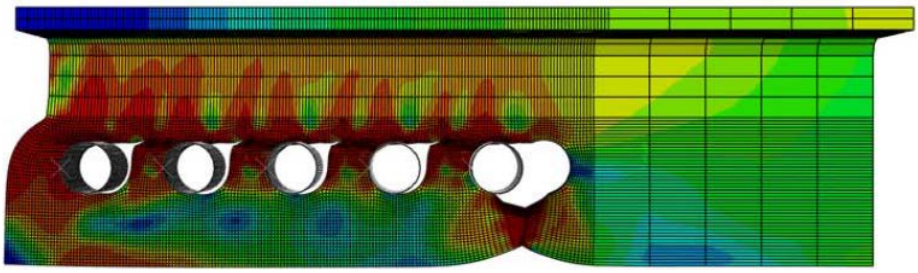

(d) 25T-800-5-60

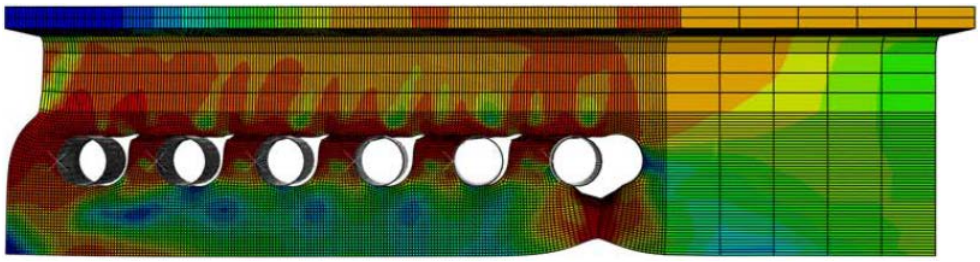

(e) 25T-800-6-60

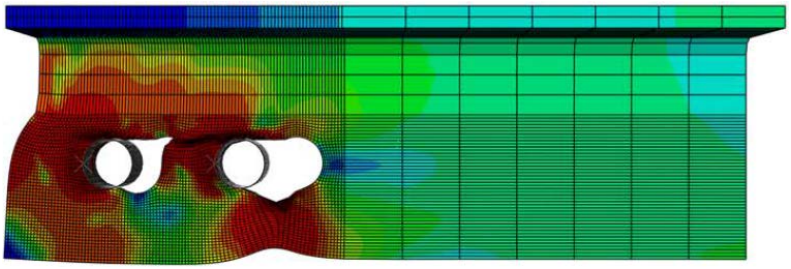

(f) 25T-800-2-80

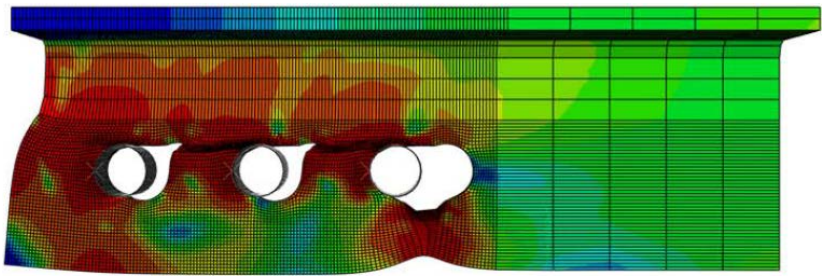

(g) 25T-800-3-80

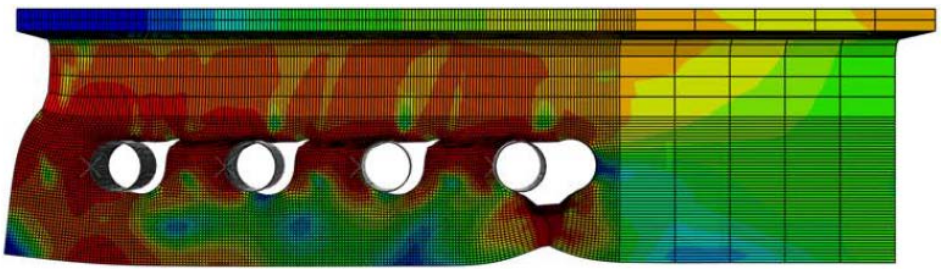

(h) 25T-800-4-80

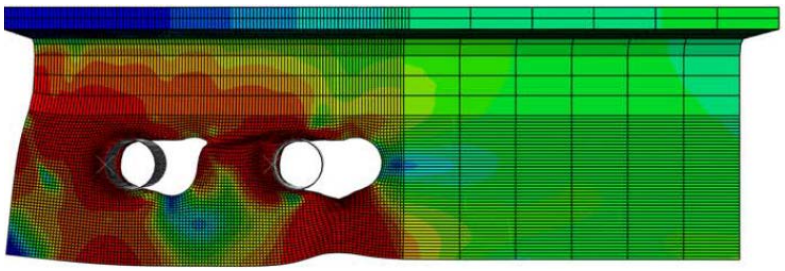

(i) 25T-800-2-100

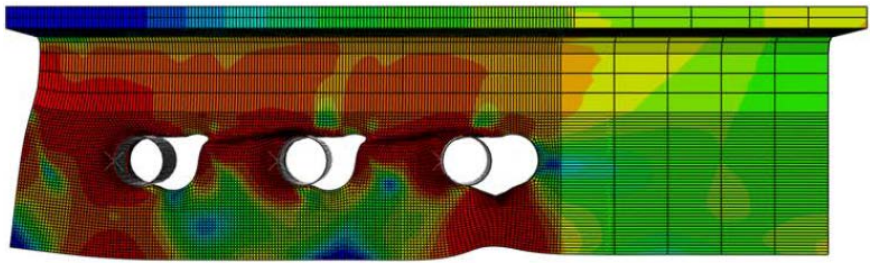

(j) 25T-800-3-100

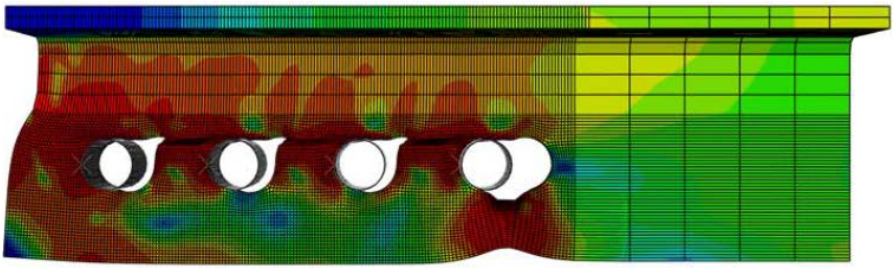

(k) 25T-800-4-75

Figure 4-12 Failure Shape of FE Analysis for 25 mm Specimen with HSA800 Steel

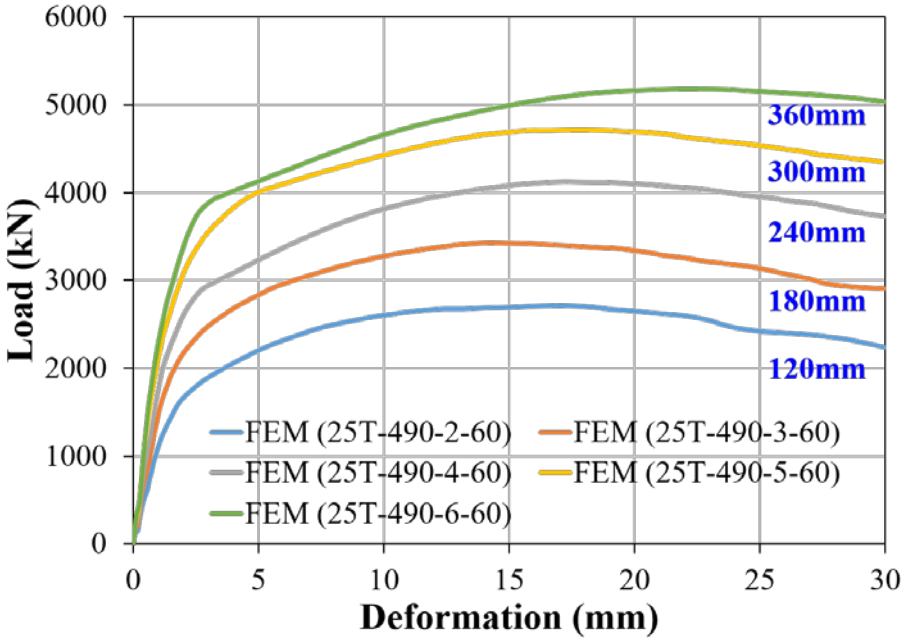

(a) 60mm Bolt Distance

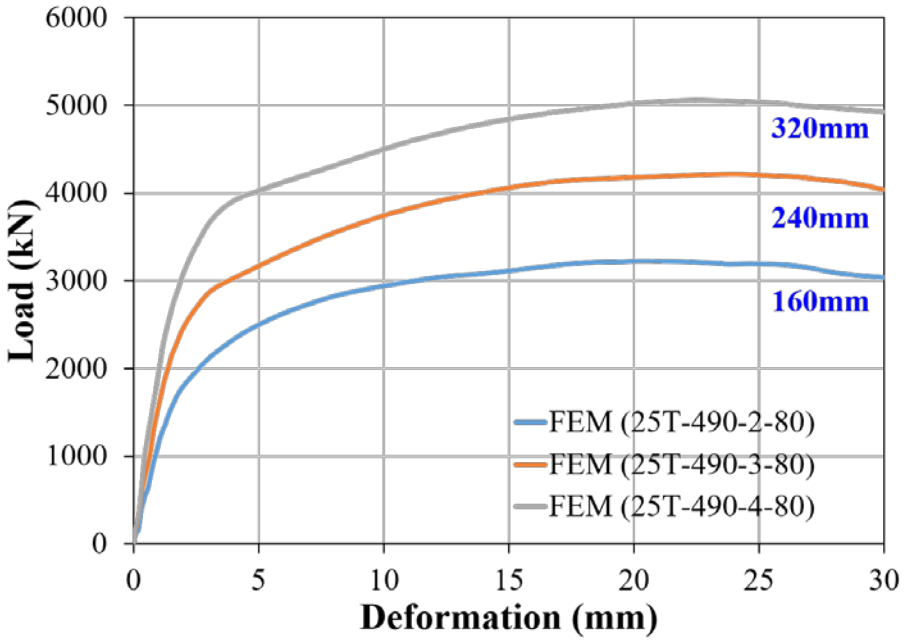

(b) 80mm Bolt Distance

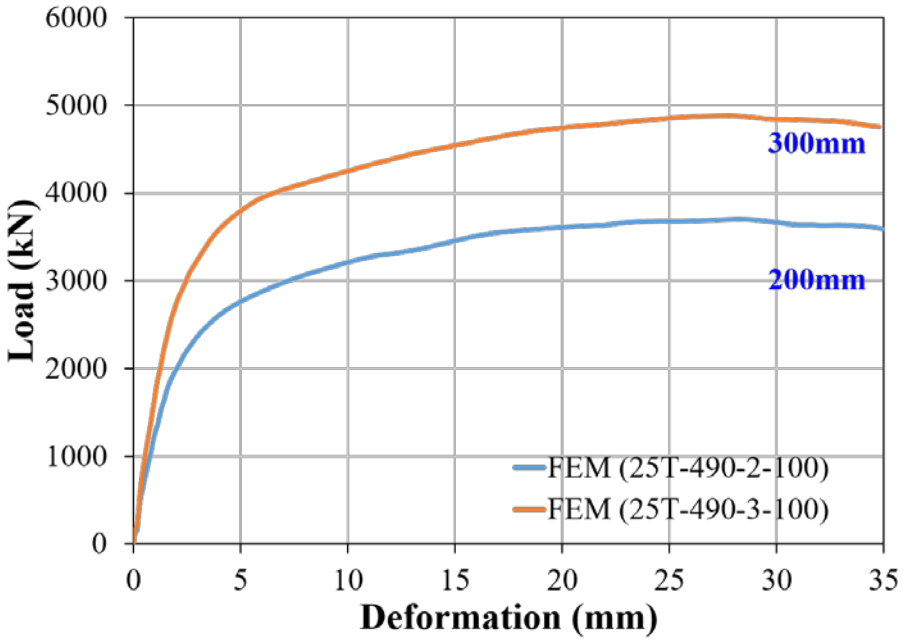

(c) 100mm Bolt Distance

Figure 4-13 Load-Deformation Curves for FE Models with 25mm Thick SM490 Steel

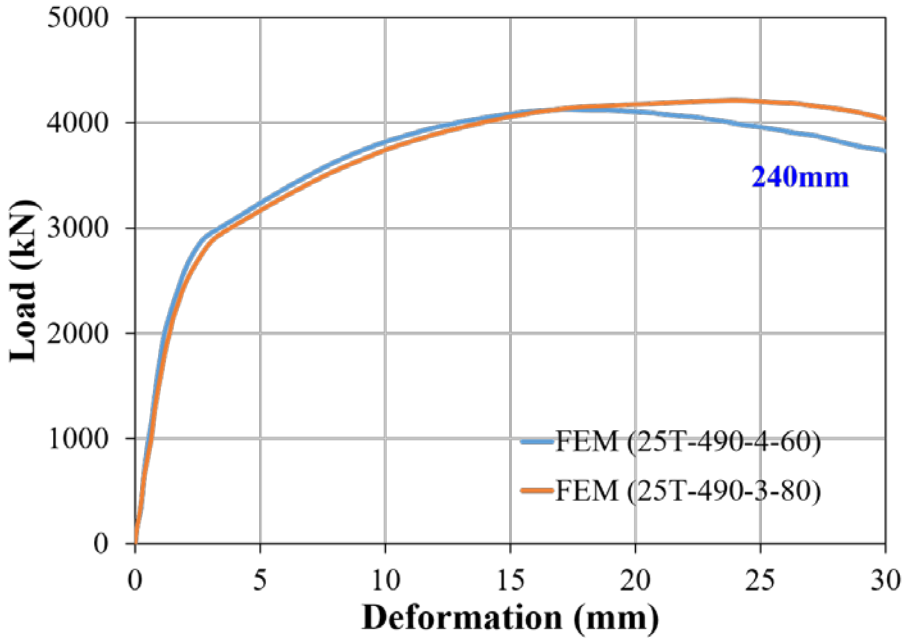

(a) 240mm Connection Length

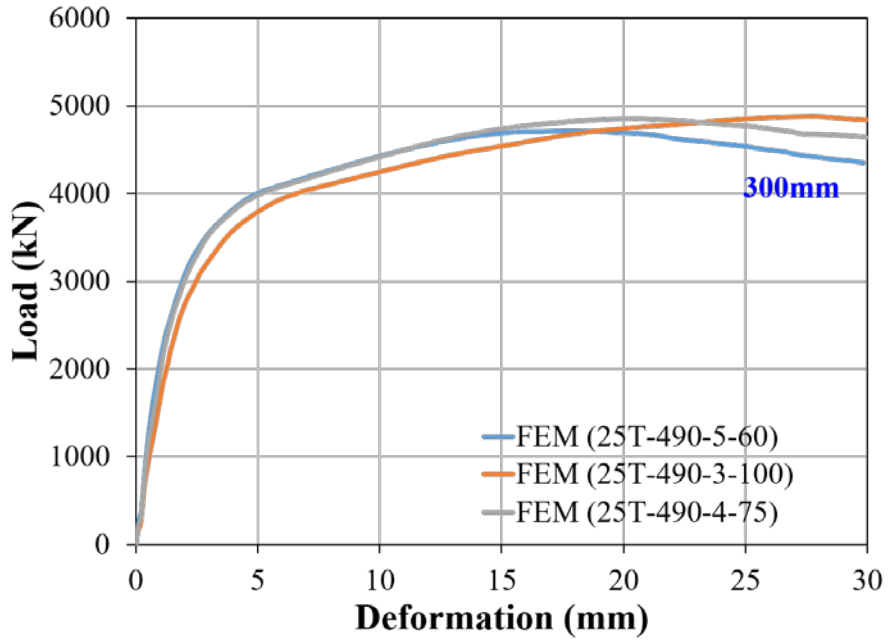

(b) 300mm Connection Length

Figure 4-14 Load-Deformation Curves of FE Models with the Same Connection Length

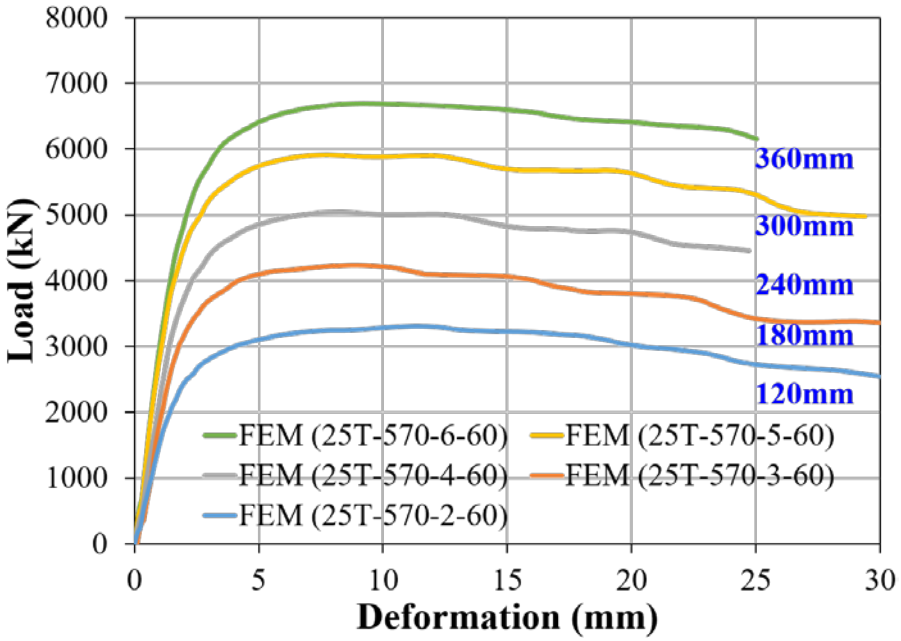

(a) 60mm Bolt Distance

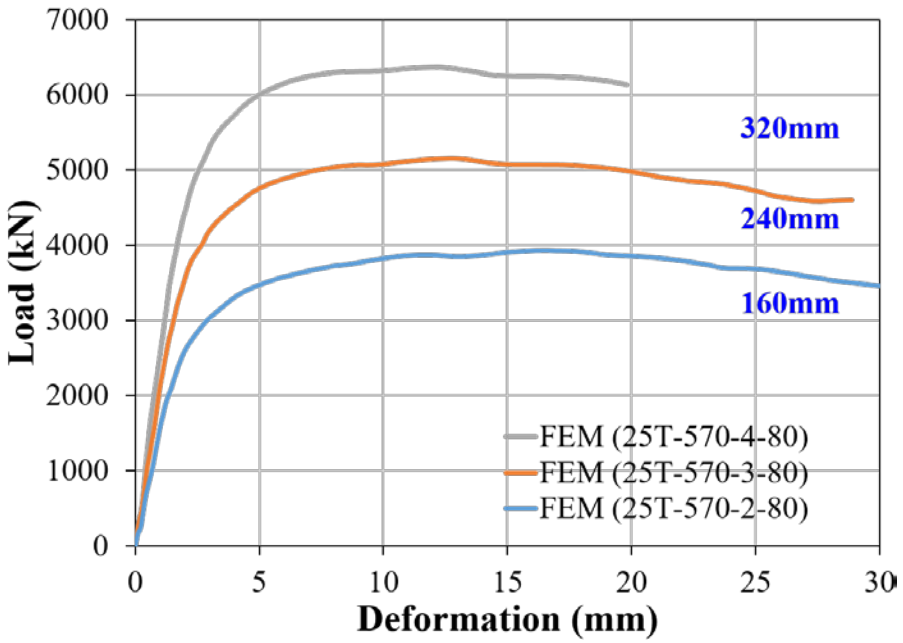

(b) 80mm Bolt Distance

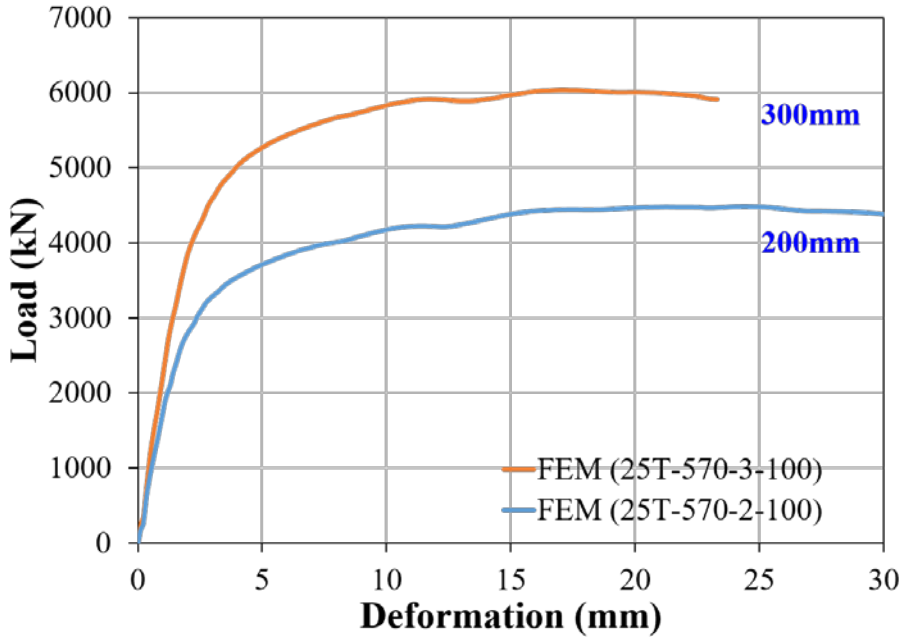

(c) 100mm Bolt Distance

Figure 4-15 Load-Deformation Curves for FE Models with 25mm Thick SM570 Steel

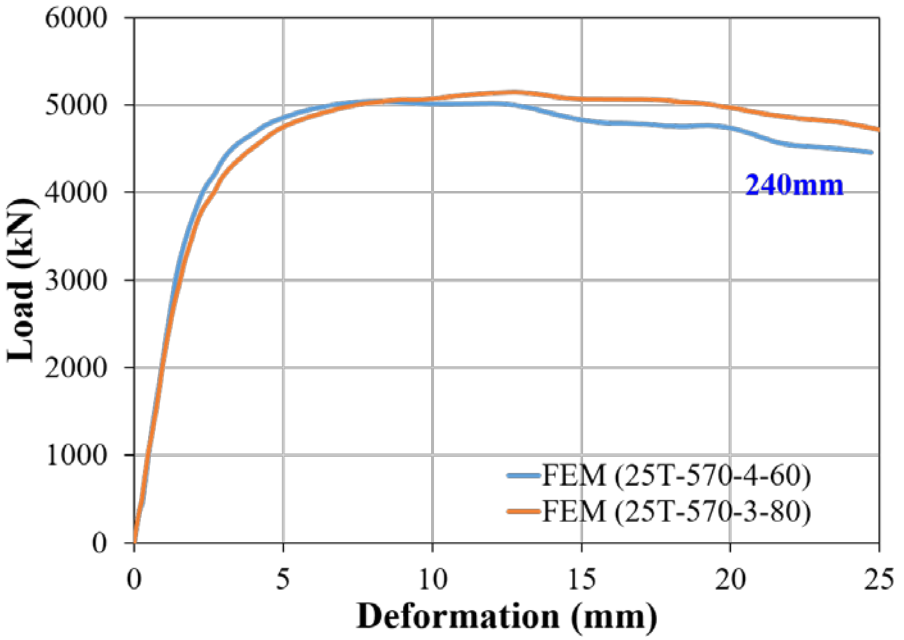

(a) 240mm Connection Length

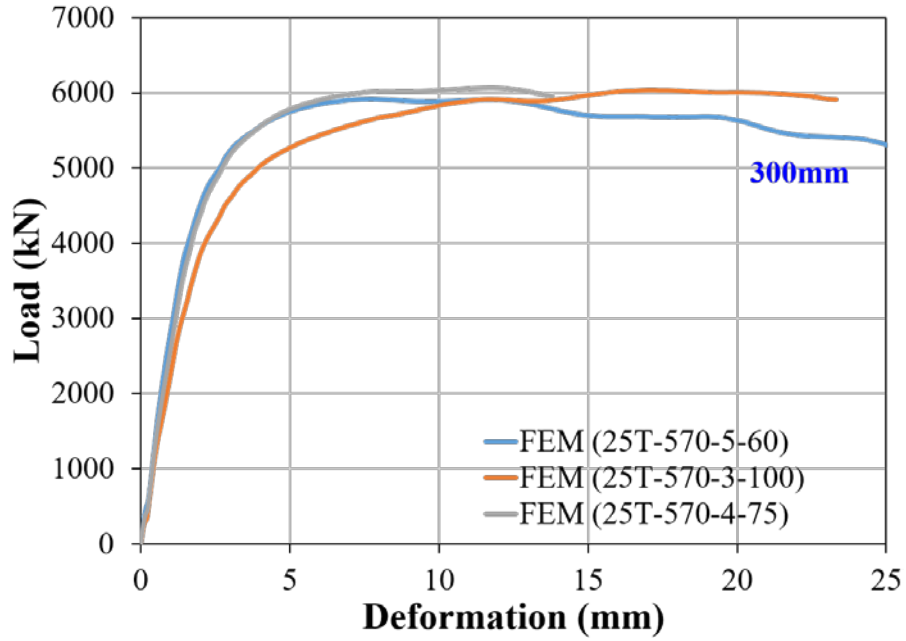

(b) 300mm Connection Length

Figure 4-16 Load-Deformation Curves of FE Models with the Same Connection Length

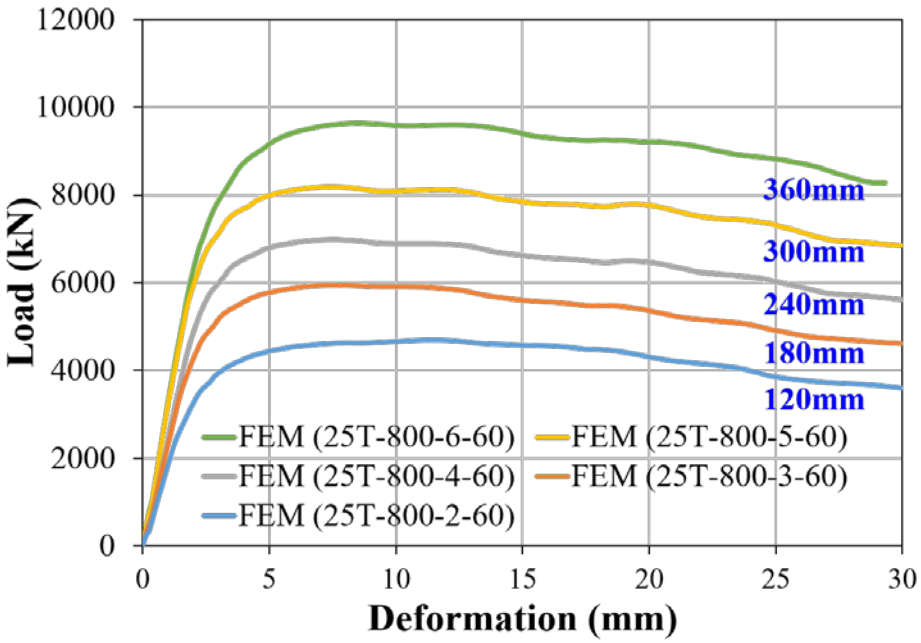

(a) 60mm Bolt Distance

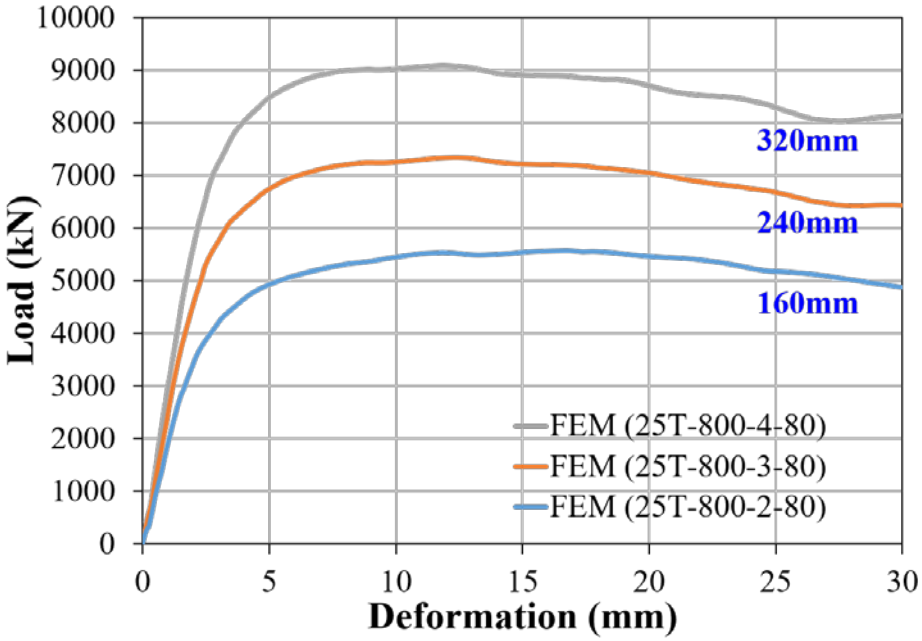

(b) 80mm Bolt Distance

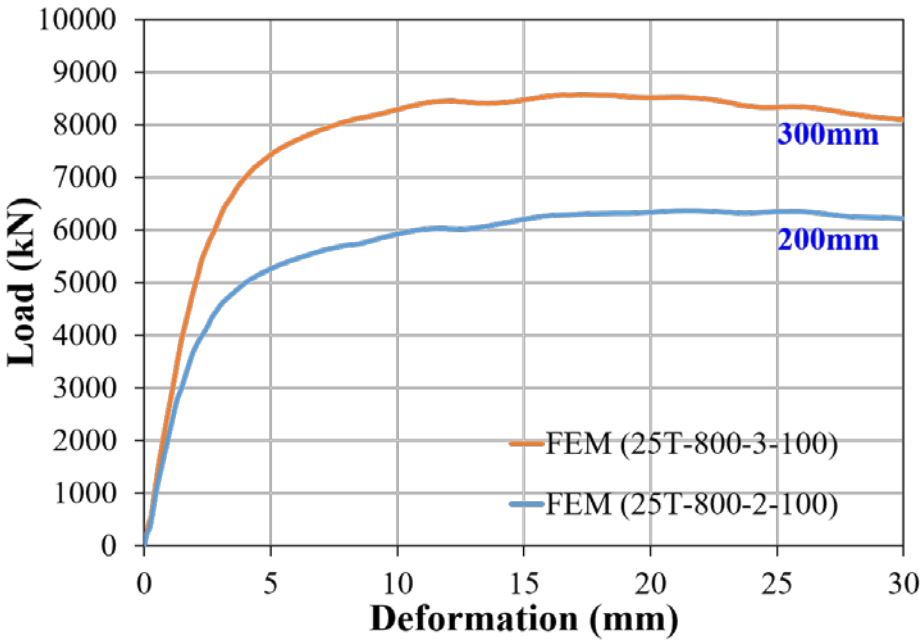

(c) 100mm Bolt Distance

Figure 4-17 Load-Deformation Curves for FE Models with 25mm Thick HSA800 Steel

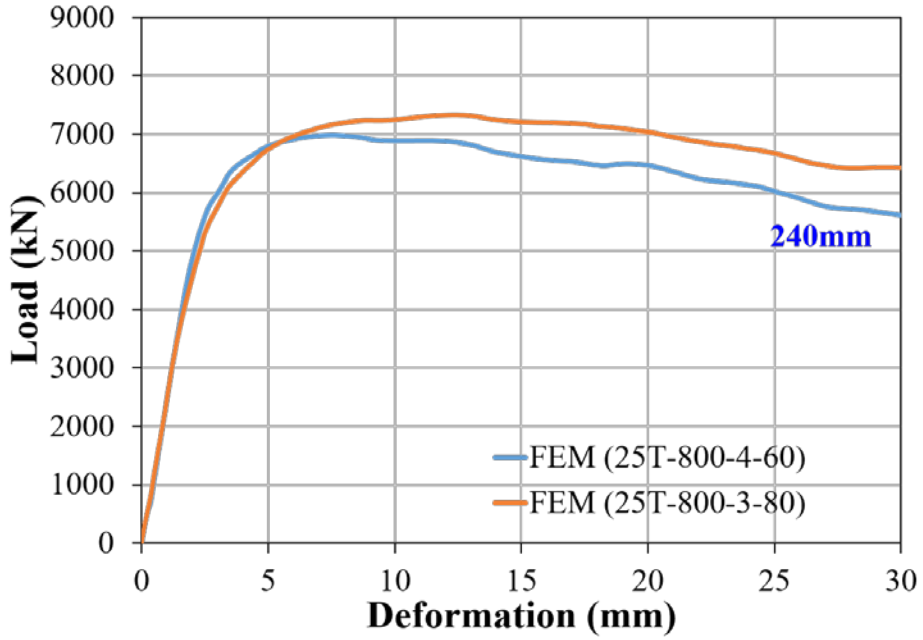

(a) 240mm Connection Length

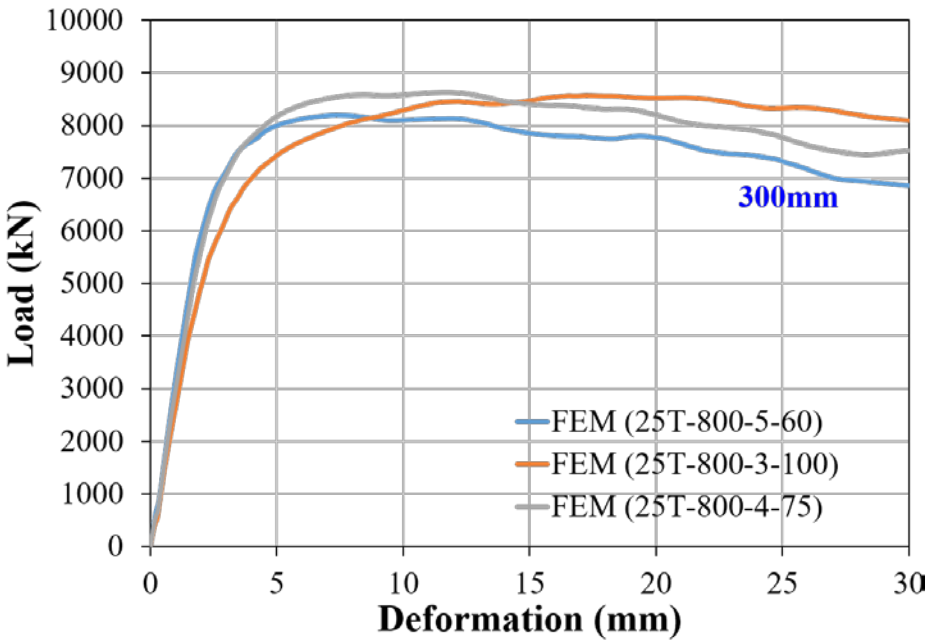

(b) 300mm Connection Length

Figure 4-18 Load-Deformation Curves of FE Models with the Same Connection Length

Table 4-2 FE Analysis Results for SM490 Steel

	Specimen	Thickness (mm)	Connection Length (mm)	A_{nt} (mm^2)	A_{gv} (mm^2)	A_{nv} (mm^2)	P_{ult} (kN)	Design Strength (kN)		
								AISC 2010	AISC 1999	CSA S16-09
	25T-490-2-60		120	2175	6000	3525	2713	2102	2236	2533
	25T-490-3-60		180	2175	9000	4875	3452	2499	3266	3266
	25T-490-4-60		240	2175	12000	6225	4127	2896	2805	4000
	25T-490-5-60		300	2175	15000	7575	4709	3293	3202	4733
	25T-490-6-60		360	2175	18000	8925	5176	3690	3599	5467
SM490	25T-490-2-80	25	160	2175	8000	5525	3226	2626	2599	3022
	25T-490-3-80		240	2175	12000	7875	4213	3381	3290	4000
	25T-490-4-80		320	2175	16000	10225	5058	4072	3981	4978
	25T-490-2-100		200	2175	10000	7525	3697	3016	3187	3511
	25T-490-3-100		300	2175	15000	10875	4879	3991	4172	4733
	25T-490-4-75		300	2175	15000	9225	4850	3778	3687	4733

Table 4-3 FE Analysis Results for SM570 Steel

	Specimen	Thickness (mm)	Connection Length (mm)	A_{nt} (mm^2)	A_{gv} (mm^2)	A_{nv} (mm^2)	P_{ult} (kN)	Design Strength (kN)		
								AISC 2010	AISC 1999	CSA S16-09
SM570	25T-570-2-60	25	120	2175	6000	3525	3308	2445	2824	3058
	25T-570-3-60		180	2175	9000	4875	4243	2907	3967	3967
	25T-570-4-60		240	2175	12000	6225	5040	3369	3449	4876
	25T-570-5-60		300	2175	15000	7575	5913	3830	3911	5785
	25T-570-6-60		360	2175	18000	8925	6688	4292	4372	6694
	25T-570-2-80		160	2175	8000	5525	3931	3129	3210	3664
	25T-570-3-80		240	2175	12000	7875	5150	3933	4013	4876
	25T-570-4-80		320	2175	16000	10225	6367	4737	4817	6088
	25T-570-2-100		200	2175	10000	7525	4478	3813	3894	4270
	25T-570-3-100		300	2175	15000	10875	6041	4959	5039	5785
	25T-570-4-75		300	2175	15000	9225	6067	4395	4475	5785

Table 4-4 FE Analysis Results for HSA800 Steel

	Specimen	Thickness (mm)	Connection Length (mm)	A_{nt} (mm^2)	A_{gv} (mm^2)	A_{nv} (mm^2)	P_{ult} (kN)	Design Strength (kN)		
								AISC 2010	AISC 1999	CSA S16-09
HSA800	25T-800-2-60	25	120	2175	6000	3525	4695	3432	4080	4350
	25T-800-3-60		180	2175	9000	4875	5948	4080	5655	5655
	25T-800-4-60		240	2175	12000	6225	6991	4728	4938	6960
	25T-800-5-60		300	2175	15000	7575	8193	5376	5586	8265
	25T-800-6-60		360	2175	18000	8925	9628	6024	6234	9570
	25T-800-2-80		160	2175	8000	5525	5572	4392	4602	5220
	25T-800-3-80		240	2175	12000	7875	7331	5520	5730	6960
	25T-800-4-80		320	2175	16000	10225	9087	6648	6858	8700
	25T-800-2-100		200	2175	10000	7525	6364	5352	5562	6090
	25T-800-3-100		300	2175	15000	10875	8571	6960	7170	8265
	25T-800-4-75		300	2175	15000	9225	8634	6168	6378	8265

4.4.2 Specimens with 15mm Plate

The FE models use the different number of bolts and the bolt distance to make various connection length of the specimen. The finite element models with 15mm plate have total fourteen different bolt configurations. The number of bolts is from 2 to 7 for 60mm bolt distance, from 2 to 5 for 80mm bolt distance, from 2 to 4 for 100mm bolt distance and 3 for 75mm bolt distance. Because SM490, SM570, and HSA800 steel were used in the finite elment analysis, the total number of FE models is 42 for 15mm thick plate. Figure 4-19 and Figure 4-20 show the failure shape of block shear from results of the finite element analysis. The tensile plane is the section of impeding fracture. Table 4-2 to Table 4-4 show the result of the finite elment analysis.

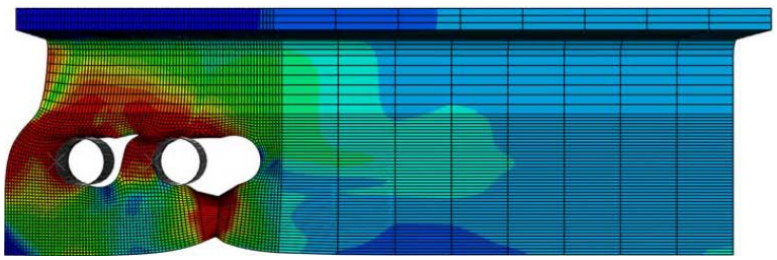

(a) 15T-490-2-60

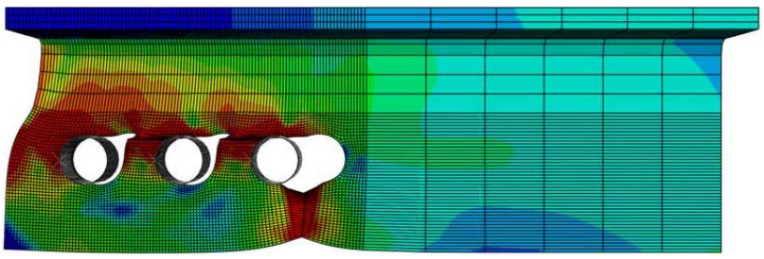

(b) 15T-490-3-60

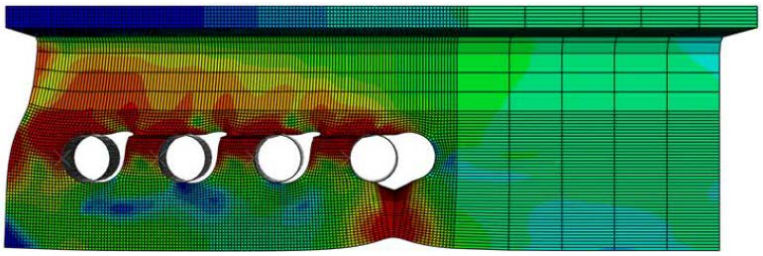

(c) 15T-490-4-60

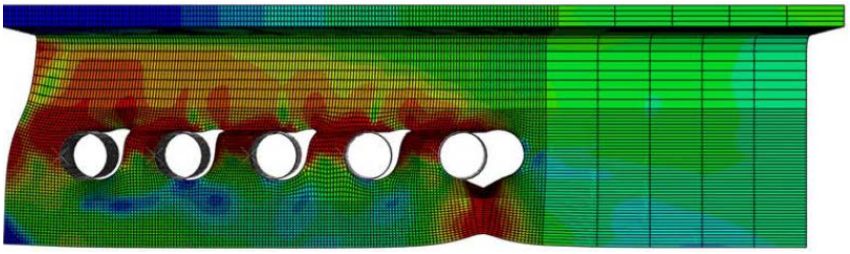

(d) 15T-490-5-60

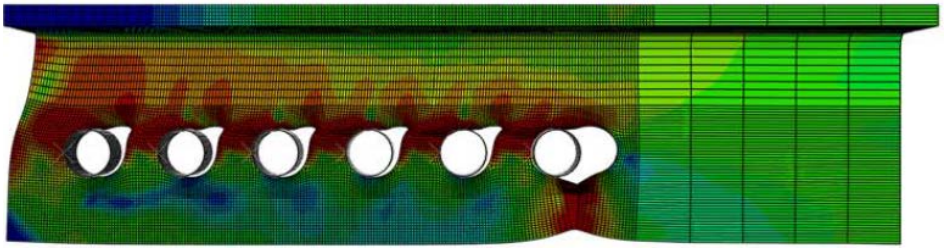

(e) 15T-490-6-60

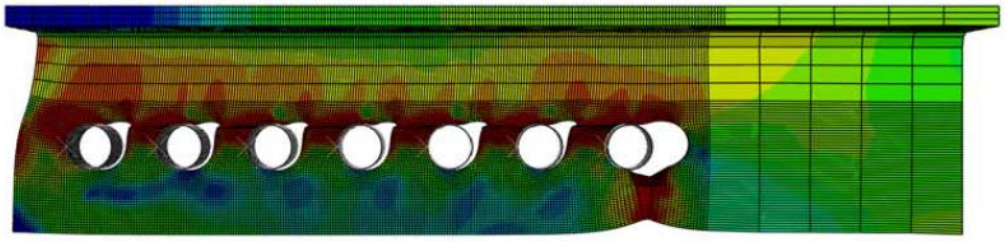

(f) 15T-490-7-60

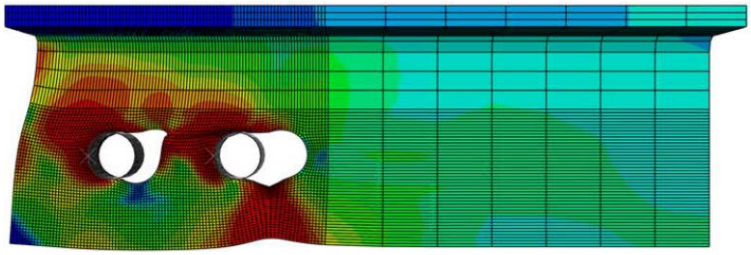

(g) 15T-490-2-80

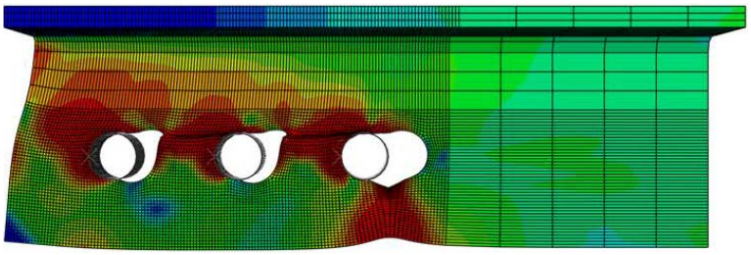

(h) 15T-490-3-80

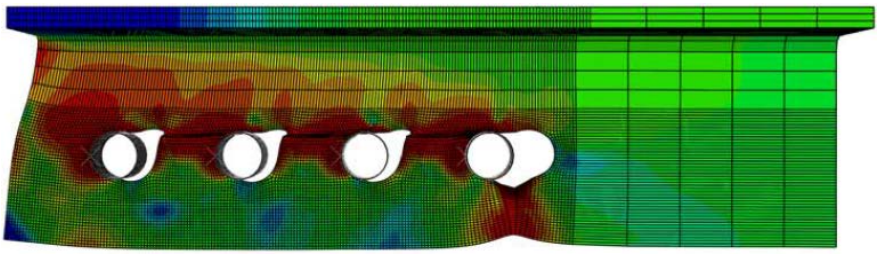

(i) 15T-490-4-80

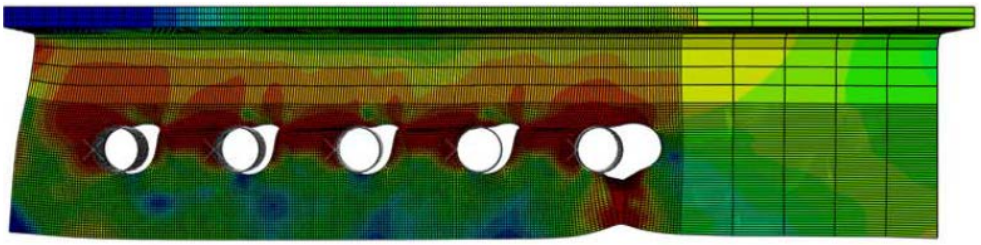

(j) 15T-490-5-80

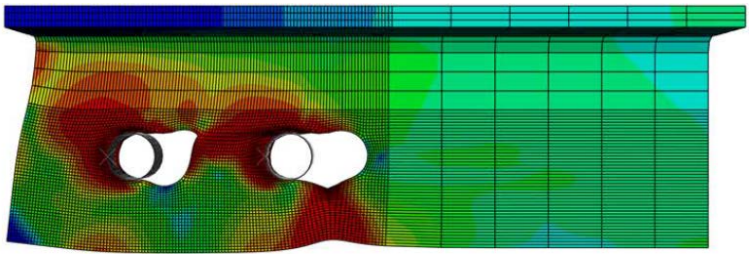

(k) 15T-490-2-100

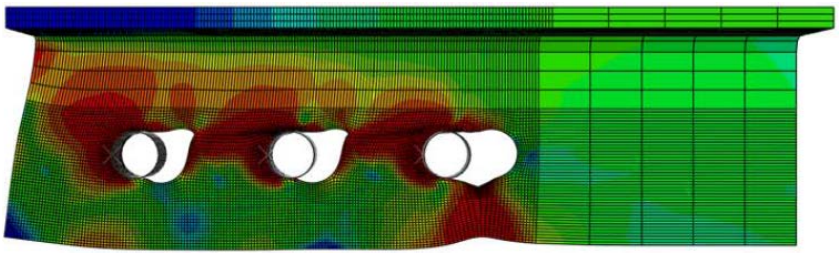

(l) 15T-490-3-100

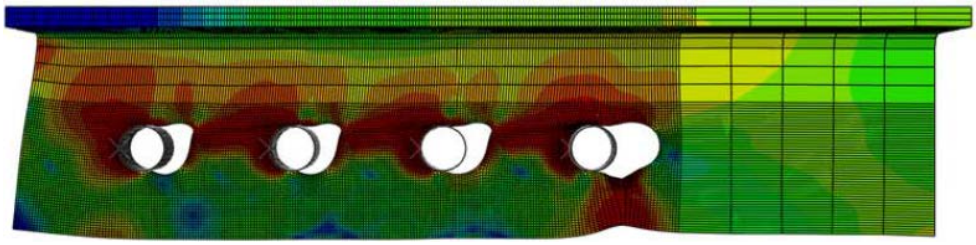

(m) 15T-490-4-100

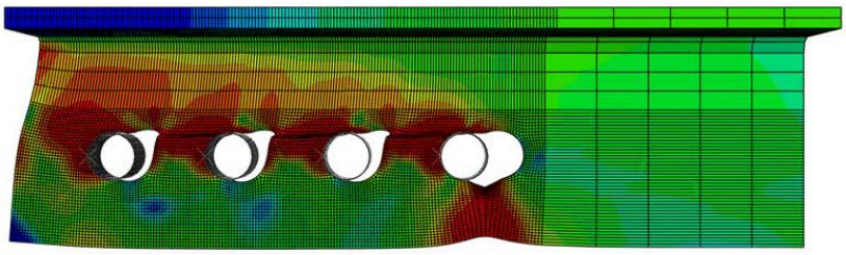

(n) 15T-490-4-75

Figure 4-19 Failure Shape of FE Analysis for 15 mm Specimen with SM490 Steel

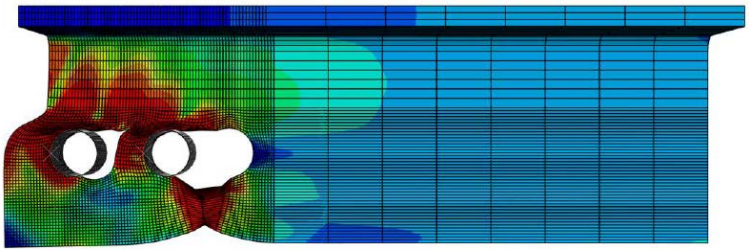

(a) 15T-800-2-60

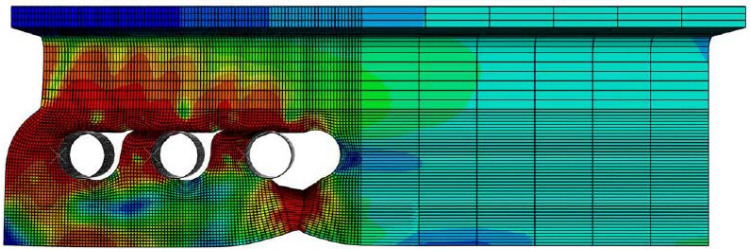

(b) 15T-800-3-60

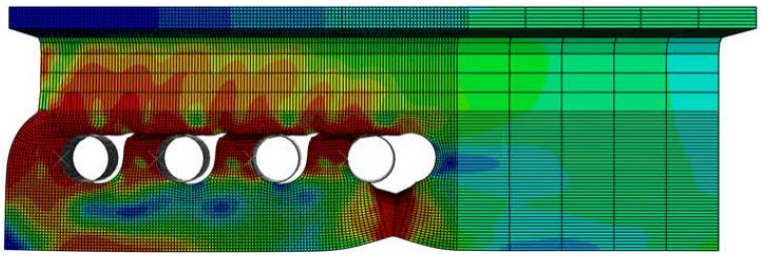

(c) 15T-800-4-60

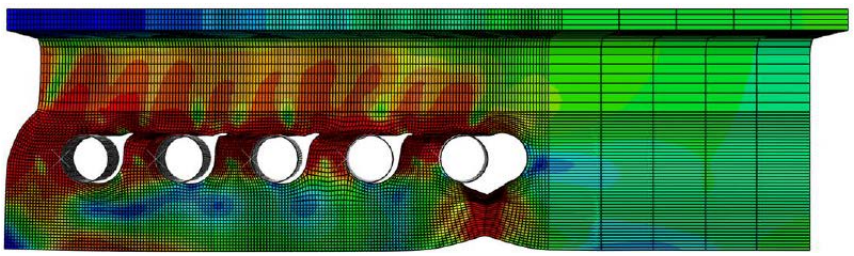

(d) 15T-800-5-60

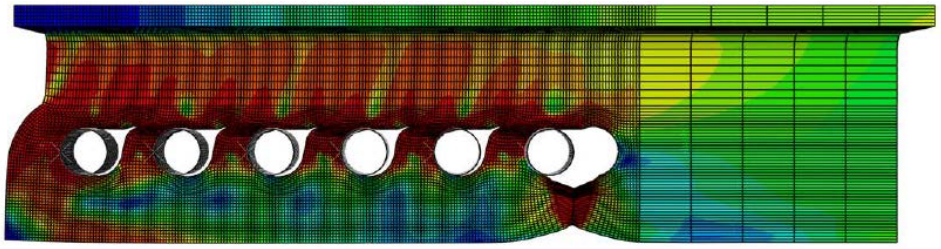

(e) 15T-800-6-60

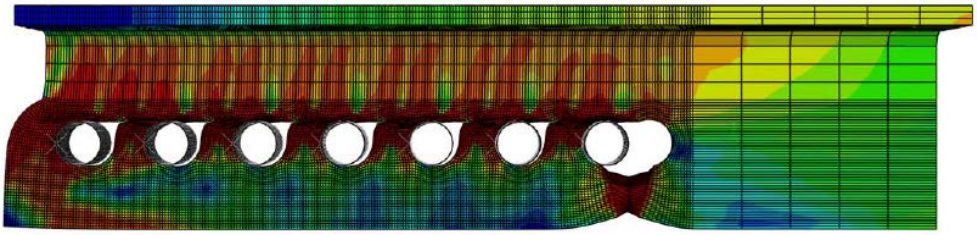

(f) 15T-800-7-60

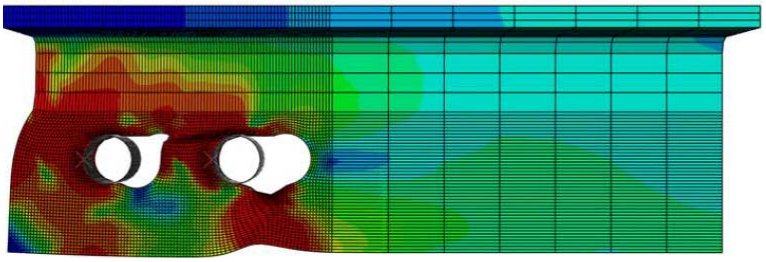

(g) 15T-800-2-80

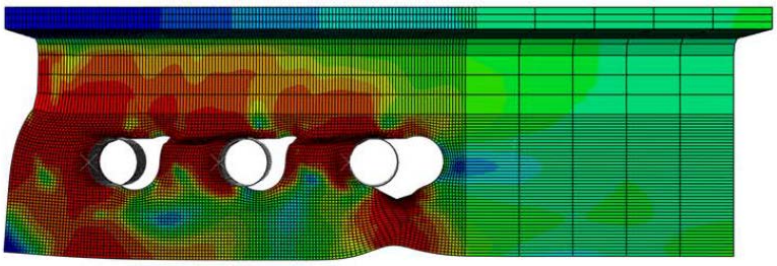

(h) 15T-800-3-80

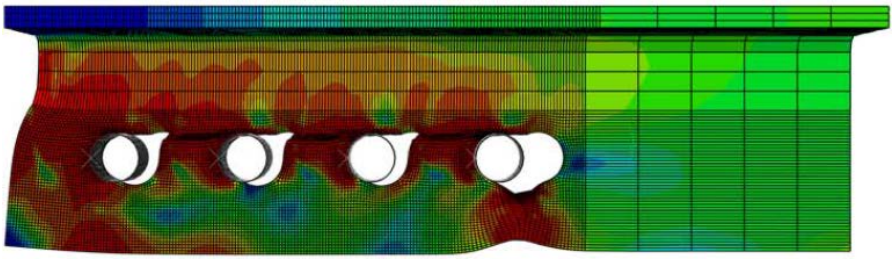

(i) 15T-800-4-80

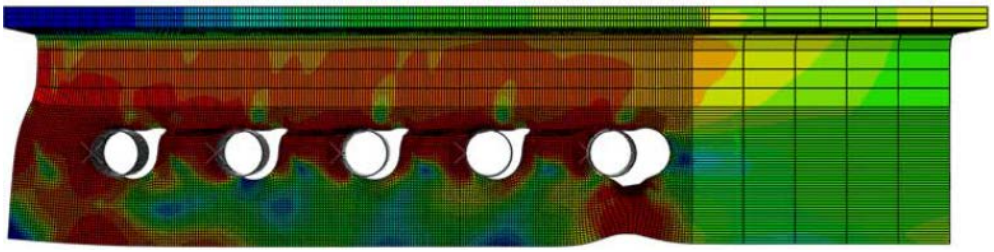

(j) 15T-800-5-80

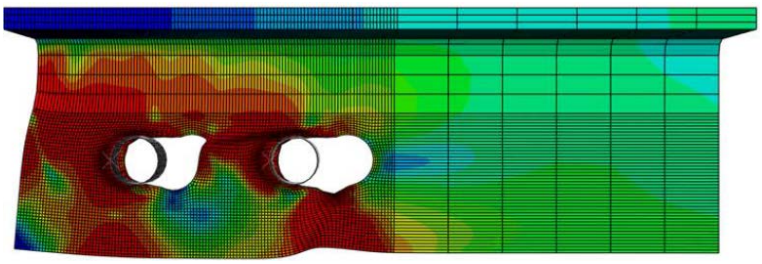

(k) 15T-800-2-100

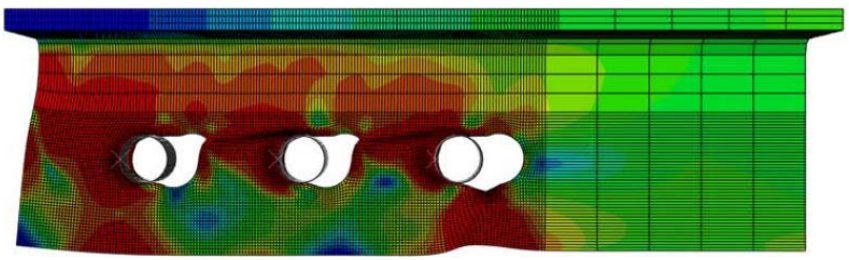

(l) 15T-800-3-100

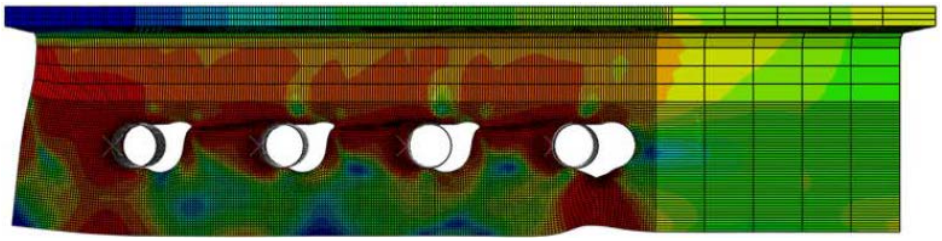

(m) 15T-800-4-100

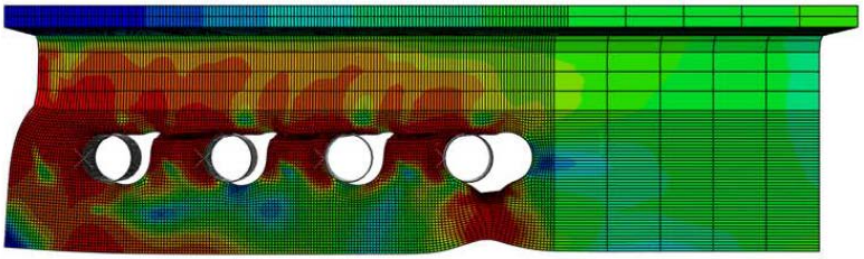

(n) 15T-800-4-75

Figure 4-20 Failure Shape of FE Analysis for 15 mm Specimen with HSA800 Steel

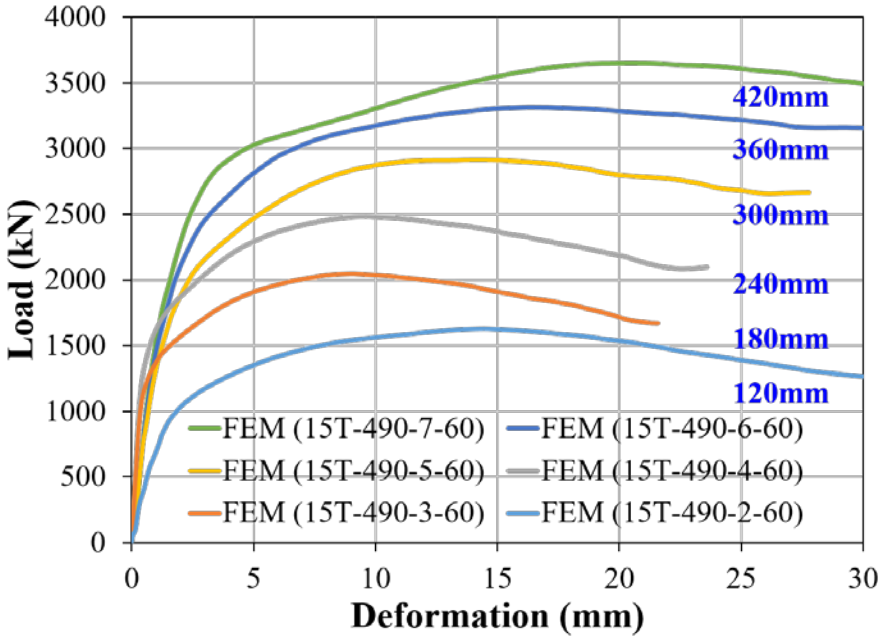

(a) 60mm Bolt Distance

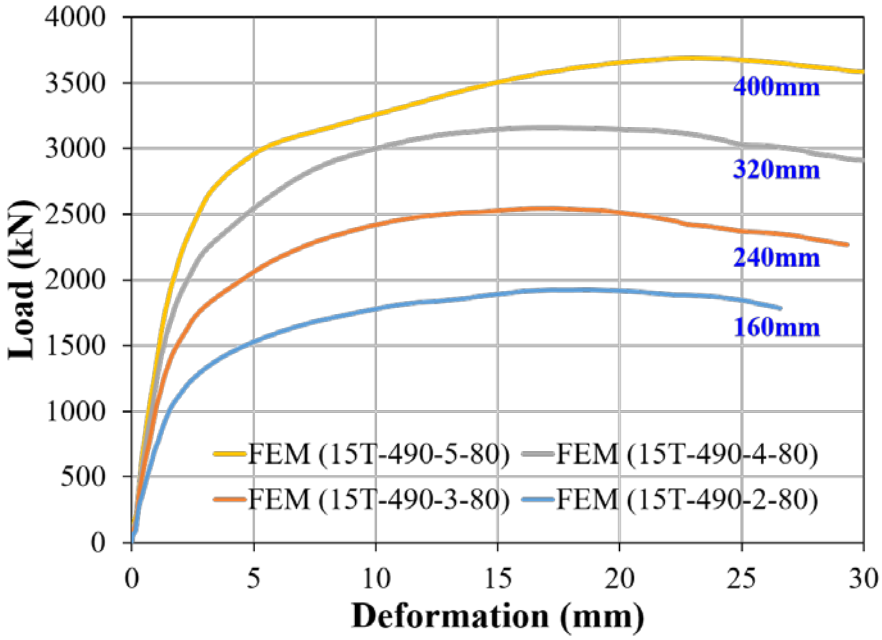

(b) 80mm Bolt Distance

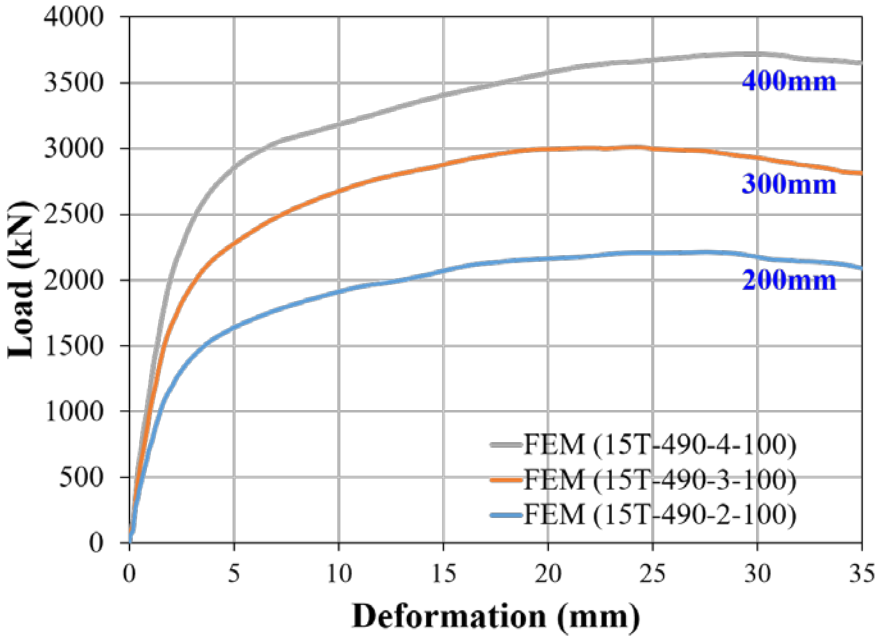

(c) 100mm Bolt Distance

Figure 4-21 Load-Deformation Curves for FE Models with 15mm Thick SM490 Steel

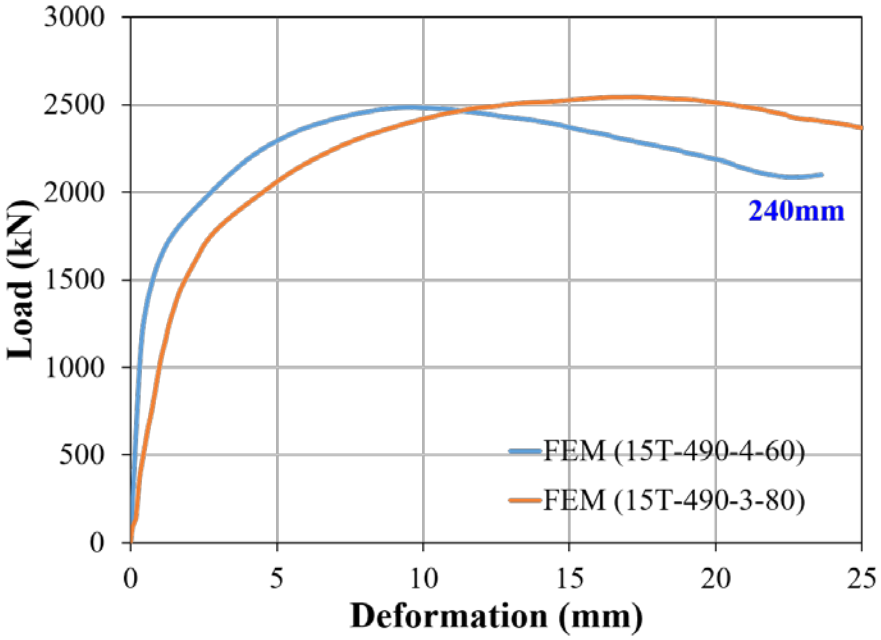

(a) 240mm Connection Length

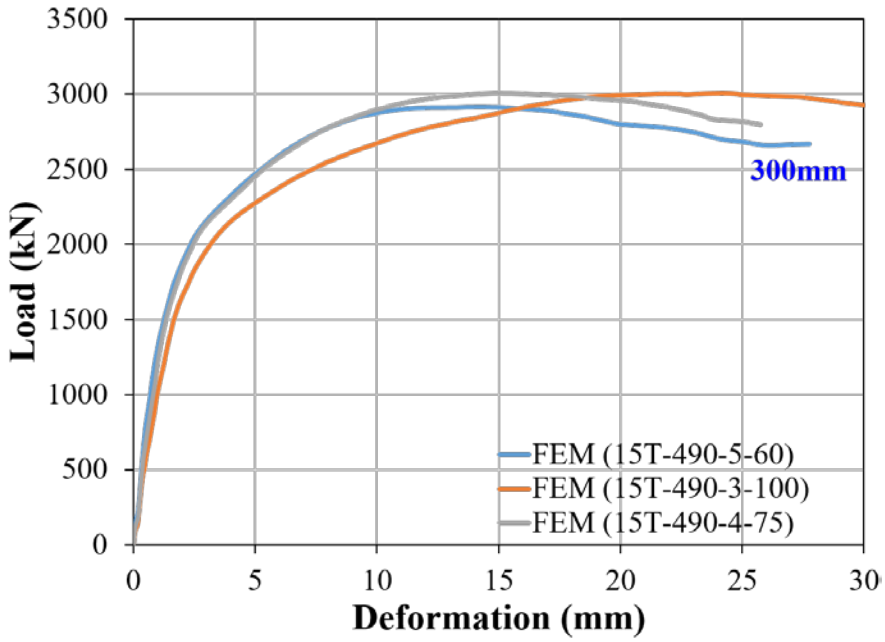

(b) 300mm Connection Length

Figure 4-22 Load-Deformation Curves of FE Models with the Same Connection Length

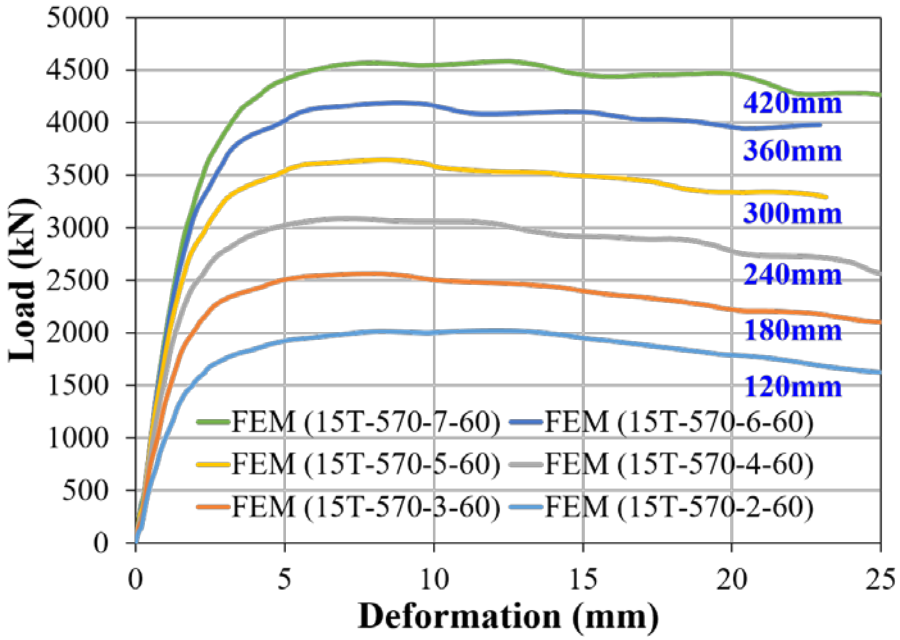

(a) 60mm Bolt Distance

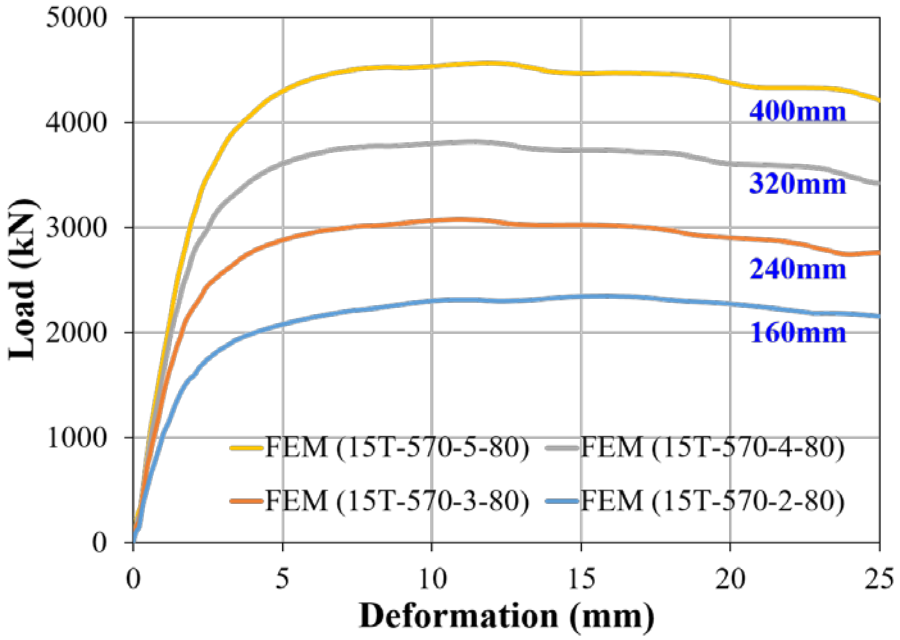

(b) 80mm Bolt Distance

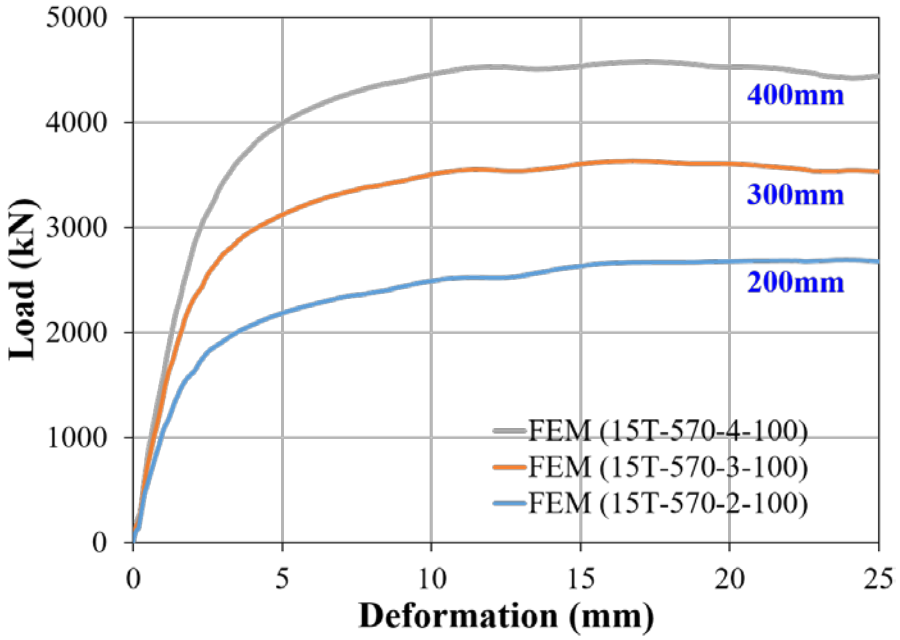

(c) 100mm Bolt Distance

Figure 4-23 Load-Deformation Curves for FE Models with 15mm Thick SM570 Steel

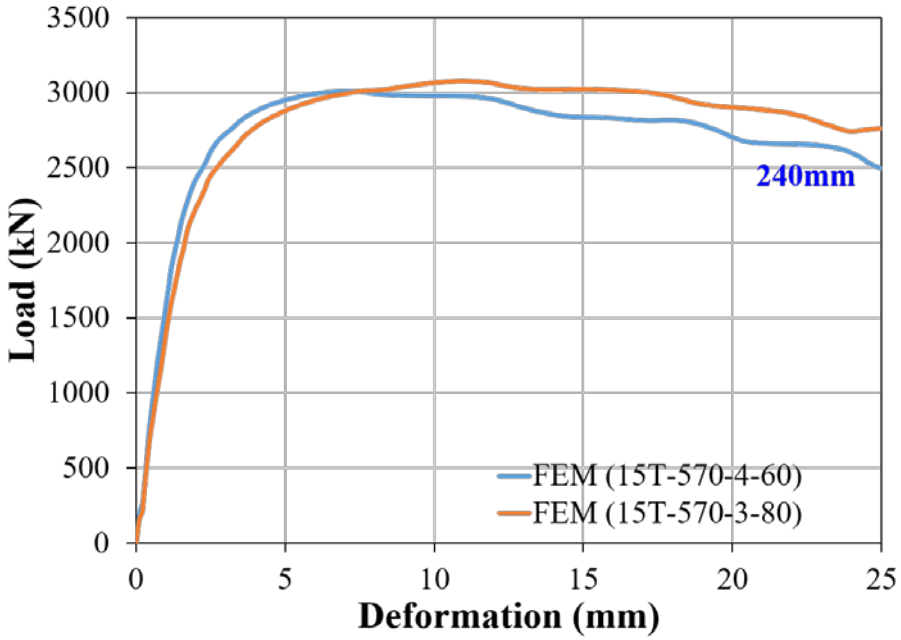

(a) 240mm Connection Length

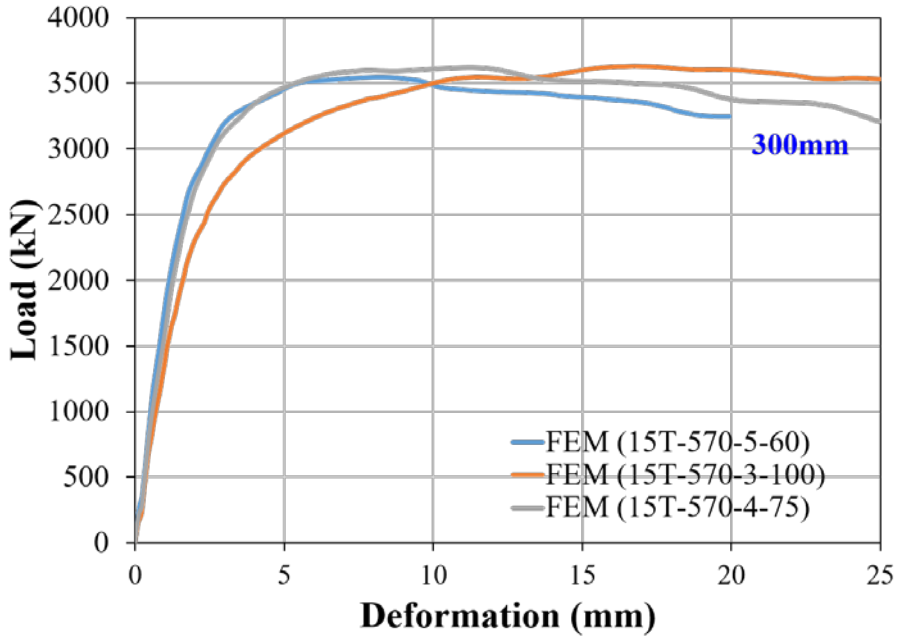

(b) 300mm Connection Length

Figure 4-24 Load-Deformation Curves of FE Models with the Same Connection Length

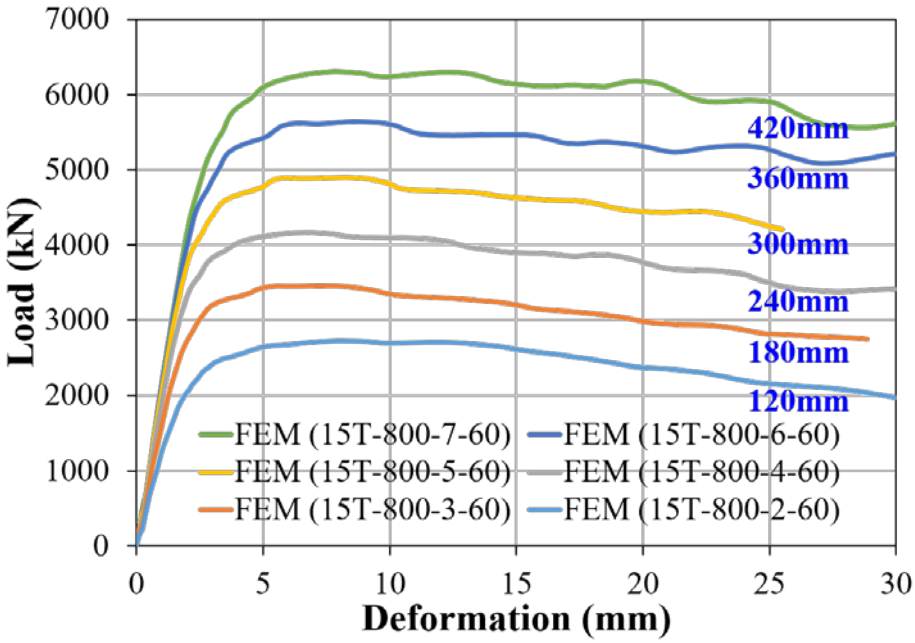

(a) 60mm Bolt Distance

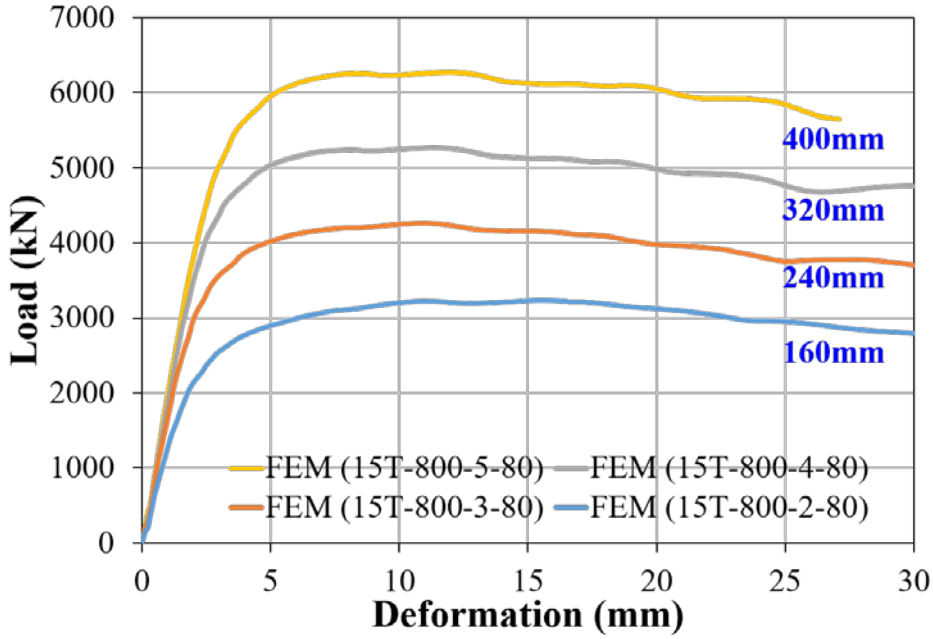

(b) 80mm Bolt Distance

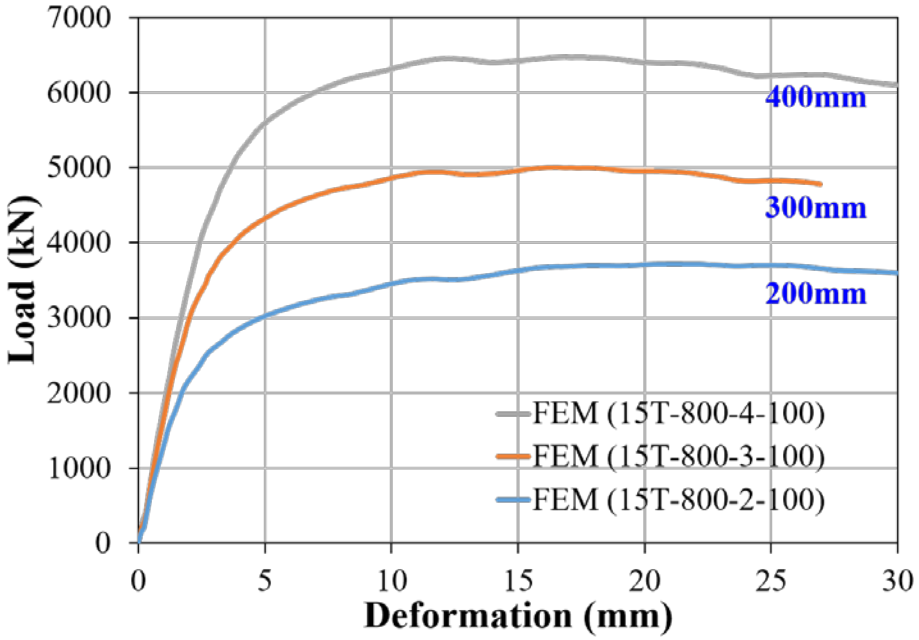

(c) 100mm Bolt Distance

Figure 4-25 Load-Deformation Curves for FE Models with 15mm Thick HSA800 Steel

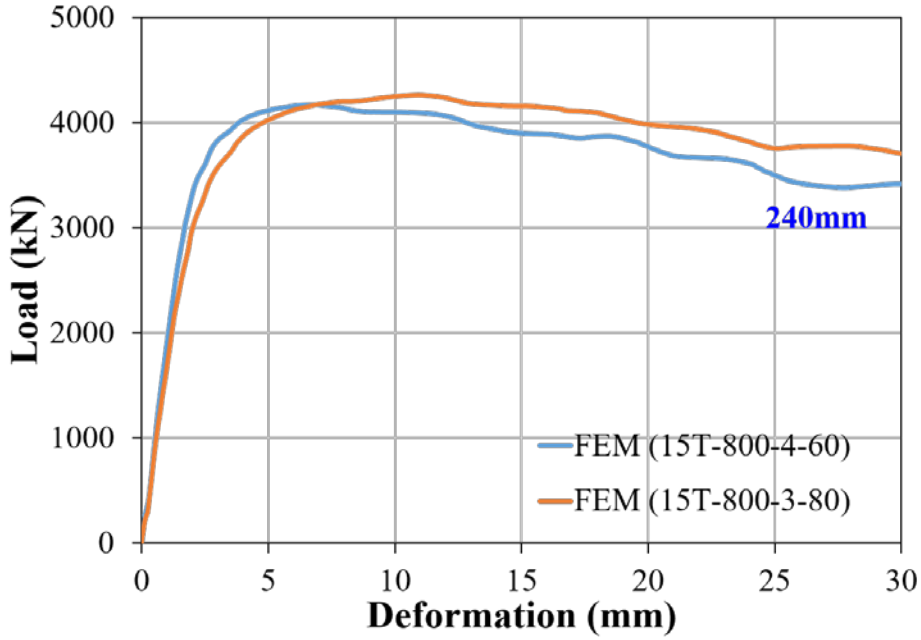

(a) 240mm Connection Length

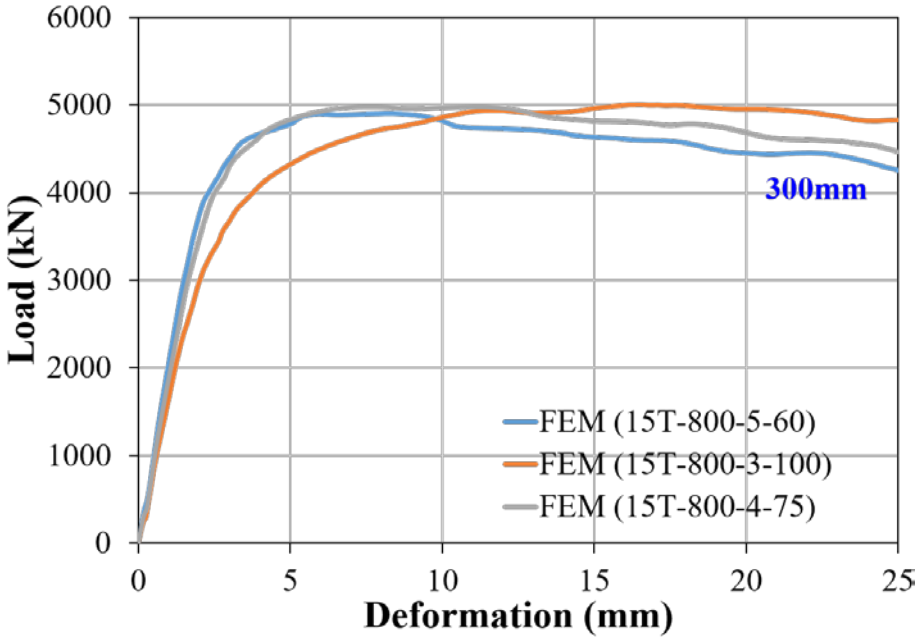

(b) 300mm Connection Length

Figure 4-26 Load-Deformation Curves of FE Models with the Same Connection Length

Table 4-5 FE Analysis Results for SM490 Steel

	Specimen	Thickness (mm)	Connection Length (mm)	A_{nt} (mm^2)	A_{gv} (mm^2)	A_{nv} (mm^2)	P_{ult} (kN)	Design Strength (kN)		
								AISC 2010	AISC 1999	CSA S16-09
SM490	15T-490-2-60	15	120	1305	3600	2115	1627	1261	1341	1520
	15T-490-3-60		180	1305	5400	2925	2045	1499	1960	1960
	15T-490-4-60		240	1305	7200	3735	2485	1738	1683	2400
	15T-490-5-60		300	1305	9000	4545	2915	1976	1921	2840
	15T-490-6-60		360	1305	10800	5355	3314	2214	2159	3280
	15T-490-7-60		420	1305	12600	6165	3651	2452	2398	3720
	15T-490-2-80		160	1305	4800	3315	1924	1575	1560	1813
	15T-490-3-80		240	1305	7200	4725	2543	2029	1974	2400
	15T-490-4-80		320	1305	9600	6135	3160	2443	2389	2987
	15T-490-5-80		400	1305	12000	7545	3688	2858	2803	3573
	15T-490-2-100		200	1305	6000	4515	2210	1809	1912	2106
	15T-490-3-100		300	1305	9000	6525	3008	2394	2503	2840
	15T-490-4-100		400	1305	12000	8535	3717	2979	3094	3573
	15T-490-4-75		300	1305	9000	5535	3006	2267	2212	2840

Table 4-6 FE Analysis Results for SM570 Steel

	Specimen	Thickness (mm)	Connection Length (mm)	A_{nt} (mm^2)	A_{gv} (mm^2)	A_{nv} (mm^2)	P_{ult} (kN)	Design Strength (kN)		
								AISC 2010	AISC 1999	CSA S16-09
SM570	15T-570-2-60	15	120	1305	3600	2115	1962	1467	1694	1835
	15T-570-3-60		180	1305	5400	2925	2495	1744	2380	2380
	15T-570-4-60		240	1305	7200	3735	3079	2021	2069	2925
	15T-570-5-60		300	1305	9000	4545	3546	2298	2346	3471
	15T-570-6-60		360	1305	10800	5355	4080	2575	2623	4016
	15T-570-7-60		420	1305	12600	6165	4586	2852	2900	4562
	15T-570-2-80		160	1305	4800	3315	2347	1878	1926	2198
	15T-570-3-80		240	1305	7200	4725	3161	2360	2408	2925
	15T-570-4-80		320	1305	9600	6135	3819	2842	2890	3653
	15T-570-5-80		400	1305	12000	7545	4560	3324	3372	4380
	15T-570-2-100		200	1305	6000	4515	2685	2288	2336	2562
	15T-570-3-100		300	1305	9000	6525	3631	2975	3024	3471
	15T-570-4-100		400	1305	12000	8535	4574	3663	3711	4380
	15T-570-4-75		300	1305	9000	5535	3619	2637	2685	3471

Table 4-7 FE Analysis Results for HSA800 Steel

	Specimen	Thickness (mm)	Connection Length (mm)	A_{nt} (mm^2)	A_{gv} (mm^2)	A_{nv} (mm^2)	P_{ult} (kN)	Design Strength (kN)		
								AISC 2010	AISC 1999	CSA S16-09
HSA800	15T-800-2-60	15	120	1305	3600	2115	2721	2059	2448	2610
	15T-800-3-60		180	1305	5400	2925	3458	2448	3393	3393
	15T-800-4-60		240	1305	7200	3735	4165	2837	2963	4176
	15T-800-5-60		300	1305	9000	4545	4901	3226	3352	4959
	15T-800-6-60		360	1305	10800	5355	5633	3614	3740	5742
	15T-800-7-60		420	1305	12600	6165	6308	4003	4129	6525
	15T-800-2-80		160	1305	4800	3315	3235	2635	2761	3132
	15T-800-3-80		240	1305	7200	4725	4264	3312	3438	4176
	15T-800-4-80		320	1305	9600	6135	5266	3989	4115	5220
	15T-800-5-80		400	1305	12000	7545	6278	4666	4792	6264
	15T-800-2-100		200	1305	6000	4515	3717	3211	3337	3654
	15T-800-3-100		300	1305	9000	6525	5002	4176	4302	4959
	15T-800-4-100		400	1305	12000	8535	6475	5141	5267	6264
	15T-800-4-75		300	1305	9000	5535	4985	3701	3827	4959

4.5 Connection Length Effect

In Figure 4-13 to Figure 4-26, load and deformation curves from the results of the finite element analysis are plotted. As depicted in Figure 4-27, the FE models with the same connection length show a similar level of block shear strength. Comparing to the finite element analysis and the experimental study, the FE models and the test results present the similar failure shape of block shear. The shear failure of the block shear occur on the gross shear plane, not on the net shear area. In spite of the number of bolts and the blot distance, the test and FE analysis results demonstrate the same level of block shear capacity. Using the gross shear area, A_{gv}, predicts more accurate block shear strength.

Effective tensile stress acting on the gross shear plane would be a value between the tensile and yield strength of the steel. For the shorter connection, the effective tensile stress, F_{eff}, has a tendency to approach F_u. On the other hand, for the longer connection, the effective tensile stress, tends to approach F_y. Although the high-strength steel has relatively low ductility, the FE models and the experimental results shows the similar failure shape of the block shear. Figure 4-27 shows the relationship between the connection length and the effective shear tensile.

$$F_{eff} = \alpha F_u + (1-\alpha) F_y \qquad 4\text{-}3$$

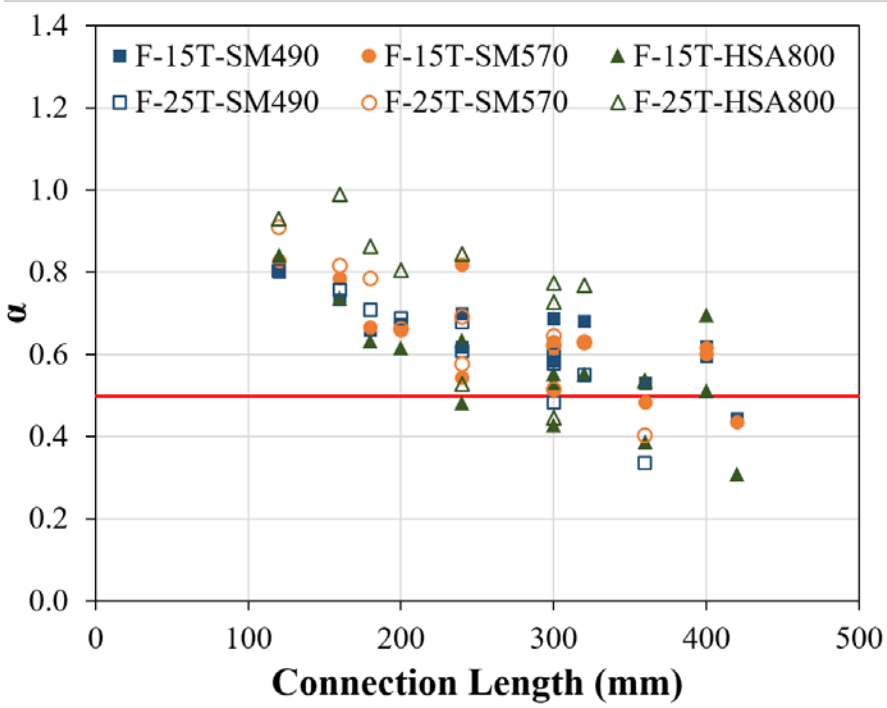

Figure 4-27 Relationship between Connection Length and α from FE Analysis

4.6 Proposed a New Design Equation

On the baisis of the data from the experimental studies and the finite element models, the regression analysis was performed. With the test and the finite element analysis results, the effective tensile stress is expressed as a function of the connection length.

$$R_n = F_u A_{nt} + 0.6 F_{eff} A_{gv} \quad \text{4-4}$$

$$F_{eff} = \alpha F_u + (1-\alpha) F_y \quad \text{4-5}$$

$$\alpha = -0.001l + 0.82 \quad \text{4-6}$$

ThepProposed equation combines the effective stress on the gross shear area. The effective stress is expressed as the relationship between the tensile and the yield stress of the steel. l means the connection length.

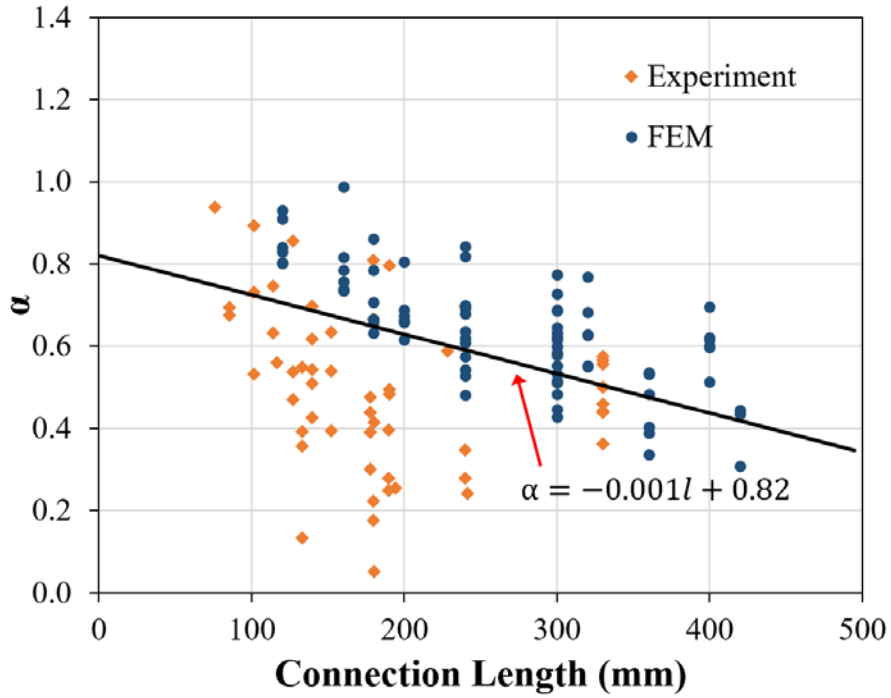

Figure 4-28 Relationship between Connection Length and α factor from FE Analysis and Experiments

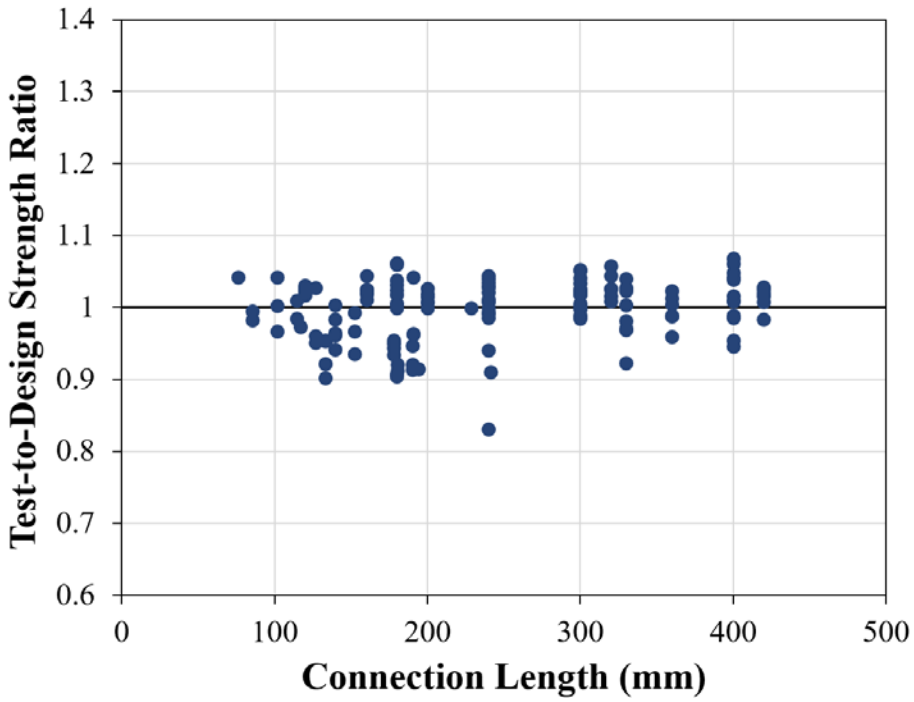

Figure 4-29 Test-to-Design Strength Ratio for New Design Equation

Table 4-8 Results of the Regression Analyses

No. of Data	R^2 (%)	Mean	CoV. (%)
156	4.07	0.91	31.96

4.7 Summary

Finite element analyses of a quarter of test specimens from Chapter 3 are conducted. As a result of the finite element analysis, the initial slope of the load-deformation curves is slightly stiffer than the experimental study. However, the FE models predict the same level of the ultimate load for the block shear

failure. In the numerical analyses, 75 different FE models that have different number of bolts and bolt distance for various connection length have been carried out. The results of finite element analyses show that the block shear strength is propotional to the connection length. The shear deformation of the bolt holes appears along the gross shear plane. Regardless of the number of bolts or the bolt distance, the specimens that have the same connection length present the same level of block shear strength.

FE models with both conventional and high-strength steel show that the effective stress on the gross shear plane varies depending on the connection length. As the connection length becomes longer, the effective stess on the gross shear area tends to approache the yield strength from the tensile strength. Due to the low ductility, the specimens with high-strength steel in the finite element analyses and experiments report the ultimate load in a small deformation, but all specimens show a similar behavior. The relationship between the effective stress and the connection length ca be expressed as a connection length parameter, α. New design equation that provides more accurate block shear strength in all steel grades includes the tendency of the effective stress.

Chapter 5. Summary and Conclusion

This chapter reports the conclusion of the experimental and numerical study into the behavior of block shear failure. The block shear failure is that the shear and tension failure occur simultaneously in perpendicular direction. Because the tensile ductility is not sufficient, the tensile rupture on the net tension area and the shear yield on the gross shear area occurred. From design to errection, the application of high-strength steel for steel structures bring about diverse technological advantages. However, most of current design standards such as AISC/KBC, and CSA S16 provide an inconsistency with the block shear strength and the failure mechanism.

In this study, a total of 10 specimens of a conventional and high-strength steel were tested and analyzed to eavaluate the current design standards. Althought the test results obtained from specimens with 25 mm thick plate showed diverse types of failure modes, the block shear failure occurred in the specimens of SM490 and SM570. All test results from specimen with 15 mm plate, including HSA800, showed the block shear failure. Comparing the test results to current design standards, the design equation of AISC 1999 and 2010 provided considerably conservative block shear strength in all specimens. The design equation from CSA S16-09 predicted most accurate block shear strength, but showed inaccurate results with the specimens of high-strength steel.

Using the symmetricity, a quarter of the test specimens were modeled in finite element analyses. According to the finite element analysis, the initial slope of the numerically obtained load-deformation curves were slightly

different, but the values of the ultimate load are in good agreement with the experimental results. In the numerical study, the finite element models had different number of bolts and bolt distance for various connection length. A total of 75 finite element models have been carried out. Based on the numerical studies and the experiments, specimens with both conventional and high-strength steel presented similar behavior of block shear failure. Regardless of the number of bolts or the bolt distance, the specimens with the same connection length indicated that the same level of block shear strength. Also, the shear deformation of the bolt holes appeared along the gross shear plane. Using the gross shear area for the equation of block shear strength is reasonable.

For shorter connection length, the effective stress on the shear plane is close to tensile strength, F_u. However, the finite element models and test specimens demonstrated a tendency that the effective stress on shear plane is close to yield strength, F_y. The effective stress varies depending on the connection length. Although the FE models and the experimental study reported that the ultimate load in small deformation because of the relatively low ductility of high-strength steel, both conventional and high-strength steel presented similar tendency of the effective stress on the gross shear plane. New design formula for block shear strength includes the tendency of the effective stress using the connection length parameter, α. The new design equation provides accurate block shear strength in all steel grades.

References

Aalberg, A., & Larsen, P. (2000). *Strength and ductility of bolted connections in normal and high strength steels.* Paper presented at the Conference Proceedings, IMPLAST.

AISC. (1978). Specification for the Design, Fabrication and Erection of Structural Steel for Buildings. *Inc., Chicago, IL*.

AISC. (1986). Load and Resistance Factor Design Specification for structural steel buildings'. American Institute of Steel Construction: American Institute of Steel Construction, Chicago, IL.

AISC. (1989). Allowable Stress Design and Plastic Design Specifications for Structural Steel Buildings: American Institute of Steel Construction, Chicago, IL.

AISC. (1993). Load and Resistance Factor Design Specification for structural steel buildings'. American Institute of Steel Construction: American Institute of Steel Construction, Chicago, IL.

AISC. (1999). Load and Resistance Factor Design Specification for structural steel buildings'. American Institute of Steel Construction: American Institute of Steel Construction, Chicago, IL.

AISC. (2005). Specification for Structural Steel Buildings (ANSI/AISC 360-05): American Institute of Steel Construction, Chicago, IL.

AISC. (2010). Specification for Structural Steel Buildings (ANSI/AISC 360-10): American Institute of Steel Construction, Chicago, IL.

Birkemoe, P. C., & Gilmor, M. I. (1978). Behavior of bearing-critical double-angle beam connections. *Engineering Journal*, *15*(4), 109-115.

Dassault Systèmes. (2009). *Abaqus/CAE User's Manual, version. 6.9*. Providence, RI, USA: Dassault Systèmes Simulia Corp.

Driver, R. G., Grondin, G. Y., & Kulak, G. L. (2006). Unified block shear equation for achieving consistent reliability. *Journal of Constructional Steel Research*, *62*(3), 210-222.

ECS. (2005). Eurocode 3: Design of steel structures, Part 1.8: Design of joints: European Committee for Standardization, Brussels, Belgium.

Hardash, S. G., & Bjorhovde, R. (1985). New design criteria for gusset plates in tension. *Engineering Journal*, *22*(2).

Huns, B. B. S., Driver, R. G., & Grondin, G. Y. (2002). *Block shear behaviour of bolted gusset plates*. Edmonton: Dept. of Civil and Environmental Engineering, University of Alberta.

Kulak, G. L., & Grondin, G. Y. (2001a). AISC LRFD rules for block shear in bolted connections- A review. *Engineering Journal, 38*(4), 199-203.

Kulak, G. L., & Grondin, G. Y. (2001b). Block shear failure in steel members–a review of design practice. *Engineering Journal, AISC*, *38*(4), 199-203.

Nast, T. E., Grondin, G. Y., & Cheng, J. R. (1999). *Cyclic Behavior of Stiffened Gusset Plate-Brace Member Assemblies*: Department of Civil and Environmental Engineering, University of Alberta.

Rabinovitch, J. S., & Cheng, J. R. (1994). *Cyclic behavior of steel gusset plate connections.* University of Alberta.

Swanson, J. A., & Leon, R. T. (2000). Bolted steel connections: tests on T-stub components. *Journal of Structural Engineering, 126*(1), 50-56.

Teh, L. H., & Yazici, V. (2013). Block shear capacity of bolted connections in hot-rolled steel plates.

Topkaya, C. (2004). A finite element parametric study on block shear failure of steel tension members. *Journal of Constructional Steel Research, 60*(11), 1615-1635.

Topkaya, C. (2007). Finite element modeling of block shear failure in coped steel beams. *Journal of Constructional Steel Research, 63*(4), 544-553.

Korean Abstract

볼트접합은 철골구조물에서 널리 사용되는 접합 방법이다. 블록전단 파단은 전단부와 인장부의 파괴가 수직인 방향으로 동시에 발생하는 것으로, 철골구조물의 설계과정에서 고려해야 하는 다양한 파괴 모드 중 하나이다. 다양한 볼트접합부의 블록전단 실험결과가 존재하지만 블록전단의 파괴메커니즘을 정확히 설명하는 연구는 드물다. 블록전단 강도 산정식은 AISC 1978에 처음 등장한 AISC 2010에 이르기까지 다양한 형태로 변형됐다. 하지만 AISC 2010은 블록전단 너무 보수적으로 예측하고, 파괴 모드도 정확하게 예측하지 못하고 있다.

고강도 강재의 적용은 철골구조물의 설계부터 시공까지 과정에서 다양한 장점이 있다. 하지만 기존 블록전단 강도 설계식은 일반강재를 이용한 실험을 바탕으로 하였기에 고강도 강재에 적용가능 여부가 불분명하였다. 본 연구에서는 인장강도 800MPa급 HSA800 강재를 적용한 볼트접합부의 거동을 실험적으로 평가하고 새로운 설계법 개발의 근거를 제시하고자 하였다.

강종 및 볼트 배열을 따른 블록전단 강도를 평가하고자 총 10개의 실대형 실험을 진행하였다. 모든 변수를 실험에 반영하지 못하기에 상용 유한요소해석 프로그램 ABAQUS를 이용하여 볼트접합부의 수치해석 연구를 진행하였다. 실험에서 반영하지 못한 볼트의

수와 간격에 따른 볼트접합부의 길이에 따른 블록전단 강도를 유한요소 해석을 이용하여 확인하고자 하였다.

본 연구에서 현행 블록전단 강도에 대한 설계기준을 평가하고 고강도 강재에 대한 적용 가능성을 연구하였다. 기존의 실험결과와 유한요소해석에 의한 데이터를 바탕으로 일반강재와 고강도 강재 모두에 적용 가능한 새로운 블록전단 강도 산정식을 제안하고자 한다.

주요어 : 블록전단, 고강도 강재, 볼트 접합부, 강도 설계식, 유한요소 해석

학번 : 2015-21095